REFLECT DELIVERABLE D2.4

Thermophysical properties of highly saline geothermal fluids

Summary:

Deliverable D2.4 reports on the activities performed within Task 2.4 "Thermophysical properties of geothermal fluids" until the end of month 36 of the REFLECT project. The task breaks down into three subtasks of different scope: Task 2.4.1 - In situ measurements of fluid thermophysical properties, Task 2.4.2 - Thermoelectrical properties, and Task 2.4.3 - Modelling of density and heat capacity. Overall, a better understanding of the thermophysical properties of highly saline geothermal fluids was obtained by a combination of analytical data evaluation, improvement of measurement devices, laboratory measurements and numerical modelling.

Authors:

Harald Milsch, Ulrike Hoffert, Juliane Kummerow, GFZ
Arnault Lassin, Laurent André, BRGM

This project has received funding from the European Union's Horizon 2020 research and innovation programme under grant agreement nº 850626.

Title:	Thermophysical properties of highly saline geothermal fluids
Lead beneficiary:	GFZ
Other beneficiaries:	BRGM
Due date:	31.12.2022
Nature:	Public
Diffusion:	All partners and general public
Status:	Final
Document code:	REFLECT_D2.4
DOI:	https://doi.org/10.48440/gfz.4.8.2022.008
License information:	CC-BY
Recommended citation:	*Milsch, H., Hoffert, U., Kummerow, J., Lassin, A., André, L. 2022, The H2020 REFLECT project: Deliverable D2.4 - Thermophysical properties of highly saline geothermal fluids, Potsdam: GFZ German Research Centre for Geosciences, DOI: https://doi.org/10.48440/gfz.4.8.2022.008*
ORCID:	Harald Milsch – ORCID: 0000-0002-5915-5862 Laurent André – ORCID: 0000-0002-8844-1585 Arnault Lassin – ORCID: 0000-0001-7414-7599 Juliane Kummerow – Scopus-ID: 36446009700

Revision history	Author	Delivery date	Summary of changes and comments
Version 01	AL, LA	14.11.2022	Input subtask 2.4.3 (BRGM)
Versions 02 / 03	HM, UH / JK	7.12.2022 / 10.12.2022	Input subtasks 2.4.1 and 2.4.2 (GFZ)
Final version	HM	16./21.12.2022	Finalization after internal/external review

Approval status				
	Name	Function	Date	Signature
Deliverable responsible	Harald Milsch	Task leader	16.12.2022	*HM*
WP leader	Chris Boeije	WP leader	19.12.2022	*CB*
Reviewer	N/A	Reviewer		
Reviewer	N/A	Reviewer		
Project Coordinator	Simona Regenspurg	Project coordinator	19.12.2022	*SR*

TABLE OF CONTENTS

1 EXECUTIVE SUMMARY

Knowing the thermophysical properties of geothermal fluids is of importance for the full value chain of geothermal site development, from exploration to operation. For highly saline fluids, however, the database is incomplete. Data become more and more scarce, the more complex the fluid composition is and the more extreme the physical conditions are. The purpose of this task was to improve the availability of thermophysical fluid data by a combined experimental (Subtasks 2.4.1 and 2.4.2) and numerical (Subtask 2.4.3) approach.

In Subtask 2.4.1 new technical developments were successfully made to permit precise viscosity measurements at reservoir conditions. Moreover, several literature-derived empirical viscosity correlations for NaCl aqueous solutions were evaluated against original viscosity data measured at GFZ. This permits to state a best matching viscosity correlation that produces accurate predictions for a broad range of salt concentrations. The temperature dependence of the inherent virial coefficients was evaluated in addition, permitting to state viscosity of NaCl fluids both as a function of concentration and temperature. This work is ongoing and expands this approach to fluids (co-)dominated by other salts, e.g. $CaCl_2$.
A second part of this subtask was to evaluate the effect of minor constituents in natural geothermal fluids on both density and viscosity. In a first attempt, measurements were performed at ambient pressure and temperatures up to 80 °C on synthetic fluids mimicking the fluid found at the Insheim, Germany geothermal site. It showed, that the measured data for density and viscosity of the solutions with lithium and/or strontium differ only slightly (i.e. < 2 %) from those of the pure solution.

In Subtask 2.4.2 an existing high-pressure/ high-temperature system for the measurement of electrical conductivity of hydrothermal fluids was technically upgraded to improve the precision of measurements of aqueous bicarbonate solutions in dependence of both temperature and concentration. These measurements allow us to determine limiting conductivities in a temperature range of 25 – 450 °C at a constant pressure of 25.5 MPa, which is a prerequisite to estimate the electrical properties of multi-component brines. To test the new data, mixed brines were investigated to deduce a mixing rule for a multi-component system.

In Subtask 2.4.3, we use geochemical modelling to predict the properties of geothermal fluids and anticipate their chemical behaviour when they are subjected to temperature and pressure variations in order to avoid exploitation issues like the precipitation of minerals in the facilities (production/injection wells, heat exchangers…). As a first step, we set-up a model to calculate the fluid properties using the tool PhreeSCALE (https://doi.org/10.1016/j.cageo.2016.03.016). The methodology relies on successive steps that include the estimation of Pitzer interaction parameters for the binary $CaCl_2$-H_2O system and for the ternary $CaCl_2$-MCl_x-H_2O (with M = Na, Ca, Mg, K, Li and x = 1 or 2) systems. With the new model, we are able to reproduce with great accuracy both recent measurements of density acquired during the REFLECT project and literature data like osmotic coefficients and heat capacities. The model can be applied at temperatures between 25 °C and 200 °C. It has also been upgraded in order to simulate the solubility of CO_2 in such saline systems. The modelling of gas solubility is of main interest in order to predict the degassing, especially within the well during the exploitation.

The results of REFLECT Task 2.4 were presented at several conferences and published as conference proceedings or in peer-reviewed scientific journals.

2 TASK 2.4.1 - IN SITU MEASUREMENTS OF FLUID THERMOPHYSICAL PROPERTIES

2.1 Experimental developments and viscosity correlations

In the past, a significant number of new thermophysical data were obtained at GFZ for the parameters density, viscosity, electrical conductivity, thermal conductivity, and speed of sound. In this subtask experimental techniques to measure viscosity at elevated pressures and temperatures were developed further using a rock physical device transformed into a capillary viscometer. The accuracy of this apparatus was tested with respect to the optimum choice of the capillary inner diameter against reference data for the viscosity of pure water at 25 °C.

Moreover, existing viscosity data obtained at GFZ for NaCl, $CaCl_2$, and mixed solutions thereof at ambient pressure and temperatures up to 80 °C were correlated using a modified Jones-Dole-Equation of the type:

$$\eta_r = \eta/\eta^0 = 1 + Ac^{1/2} + Bc + Dc^2 + Ec^{3.5},$$

where η_r, η, η^0 are the viscosity ratio, the viscosity of the solution, and the viscosity of pure water, respectively, A, B, D, and E are temperature dependent virial coefficients, and c is salt concentration.

Regarding viscosity measurements, after the modification of the apparatus, systematic investigations with different capillary diameters and lengths as well as different flow rates were required. In addition, a sufficiently accurate determination of the fluid temperature within the measuring capillary had to be ensured. For measurements of pure water, the current setup (inner capillary diameter: 130 µm and length: 1.6 m) allows an accuracy better than about 2% as shown in Figure 1, where the relative error of the viscosity data of pure water compared to NIST-REFPROP (https://www.nist.gov/programs-projects/reference-fluid-thermodynamic-and-transport-properties-database-refprop) is shown for different pressure and flow conditions.

These results were presented during the last World Geothermal Congress held in Iceland in 2021 and are summarized in the following extended abstract referenced as:

Hoffert, U., Milsch, H. (2021): *Methods for measuring the density and viscosity of saline geothermal fluids under reservoir conditions.* **Papers, World Geothermal Congress 2020+1 (Reykjavik, Iceland Online 2021), 13131.**

The publication is attached to this report as Appendix 1.

For viscosity, different literature-derived virial correlations were tested against existing data as shown in Figure 2 for the example of NaCl solutions at 25 °C as a function of molarity. It shows that the correlation established by Zhang and Han (1996) with four virial coefficient performs better than the original Jones-Dole-Equation (e.g. in Falkenhagen, 1970) and the one established by Out and Los (1980). The experimental viscosity is reproduced fairly well by the former within the limits of experimental precision.

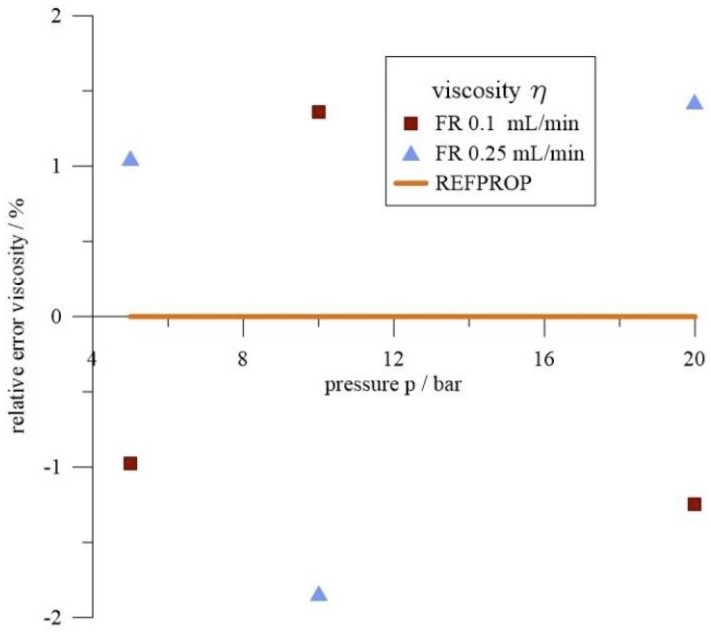

Figure 1 - Relative error for viscosity measurements of pure water at room temperature (25 °C), different pressures and flow rates, compared to NIST-REFPROP. FR in the legend indicates flow rate.

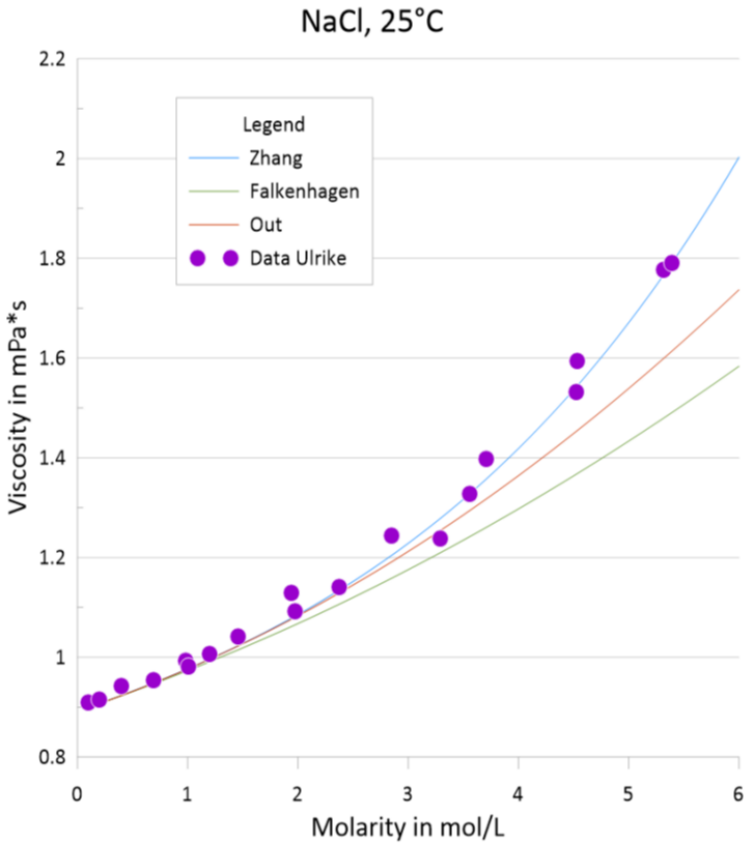

Figure 2 - Comparison of three different viscosity correlations (established by Zhang and Han, Jones-Dole / Falkenhagen, and Out and Los) with original experimental data (Ulrike Hoffert, GFZ) for NaCl solutions of various molarity at 25 °C.

2.2 Evaluating the effect of minor compounds on density and viscosity

Geothermal fluids display a huge variability in chemical composition. It is therefore impossible to determine their thermophysical properties for all possible sites and at any conditions. Consequently, the approach that is pursued at GFZ is to fill the existing data gaps systematically by determining the properties of synthetic fluids containing the main salts only, i.e. typically NaCl, $CaCl_2$, and KCl. This, however, neglects the minor constituents of natural fluids. To evaluate the effect of this approach on the respective property, density and viscosity measurements were performed at ambient pressure and temperatures ranging between 20 °C and 80 °C. The fluid sampled at the Insheim, Germany geothermal site was used as an example of a highly saline fluid. Four synthetic samples were prepared, one containing the main salts only and three others containing two dominant minor salts as pure and mixed additions to the base solution.

Table 1: Composition of the deep fluid in Insheim; mass m of dissolved cations and anions in water and their molality b.

Cations/Anions	*m mg/L*	*b mol/kg*	*Cations/Anions*	*mg/L*	*b mol/kg*
Sodium	29000.0	1.2614	Antimony	0.3	0.0000
Potassium	4000.0	0.1023	Barium	26.0	0.0002
Calcium	7100.0	0.1772	Lithium	167.0	0.0241
Magnesium	70.0	0.0029	Silicon	73.4	0.0026
Ammonium	39.2	0.0022	Strontium	130.0	0.0015
			Arsenic	16.0	0.0002
Chloride	61000.0	1.7207	Lead	1.6	0.0000
Bicarbonate	150.0	0.0025	Iron	26.3	0.0005
Sulfate	140.0	0.0015	Copper	0.0	0.0000
Nitrate	1.6	0.0000	Manganese	30.7	0.0006
Bromide	181.0	0.0023	Zinc	8.8	0.0001

As shown in Table 1, the main solutes in the Insheim fluid are sodium, potassium, calcium and chloride. Consequently, we chose the main components sodium, potassium and calcium as its chloride salts[1] for our synthetic fluid model. To study the influence of minor salt components on the fluid properties, we chose lithium and strontium, also as chloride salts[2]. The added molality of these salts was chosen to correspond to the total mass of all cations in the fluid without the main components. The composition of the synthetic samples is shown in Table 2.

[1] Carl Roth GmbH + CO. KG.:
Natriumchlorid, min. 99,5 %, CELLPURE®, CAS Nr. [7647-14-5], Order Nr. HN00.2
Calciumchlorid-Hexahydrat, min. 98 %, p.a., CAS Nr. [7774-34-7], Order Nr. T886.3
Kaliumchlorid, min. 99,5 %, p.a., CAS Nr. [7447-40-7], Order Nr. 6781.1

[2] Carl Roth GmbH + CO. KG.:
Lithiumchlorid, min. 99 %, p.a., CAS Nr. [7447-41-8], Order Nr. 6698.1
Strontiumchlorid Hexahydrat, min. 99 %, p.a., CAS Nr. [10025-70-4], Order Nr. 4473.1

Table 2: Composition of the synthetic fluid samples; for sample 1: salts in water, for sample 2-4: salts in sample 1.

sample	*component*	*b / mol·kg^{-1}*
1: IH_pure	sodium chloride	1.2994
	potassium chloride	0.1064
	calcium chloride	0.1829
2: IH_Li	lithium chloride	0.0298
3: IH_Sr	strontium chloride	0.0296
4: IH_LiSr	lithium chloride	0.0148
	strontium chloride	0.0148

The samples were weighed in with a scale[3] whose reproducibility is given as less than 1 ‰ relative to the weighed quantities. To measure the density and viscosity of the samples, a combined setup of a densitometer[4] and a viscometer[5] was used. Before injection into the measuring devices, the samples were heated up to 80°C to avoid bubbles interfering with the measuring process. Density and viscosity were obtained in 10 K steps beginning with 80°C to 20°C and at 25°C. After the measurement, the samples were dried in an oven to verify the molality by weighing and recalculating the resultant water loss.

Table 3: Measured density and viscosity data

	1: IH_pure		***2: IH_Li***		***3: IH_Sr***		***4: IH_LiSr***	
ϑ / °C	*η / mPa·s*	*ρ / g·cm^{-3}*	*η / mPa·s*	*ρ / g·cm^{-3}*	*η / mPa·s*	*ρ / g·cm^{-3}*	*η / mPa·s*	*ρ / g·cm^{-3}*
80	0.4652	1.0398	0.4701	1.0423	0.4746	1.0458	0.4706	1.0423
70	0.5173	1.0457	0.5236	1.0482	0.5259	1.0518	0.5224	1.0483
60	0.5838	1.0513	0.5903	1.0538	0.5929	1.0574	0.5881	1.0539
50	0.6709	1.0565	0.6794	1.0590	0.6813	1.0626	0.6760	1.0591
40	0.7887	1.0613	0.7975	1.0638	0.8012	1.0674	0.7951	1.0638
30	0.9508	1.0655	0.9615	1.0681	0.9654	1.0717	0.9582	1.0681
25	1.0551	1.0675	1.0678	1.0700	1.0708	1.0737	1.0632	1.0701
20	1.1804	1.0693	1.1929	1.0718	1.1975	1.0755	1.1892	1.0719

The measured data (Table 3) for density and viscosity of the solutions with lithium and/or strontium differ only slightly from those of the pure solution. While the values of the sample IH_Sr deviate the most, the results for IH_Li and IH_LiSr lie closer together. Table 4 shows the percentage deviation of the measured data for the solutions with lithium and/or strontium compared to IH_pure.

[3] KERN & SOHN GmbH. ABJ 220-4M

[4] DMA 4500M, Anton Paar GmbH, precision: 0.00005g·cm -3 (manufacturer's specifications)

[5] AMVn, Anton Paar GmbH, precision: 0.5% (manufacturer's specifications)

Table 4: Average deviation of the measured values compared to IH_pure over all measured temperatures.

	IH_Li	***IH_Sr***	***IH_LiSr***
	difference to IH_pure / %		
viscosity	1.15	1.61	0.84
density	0.24	0.58	0.24

In terms of viscosity, the deviation from the measured values is less than 2%. The observed measurement error for the higher temperatures and higher concentrations is also around 2%. The influence of minor salt components on the viscosity can therefore be neglected. With regard to the density, the deviations are above the observed measurement error. However, the differences to the pure solution are so slight that they may also be neglected in the context of geothermal applications.

3 TASK 2.4.2 - THERMOELECTRICAL PROPERTIES

3.1 Objectives

The measurement of electrical conductivity is a classical experimental technique, predominantly used for the determination of transport and thermodynamic properties of dilute electrolyte solutions. Also, the reliability of the interpretation of resistivity data from geoelectric surveys in the frame of geothermal exploration initiatives highly depends on the proper knowledge of electrical conductivities of geothermal brines. Most natural brines are sodium chloride dominated solutions. Thus, geothermal fluids are commonly regarded as pure NaCl – H_2O systems, for which the electrical properties are fairly well known up to 800 °C (e.g. Quist & Marshall, 1968; Ho et al., 1994; Zimmerman et al., 2012) and numerical models were developed to accurately predict the conductivity of aqueous NaCl solutions for various concentrations under crustal and upper mantle conditions (e.g. Sinmyo & Keppler, 2017; Watanabe et al., 2021). In contrast, although carbonates are important constituents of natural subsurface fluids, no data on aqueous carbonate systems are documented in literature, at least for elevated temperatures and pressures. This is a major obstacle in developing adequate numerical tools to estimate the electrical properties of multi-component brines.

Therefore, the electrical conductivities of binary carbonate solutions ($NaHCO_3$) were measured at various concentrations, to determine limiting conductivities in a temperature range of 25 to 450 °C at 25.5 MPa. These data are the prerequisite to predict the electrical conductivity of a solution of any concentration. Additionally, the electrical conductivity of a mixed brine, containing both NaCl and $NaHCO_3$ was measured at similar conditions to test fitting models.

3.2 Experimental methods and procedures

A self-constructed high-temperature/ high-pressure flow-through cell was used for electrical conductivity measurements at temperatures ranging from 25 to 450 °C at a constant pressure of 25.5 MPa (Figure 3). The cell consists of two pairs of current and potential electrodes (Pt wires, embedded in electrically insulating corundum capillaries), which are sealed in both ends

of a corundum-lined high-pressure tube that is placed in a tube furnace. A free interspace of 2 cm between the electrodes serves as conductivity measuring cell.

An impedance spectrometer (Zahner-Zennium electrochemical workstation) was used to measure impedance, Z, and the phase angle, φ, at distinct frequencies ranging from 10 mHz to 10 kHz with the 4-wire electrode layout. The electrical conductivity of the solution, σ, is given by

$$\sigma = k_{cell}/R \,, \qquad (1)$$

whereby R is the fluid resistance, calculated from

$$R = cos\varphi \cdot Z \,, \qquad (2)$$

and the cell constant, k_{cell}, which considers the geometry of the 4-electrode layout. The cell constant of the set-up was experimentally determined before and after the test series by using standard NaCl solutions of 0.05 mol·kg^{-1}, 0.01 mol·kg^{-1}, 0.001 mol·kg^{-1}, and bi-distilled water at ambient conditions. For more details see Kummerow and Raab (2015a, b) and Kummerow et al. (2020).

For temperature control a Pt/Pt-Rh-thermocouple is additionally installed in the fluid pipe, allowing direct measurements in the hot zone. Temperatures were constant at ± 0.2 °C below supercritical conditions, while above the critical point temperature fluctuations of up to ± 0.3 °C within milliseconds were observed, which were possibly caused by flow perturbations. No corrections were made for the temperature influence. Hence, the experimental error on fluid conductivities cumulates usually to ±3 % at maximum due to instrumental accuracy and variations in the set-up dimension caused by differences in the thermal expansion coefficients of the stainless-steel pressure tube, corundum ceramic and the Pt-wires at elevated pressure and temperature. The accuracy is higher at lower temperatures.

Sodium bicarbonate test solutions were prepared from highly pure $NaHCO_3$ powder (Merck) and bi-distilled, degassed water (conductivity = 2.4 µS/cm) at four different concentrations with molalities, m, of 0.00110 mol·kg^{-1}, 0.01137 mol·kg^{-1}, 0.05203 mol·kg^{-1}, and 0.08800 mol·kg^{-1}, respectively. The conductivity of the four test solutions was measured at the same temperature, pressure, and flow rate. The NaCl – $NaHCO_3$ brine was mixed from degassed and deionised water and high purity salts after unpublished information of geothermal well fluid chemistry from a carbonate reservoir (person. comm.).

After each test series the flow-through system was rinsed with 200 ml of diluted HCl, followed by the injection of 1000 ml of deionised water to return to baseline conductance values.

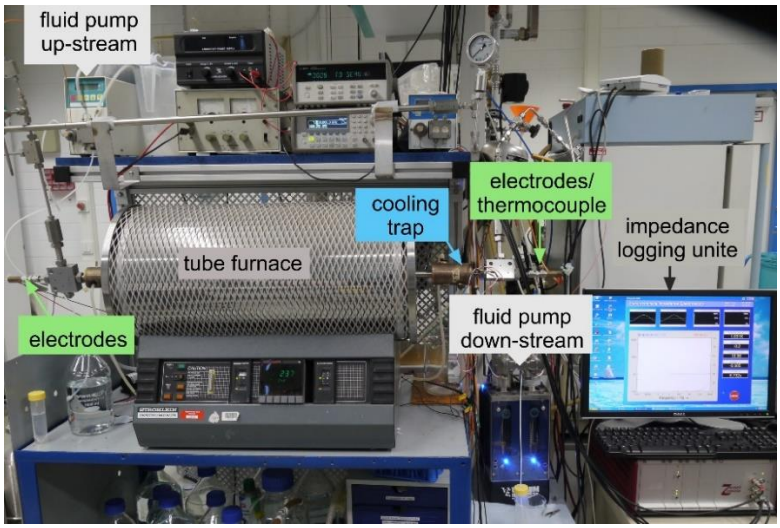

Figure 3 - High-temperature/high-pressure electrical conductivity cell.

3.3 Results and conclusions

In a series of first test runs with sodium bicarbonate solutions, especially for temperatures between 150 °C and 350 °C, highly unstable electrical signals where observed, leading to a high variability of conductivity data of up to 15 %, whereby variations were highest for the solution with the lowest concentration (Figure 4). This behavior was accompanied by an unintentional decrease in flow rate till stagnancy, indicating a gas phase in the flow-through system. Moreover, gas bubbles were observed in produced fluid samples, while pH values increased from neutral (pH 7.3) to pH 8.4 at 350 °C, and became neutral again after applying supercritical conditions.

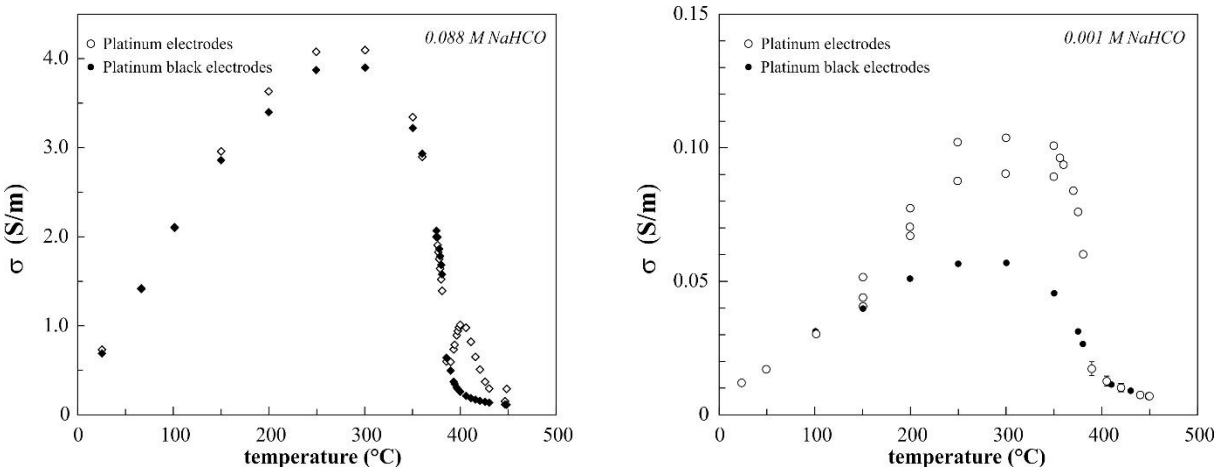

Figure 4. - Electrical conductivities of NaHCO3 solutions of two different concentrations in dependence of temperature. Open symbols represent measurements with uncoated Pt electrodes, while black data points were measured with Pt-black coated electrodes.

In a bench top test, it could be demonstrated that this effect was not only linked to increasing temperatures, but that applying an alternating current, induced the development of a free gas phase, which deposited at the electrode surface (Figure 5) and lead to an electrode polarisation. The gas phase was identified as CO_2 by a limewater precipitation test.

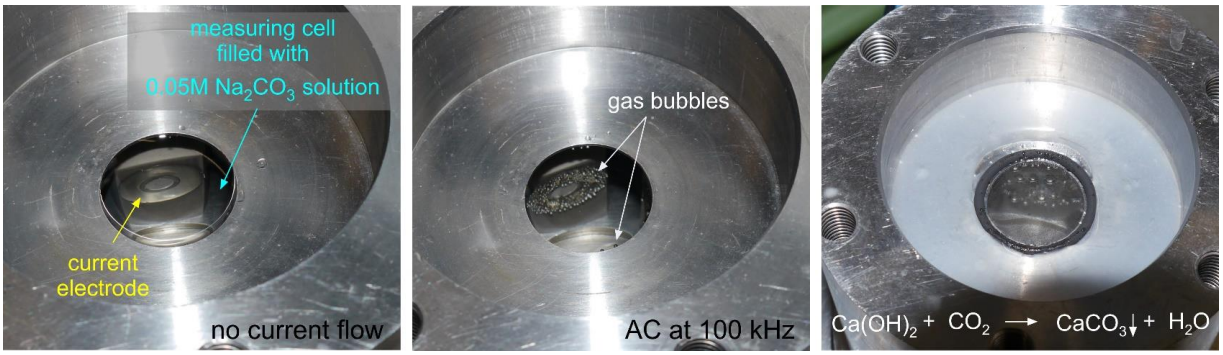

Figure 5. - A fluid conductivity measuring cell is filled with 0.05 M Na2CO3 solution (left). After applying an alternative current gas bubbles form at the surface of the current electrodes (middle). The development of CO_2 was verified by precipitation of $CaCO_3$ (white deposit) after discharging the gas phase into limewater (right).

Inherently, the dissociation of $NaHCO_3$ can be described by a series of equilibria that occur:

$$\overset{A}{NaHCO_3} \rightleftharpoons Na^+ + HCO_3^- + H_2O \overset{B}{\rightleftharpoons} Na^+ + H_2CO_3 + OH^- \overset{C1}{\rightleftharpoons} Na^+ + OH^- + H_2O + (CO_{2(aq)} \overset{C2}{\rightleftharpoons} CO_{2(sc)})$$

At equilibrium conditions, all of the species are present in different amounts. While at low temperature the first dissociation step (A) seems to be favored (solution pH is neutral), steps B and C seem to become increasingly important between 150 °C and 374 °C, indicated by an increasing pH and fizzing fluid samples. However, it could be shown that the shift in equilibrium to the right side was, at least partly, due to experimental artefacts caused by unsuitable electrode surfaces. The disproportional increase in electrical conductivity above 150 °C can also be explained by an increase of OH^- concentration in the solution, as the ionic conductivity of OH^- (at ambient conditions) exceed that of most other ions by the 4-fold. The higher conductivity is due to the special shifting mechanism of bonding electrons between the OH^- ion and water molecules. As this mechanism is most effective due to fast charge transport via hydrogen bonds, with decreasing dielectric properties of water and the reorganization of H_2O clusters this effect becomes less decisive near the critical point, which is at about 380 to 385 °C for the studied solutions.

The electrochemical decomposition of the carbonate phase at the electrode surface could be reduced significantly by coating the electrodes with Pt black, a highly porous powder, which enlarges the electrode surfaces and consequently reduces the current density. This measure considerably improved the quality of electrical signals.

In the temperature range of 25 to 450 °C, electrical conductivities of the aqueous $NaHCO_3$ solutions were measured with the modified electrodes and transformed into molar equivalence conductivities, Λ_{eq},

$$\Lambda_{eq} = \sigma/c \cdot n^e \,, \qquad (3)$$

which is the electrical conductivity in electrolytes related to the molar concentration, *c*, and the charge number, n^e. For strong electrolytes, plotting the molar equivalence conductivity of the solutions as a function of the square root of the corresponding concentration gives a set straight lines for each temperature, which is known as Kohlrausch's square root law. By extrapolating these lines to $c^{-1/2} = 0$ the molar limiting conductivity, Λ_{lim}, at infinite dilution is found (Figure 6a), which is a characteristic constant of the respective type of salt. For weak electrolytes, such as sodium bicarbonate, Ostwald's law of dilution applies. Here, the reciprocal value of the equivalent conductivity is plotted against the specific conductivity and the limiting conductivity is given by the reciprocal of the intercept with the ordinate (Figure 6b). In this study, both models lead to a series of linear functions. However, the respective values for Λ_{lim} differ (Table 5), whereby the values determined according to Ostwald's dilution law show better agreement with the measured electrical conductivities (Figure 6c).

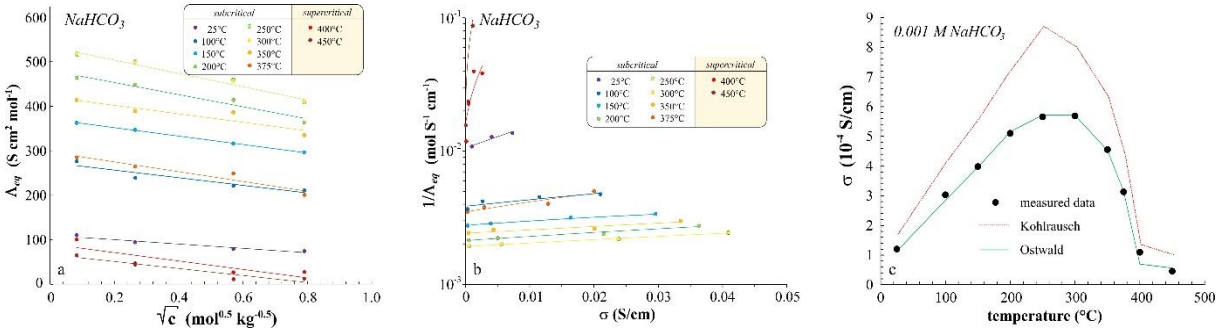

Figure 6. - (a) Kohlrausch plot: Λ_{eq} of bi-carbonate solutions, measured in dependence of temperature are plotted versus square root of the molar concentration. (b) Ostwald plot: 1/ Λ_{eq} plotted versus electrical conductivity of the solutions. The extension of these linear functions to zero concentration and electrical conductivity, respectively defines the limiting equivalent conductivity at infinite dilution. (c) Measured electrical conductivities (black symbols) in comparison with conductivities estimated from Kohlrausch and Ostwald limiting conductivity values.

Table 5: Limiting equivalent conductivities for the $NaHCO_3$ – H_2O system under hydrothermal conditions determined from Ostwald and Kohlrausch plots, respectively.

T (°C)	P (MPa)	Λ_{lim} (S cm² mol⁻¹)	Λ_{lim} (S cm² mol⁻¹)
20	25.5	93.20	118.53
25	25.5	102.91	109.81
100	25.5	259.23	273.12
150	25.5	359.80	343.59
200	25.5	468.35	473.50
250	25.5	520.03	479.03
300	25.5	518.88	507.43
350	25.5	411.58	421.70
375	25.5	287.12	288.43
400	25.5	63.28	88.98
450	25.5	51.28	74.45
		Ostwald model	*Kohlrausch model*

Also, extrapolated to 20 °C, Λ_{lim} is 93.20 S cm^2 mol^{-1} and thus, in excellent agreement with the value of 94.57 S cm^2 mol^{-1}, which is documented in literature. Limiting conductivities allow to calculate electrical conductivities of given solutions at any concentration. This was tested by recalculating the electrical conductivity of all tested $NaHCO_3$ solutions by using the determined Λ_{lim}. Above the critical point, the agreement between the model and the measured data is generally weak. However, between 24 and about 380 °C the match is remarkable well, though between the 200 – 300 °C calculated and measured conductivities deviate by 5 % at maximum for the 0.052 mol·kg^{-1} solution and by 10 % for the 0.088 mol·kg^{-1} solution (Figure 7).

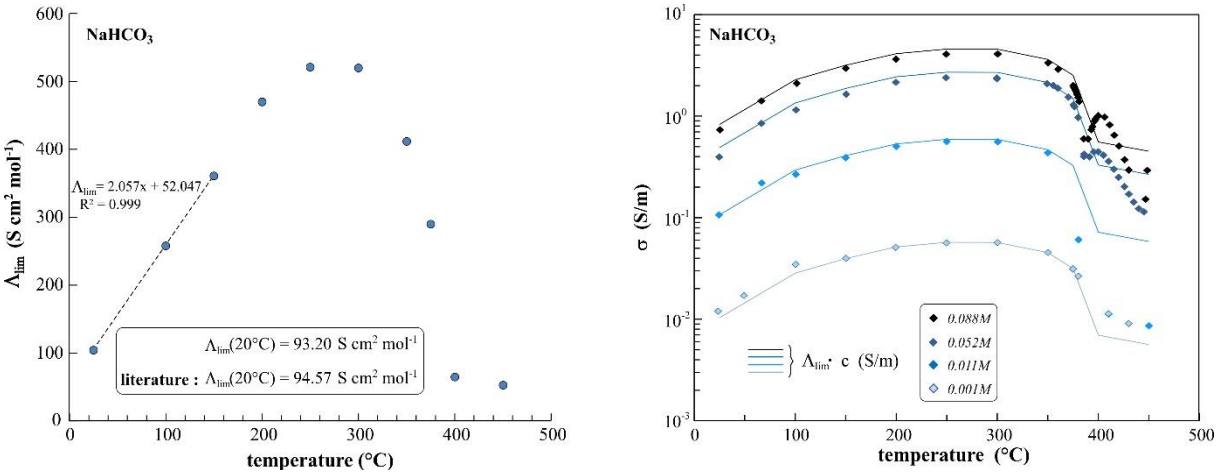

Figure 7. - (left) Λ_{lim} of $NaHCO_3$ determined after Ostwald's law as function of temperature. (right) Electrical conductivities of $NaHCO_3$ solutions of different concentrations. Dots represent measured data, the lines depict conductivities, calculated from Λ_{lim}.

Figure 8 shows measured conductivities of a diluted, nearly 1:1 aqueous NaCl – $NaHCO_3$ mixture. Fitting the data with the well-established binary model function of Sinmyo and Keppler (2017):

$$\log \sigma = A + B/T + C \log c + D \log \rho + \log \lambda_{lim}\,(T, p)\,, \qquad (4)$$

where ρ is the density of water and *A, B, C, D* are fitting parameters, is unsatisfying, pointing to the limitation of the use of models of binary systems to describe natural brines. A simple ternary fitting model was set-up, based on the summation of individual conductivities of NaCl and $NaHCO_3$ solutions, calculated from limiting conductivities of the components (this study; Zimmerman et al., 2012) and their respective molar concentration.

$$\sigma = \lambda_{lim}(NaCl) \cdot c_{NaCl} + \lambda_{lim}(NaHCO_3) \cdot c_{NaHCO3} \qquad (5)$$

With this model, the electrical conductivity of the given NaCl – $NaHCO_3$ solution can be adequately predicted, whereby an assessment of the general validity of this approach requires further measurements with higher absolute concentrations and different stochiometric weightings. Future work should thus be directed both to systematically broaden the database for complex brines and to determine limiting conductivities for relevant pressure and temperature conditions.

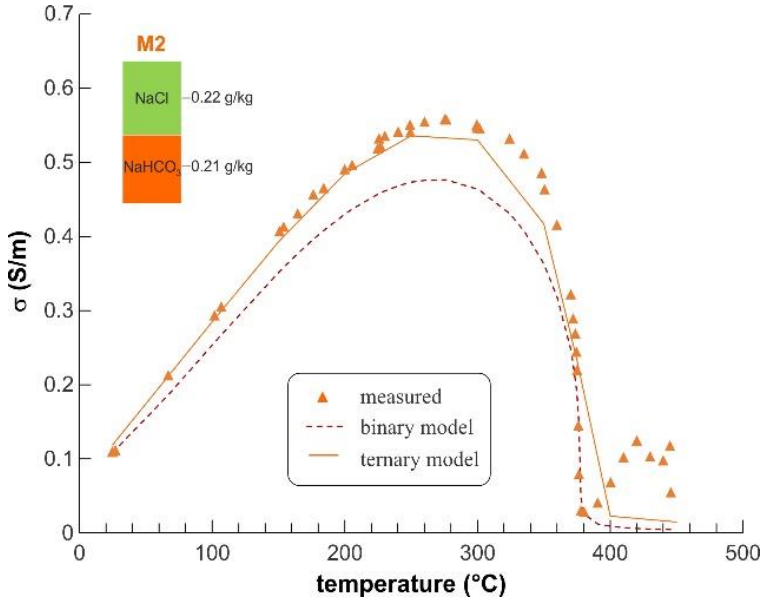

Figure 8. - Measured conductivities of an aqueous NaCl – $NaHCO_3$ mixture (symbols), fitted with the binary model function of Sinmyo and Keppler, 2017 (red dotted line) and a simple fitting model based on the summation of individual conductivities of NaCl and $NaHCO_3$ solutions, calculated from limiting conductivities of the components and their respective molar concentration (orange line/ this study).

More detailed information on the

4 TASK 2.4.3 - MODELLING OF DENSITY AND HEAT CAPACITY

4.1 A thermodynamic model for brines

The physicochemical properties of geothermal fluids (such as density, viscosity, heat capacity) are of interest due to their impact on the exploitation of the geothermal sites. It is therefore crucial to have robust thermodynamic models able to simulate the properties of these hot aqueous brines.

In this context, the work presented hereafter focuses on aqueous brines that are mainly of NaCl or $CaCl_2$-type. Existing models are able to simulate mineral solubility and heat capacity up to 200 °C and halite solubility in NaCl-H_2O systems, but this is not the case for $CaCl_2$-type waters, especially at high salinity and temperature.

To this end, a new thermodynamic model for the H-Li-Na-K-Ca-Mg-Cl-H_2O chemical system was developed, which is applicable from dilute solutions up to the salt solubility limit, and for temperatures up to 250 °C. This model relies on the Helgeson-Kirkham-Flowers (HKF) and the Pitzer equations. It takes the aqueous speciation of the $CaCl_2$ electrolyte into account, according to the partial molar properties of the Ca^{2+}, $CaCl^+$, $CaCl_2^0$ and Cl^- aqueous species described by the HKF theory.

The new model applies to the binary $CaCl_2$ aqueous systems (up to 250 °C), but also to ternary systems containing other major alkaline and alkaline earth cations, namely Li, Na, K and Mg, up to temperatures generally above 100 °C. The model becomes unstable when approaching the salt solubility limit for ternary systems and temperatures above 200 °C. Therefore, it needs improvements, but at this time and to our knowledge it is the only model with such capabilities

that can be used with a free geochemical code like PhreeSCALE (Lach et al., 2016; https://doi.org/10.1016/j.cageo.2016.03.016).

The model is presented in an open access published paper referenced as:

Lassin A., André L. (2023). *A revised description of the binary $CaCl_2$-H_2O chemical system up to solution-mineral equilibria and temperatures to 250°C using Pitzer equations. Extension to the multicomponent H^+-Li^+-Na^+-K^+-Mg^{2+}-Ca^{2+}//Cl^- aqueous system.* **Journal of Chemical Thermodynamics. 176, pp. 106927.** https://doi.org/10.1016/j.jct.2022.106927

The publication is attached to this report as Appendix 3.

A brief summary of the Pitzer equations

The ion specific interaction model developed by Pitzer [1,2] enables the description of the thermodynamic properties of aqueous solutions, such as the osmotic coefficient, heat capacity, density, or solute activity coefficients by deriving the excess Gibbs free energy with respect to temperature, pressure, or solute content. The basic theoretical framework of this approach relies on the expression of the excess Gibbs energy, G^{ex}, of the real aqueous solution (by comparison with the equivalent ideal solution):

$$\begin{aligned}\frac{G^{ex}}{w_w RT} = &-\frac{4IA^{\phi}}{b}\ln\left(1+bI^{\frac{1}{2}}\right)+2\sum_c\sum_a m_c m_a\left(B_{ca}+\left(\sum_c m_c z_c\right)C_{ca}\right)\\&+\sum_c\sum_{c'} m_c m_{c'}\left(2\Phi_{cc'}+\sum_a m_a\psi_{cc'a}\right)\\&+\sum_a\sum_{a'} m_a m_{a'}\left(2\Phi_{aa'}+\sum_c m_c\psi_{aa'c}\right)+\sum_n m_n^2(\lambda_{nn}+m_n\mu_{nnn})\\&+2\sum_n\sum_{n'} m_n m_{n'}\lambda_{nn'}+3\sum_n\sum_{n'} m_n^2 m_{n'}\mu_{nnn'}\\&+6\sum_n\sum_{n'}\sum_{n''} m_n m_{n'} m_{n''}\mu_{nn'n''}+2\sum_n\sum_c m_n m_c\lambda_{nc}+3\sum_n\sum_c m_n^2 m_c\mu_{nnc}\\&+2\sum_n\sum_a m_n m_a\lambda_{na}+3\sum_n\sum_a m_n^2 m_a\mu_{nna}+\sum_n\sum_c\sum_a m_n m_c m_a\zeta_{nca}\\&+\sum_n\sum_c\sum_{c'} m_n m_c m_{c'}\eta_{ncc'}+\sum_n\sum_a\sum_{a'} m_n m_a m_{a'}\eta_{naa'}\\&+6\sum_c\sum_n\sum_{n'} m_c m_n m_{n'}\mu_{cnn'}+6\sum_a\sum_n\sum_{n'} m_a m_n m_{n'}\mu_{ann'}\end{aligned} \quad \text{(A1)}$$

Where (A2)

$A^{\phi} = \frac{1}{3}\left(\frac{2\pi N_a d_w}{1000}\right)^{1/2}\left(\frac{e^2}{\varepsilon_w k_b T}\right)^{3/2}$ is the Debye-Hückel coefficient,

$I = \frac{1}{2}\sum_j z_j^2 m_j$ is the ionic strength (in mol kg^{-1}), (A3)

with z_j and m_j the electric charge and the molality of species *j*, respectively.

b is an empirical parameter with a value of 1.2; w_w is the mass of water.

The Debye-Hückel coefficient depends on the density d_w (in kg m^{-3}) and the dielectric constant ε_w (in F m^{-1}) of pure water. N_a is the Avogadro number (6.02 × 10^{23} compound mol^{-1}).

The subscripts a and a' represent anions, c and c' represent cations, and n, n' and n'' represent neutral species.

B_{ca} describes the interaction of pairs of oppositely charged ions (c and a). It is defined as an explicit function of the ionic strength by:

$$B_{ca} = \beta^0_{ca} + \beta^1_{ca} g(x_1) + \beta^2_{ca} g(x_2), \quad \text{with } x_1 = \alpha_1\sqrt{I},\ x_2 = \alpha_2\sqrt{I}, \qquad \text{(A4)}$$

$$g(x) = -2[1 - (1 + x)\mathrm{e}^{-x}]/x^2. \qquad \text{(A5)}$$

β^0_{ca}, β^1_{ca}, β^1_{ca} are the Pitzer binary interaction parameters, and α_1 = 2 for 1:2 electrolytes. In general, α_2 = 0 for 1:2 electrolytes. The term C_{ca} describes ternary short-range interactions between two cations c and one anion a, and one cation c and two anions a. It is expressed by:

$C_{ca} = \frac{C^{\phi}_{ca}}{2\sqrt{z_c z_a}}$, where C^{ϕ}_{ca} is an adjustable interaction parameter. (A6)

$\Phi_{ij}(I, \rho, T) = \theta_{ij} + {}^{E}\theta_{ij}(I, \rho, T)$, is a mixing term that accounts for like-charge ions: *i* and *j* represent either *c* and *c'*, or *a* and *a'* ions. (A7)

${}^{E}\theta_{ij}(I, \rho, T)$ accounts for the contribution of non-symmetrical electrostatic effects. It is a function of the ionic strength, the solution density and the temperature, but it is not specific to the pair of cations or of anions. On the contrary, θ_{ij} is an adjustable parameter, specific to the *i,j* ion pair.

ψ represents specific interactions between two different cations and one anion, or between one cation and two different anions. It is an adjustable parameter.

Other parameters λ, ζ, η, and μ are adjustable interaction parameters related to one neutral species, at least.

By deriving equation (A1) with respect to the mass of water, we obtain the expression of the water activity a_w, which is related to the osmotic coefficient ϕ according to:

$$\phi = -\frac{1000 \ln(a_w)}{M_w \sum_i \nu_i m_i}, \qquad \text{(A8)}$$

where M_w is the molar mass of water and ν_i is the number of ions formed by the complete dissociation of one molecule of solute *i* [3]. One has:

$$\frac{(\phi-1)}{2}\sum_i m_i = -\frac{A^\phi I^{\frac{3}{2}}}{1+bI^{\frac{1}{2}}} + \sum_c\sum_a m_c m_a\left(B_{ca}^\phi + ZC_{ca}\right) + \sum_c\sum_{c'>c} m_c m_{c'}\left(\Phi_{cc'}^\phi + \sum_a m_a\psi_{cc'a}\right)$$
$$+ \sum_a\sum_{a'>a} m_a m_{a'}\left(\Phi_{aa'}^\phi + \sum_c m_c\psi_{aa'c}\right)$$
$$+ \sum_n m_n\left(\sum_a m_a\lambda_{na} + \sum_c m_c\lambda_{nc} + \sum_c\sum_a m_c m_a\zeta_{nca}\right) + \sum_n\frac{m_n^2}{2}\left(\lambda_{nn} + m_n\mu_{nnn}\right)$$
$$+ \sum_n\sum_{n'>n} m_n m_{n'}\lambda_{nn'} + 3\sum_n m_n^2\left(\sum_c m_c\mu_{nnc} + \sum_a m_a\mu_{nna} + \sum_{n'>n} m_{n'}\mu_{nnn'}\right)$$
$$+ \sum_n m_n\left(\sum_c\sum_{c'>c} m_c m_{c'}\eta_{ncc'} + \sum_a\sum_{a'>a} m_a m_{a'}\eta_{naa'}\right)$$
$$+ 6\sum_n m_n\left(\sum_{n'>n}\sum_c m_{n'}m_c\mu_{cnn'} + \sum_{n'>n}\sum_a m_{n'}m_a\mu_{ann'} + \sum_{n'>n}\sum_{n">n'} m_{n'}m_{n"}\mu_{nn'n"}\right) \quad \textbf{(A9)}$$

With $Z = \sum_i m_i|z_i|$.

By deriving equation (A1) with respect to the number of moles of solute i in the aqueous solution, we obtain its activity coefficient γ_i, with i = M (for a cation), X (for an anion), N (for a neutral species)

$$\ln\gamma_M = z_M^2 F + \sum_a m_a\left(B_{Ma} + ZC_{Ma}\right) + \sum_c m_c\left(2\Phi_{Mc} + \sum_a m_a\psi_{Mca}\right) + \sum_a\sum_{a'>a} m_a m_{a'}\psi_{aa'M}$$
$$+ |z_M|\sum_c\sum_a m_c m_a C_{ca} + 2\sum_n m_n\lambda_{nM} + \sum_n\sum_a m_n m_a\zeta_{naM} \quad \textbf{(A10)}$$
$$+ 6\sum_n\sum_c m_n m_c\mu_{ncM} + 3\sum_n m_n^2\mu_{nnM} + 6\sum_n\sum_{n'>n} m_n m_{n'}\mu_{nn'M}$$

$$\ln\gamma_X = z_X^2 F + \sum_c m_c\left(B_{Xc} + ZC_{Xc}\right) + \sum_a m_a\left(2\Phi_{aX} + \sum_c m_c\psi_{caX}\right) + \sum_c\sum_{c'>c} m_c m_{c'}\psi_{cc'X}$$
$$+ |z_X|\sum_c\sum_a m_c m_a C_{ca} + 2\sum_n m_n\lambda_{nX} + \sum_n\sum_c m_n m_c\zeta_{ncX} + 6\sum_n\sum_a m_n m_a\mu_{naX} \quad \textbf{(A11)}$$
$$+ 3\sum_n m_n^2\mu_{nnX} + 6\sum_n\sum_{n'>n} m_n m_{n'}\mu_{nn'X}$$

$$\ln\gamma_N = 2\sum_c m_c\lambda_{Nc} + 2\sum_a m_a\lambda_{Na} + 2\sum_n m_n\lambda_{Nn} + \sum_c\sum_a m_c m_a\zeta_{Nca} + 6\sum_n\sum_c m_n m_c\mu_{Nnc}$$
$$+ 6\sum_n\sum_a m_n m_a\mu_{Nna} + 6\sum_c\sum_{c'>c} m_c m_{c'}\mu_{Ncc'} + 6\sum_a\sum_{a'>a} m_a m_{a'}\mu_{Naa'} \quad \textbf{(A12)}$$
$$+ 3\sum_n m_n^2\mu_{Nnn} + 6\sum_{n\neq N} m_N m_n\mu_{NNn} + 6\sum_{n\neq N}\sum_{n'\neq N} m_n m_{n'}\mu_{Nnn'}$$

$$F = \frac{f'(I)}{2} + \sum_c \sum_a m_c m_a B'_{Nca} + \sum_c \sum_{c'>c} m_c m_{c'} \Phi'_{cc'} + \sum_a \sum_{a'>a} m_a m_{a'} \Phi'_{aa'} \quad \textbf{(A13)}$$

$$f'(I) = \left(\frac{\partial f}{dI}\right)_{\rho,T} = -2A^{\phi}\left(\frac{\sqrt{I}}{1+b\sqrt{I}} + \frac{2}{b}\ln(1+b\sqrt{I})\right) \quad \textbf{(A14)}$$

$$B^{\phi}_{ca} = \beta^0_{ca} + \beta^1_{ca} e^{-\alpha_1\sqrt{I}} + \beta^2_{ca} e^{-\alpha_2\sqrt{I}} \quad \textbf{(A15)}$$

$$B'_{ca} = \left(\frac{\partial B_{ca}}{dI}\right)_{\rho,T} = -\left[\frac{\alpha_1\beta^1_{ca} g'(\alpha_1\sqrt{I}) + \alpha_2\beta^2_{ca} g'(\alpha_2\sqrt{I})}{\sqrt{I}}\right], \text{ after (A4)} \quad \textbf{(A16)}$$

$$g'(x) = \frac{dg}{dx} = -\frac{4}{x^3}\left(1 - \left(1 + x + \frac{x^2}{2}\right)e^{-x}\right), \text{ after (A5)} \quad \textbf{(A17)}$$

General description of model development

A - Numerical simulation tools and initial results

The geochemical calculation code used in the present work is PhreeSCALE [4,5], which is an evolution of PhreeqC [6], software that is widely used in the geochemical modelling community. The Pitzer equations implemented in these two calculation codes can handle partial dissociation of electrolytes but are limited to ionic strength-dependent second-order virial contributions. Compared to PhreeqC, PhreeSCALE includes a more rigorous treatment of the partial derivatives of the Pitzer equations for the excess Gibbs free energy of solutes in order to compute consistent thermal and volumetric properties of aqueous solutions. Therefore, the set of interaction parameters corresponding to model (*iii)* of Sterner et al. [7] was implemented in the thermodynamic database associated with the PhreeSCALE software. Before developing a new set of interaction parameters from the $CaCl_2$-H_2O binary system, the objective was to test model (III) of Sterner et al. [7], which is *a priori* compatible with the PhreeSCALE calculation code. The results plotted in Figure 9 illustrate that the calculated osmotic coefficient values of $CaCl_2$ aqueous solution match the values recommended by Pitzer and Oakes [8] for concentrations below 7 M $CaCl_2$ only. Although Sterner et al. [7] could describe the osmotic coefficient for higher concentrations with their model, important discrepancies can be noticed between our calculated values and the recommended ones. Given the discrepancies observed at high concentrations (Figure 9), it was concluded that this model could not apply and that a new model was needed. Then, the introduction of other major cations (H^+, Li^+, Na^+, K^+ and Mg^{2+}) is considered to check the extension capability of the new model to multicomponent mixtures.

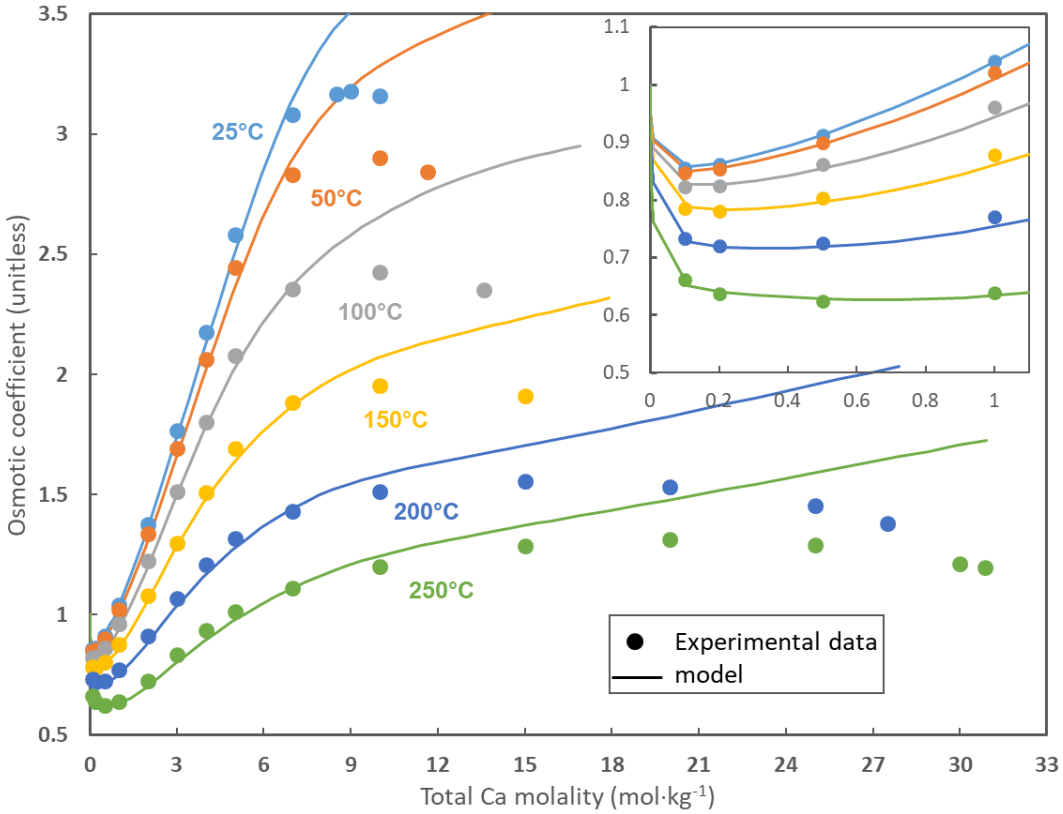

Figure 9 – Osmotic coefficient of $CaCl_2$ aqueous solutions as a function of electrolyte concentration, over the temperature range 25-250°C. Symbols represent recommended data from Pitzer and Oakes [8]; lines represent calculated values using model (iii) from Sterner et al. [7].

B - Model constraints

While Sterner et al. [7] published their thermodynamic model for the $CaCl_2$-H_2O system, Sverjensky et al. [9] proposed standard partial molar thermodynamic properties for $CaCl^+$ and $CaCl_2^0$ aqueous species and the associated formation constant, according to the following reactions:

$$Ca^{2+} + Cl^- = CaCl^+ \quad \text{and} \quad Ca^{2+} + 2\ Cl^- = CaCl_2^0.$$

The temperature functions of the formation constant of these aqueous species significantly differ from the estimations made by Sterner et al. [7] (see also Appendix 3). More specifically, the formation constants proposed by Sverjensky et al. [9] represent a much greater stability of the aqueous complexes, and of $CaCl_2^0$ in particular, compared to those estimated by Sterner et al. [7]. Recent determinations of the formation constant of the $CaCl^+$ aqueous species [10] confirm the values of Sverjensky et al. [9]. For the sake of thermodynamic consistency, it was thus necessary to include the formation constants of Sverjensky et al. [9] in the adjustment procedure of the new set of Pitzer interaction parameters. Given the very large differences between the formation constants proposed by Sterner et al. [7] and Sverjensky et al. [9], the new set of Pitzer interaction parameters is also expected to strongly differ from that of Sterner et al. [7].

In addition to the osmotic coefficient data recommended by Pitzer and Oakes [8], experimental osmotic coefficient data [11–13], as well as thermal properties of $CaCl_2$ aqueous solutions [14,15], were taken from the literature. With the exception of the hygroscopic

measurements made at 25°C by Azougen et al. [11], the above data do not cover the whole concentration range, from very low values to saturation with respect to the solid salts. Therefore, considering such data in the optimization procedure would result in an imbalance in the weight distribution of the observable data and thus complicate the process rather than helping it. Consequently, these new data were used for final verification of the model, only.

C - Parameter estimation procedure

The parameter optimization procedure [16] relies on the combined used of PhreeSCALE for calculating the osmotic coefficients of aqueous solutions of given composition and temperature, and on the PEST code [17]. The latter proposes values for the set of parameters to estimate and calls PhreeSCALE to run the model. The osmotic coefficients calculated with this set of parameters are then compared to the recommended observable data. If the resulting error is smaller than a predefined convergence criterion, the estimation procedure stops. If the error is greater than the convergence criterion, PEST proposes new parameter values to PhreeSCALE. The process runs until the convergence criterion is met, or a given number of iterations is reached. The convergence criterion is a minimal value of the standard error as defined by Christov and Møller [18]. In the present work, it is calculated for solution properties and salt solution equilibria (see Appendix 5). The solution properties are the osmotic coefficient and mean activity coefficient of HCl in the HCl-$CaCl_2$-H_2O ternary system (the only available activity coefficient data related to our study). Salt solution equilibria are studied on the basis of saturation index calculations, i.e. log (IAP/K), where IAP is the ionic activity product for the considered dissolution reaction, and K is the related solubility product. The philosophy of the parameter optimization procedure is to find the best compromise between a minimized number of interaction parameters and a good overall accordance of the model calculations with the experimental data. This means that several combinations of interaction parameters were tested, and only the set of interaction parameters that gave the best results are reported here. We also note that the "binary" chemical system is actually composed of 4 aqueous species: 2 cations (Ca^{2+}, $CaCl^+$), 1 anion (Cl^-) and 1 neutral species ($CaCl_2^0$), and thus represents an equivalent combination of 3 ternary systems: Ca^{2+}/$CaCl^+$/Cl^-, Ca^{2+}/Cl^-/$CaCl_2^0$, and $CaCl^+$/Cl^-/$CaCl_2^0$. In principle, the following interaction parameters are required to describe the chemical behavior of each ternary system:

- $\beta^{(0)}_{Ca^{2+}/Cl^-}$, $\beta^{(1)}_{Ca^{2+}/Cl^-}$, $C^{\phi}_{Ca^{2+}/Cl^-}$, $\beta^{(0)}_{CaCl^+/Cl^-}$, $\beta^{(1)}_{CaCl^+/Cl^-}$, $C^{\phi}_{CaCl^+/Cl^-}$, $\theta_{Ca^{2+}/CaCl^+}$, and $\psi_{Ca^{2+}/CaCl^+/Cl^-}$ for the Ca^{2+}/$CaCl^+$/Cl^- system;
- $\beta^{(0)}_{Ca^{2+}/Cl^-}$, $\beta^{(1)}_{Ca^{2+}/Cl^-}$, $C^{\phi}_{Ca^{2+}/Cl^-}$, $\lambda_{Ca^{2+}/CaCl_2^0}$, $\lambda_{Cl^-/CaCl_2^0}$, $\zeta_{Ca^{2+}/Cl^-/CaCl_2^0}$, $\mu_{Ca^{2+}/CaCl_2^0/CaCl_2^0}$, $\mu_{Cl^-/CaCl_2^0/CaCl_2^0}$, and $\mu_{CaCl_2^0/CaCl_2^0/CaCl_2^0}$ for the Ca^{2+}/Cl^-/$CaCl_2^0$ system;
- $\beta^{(0)}_{CaCl^+/Cl^-}$, $\beta^{(1)}_{CaCl^+/Cl^-}$, $C^{\phi}_{CaCl^+/Cl^-}$, $\lambda_{CaCl^+/CaCl_2^0}$, $\lambda_{Cl^-/CaCl_2^0}$, $\zeta_{CaCl^+/Cl^-/CaCl_2^0}$, $\mu_{CaCl^+/CaCl_2^0/CaCl_2^0}$, $\mu_{Cl^-/CaCl_2^0/CaCl_2^0}$, and $\mu_{CaCl_2^0/CaCl_2^0/CaCl_2^0}$ for the Ca^{2+}/Cl^-/$CaCl_2^0$ system;
- And finally, $\eta_{Ca^{2+}/CaCl^+/CaCl_2^0}$ for the full Ca^{2+}/$CaCl^+$/Cl^-/$CaCl_2^0$ system.

Thus, it was expected that up to 18 interaction parameters could be necessary to describe the whole system. In addition, the relative amount of each constituent varies with the total electrolyte concentration, which adds complexity to the optimization process as the concentration range within which a given interaction parameter plays a significant role on the excess Gibbs energy and its derivatives cannot be clearly defined.

Comparison of the thermodynamic functions for the formation reactions of the aqueous complexes $CaCl^+$ and $CaCl_2^0$

The thermodynamic functions for the formation reactions of the aqueous complexes $CaCl^+$ and $CaCl_2^0$ are plotted against temperature in Figure 10. For comparison, the experimental values from various sources cited in [10] for the formation of the $CaCl^+$ complex are also plotted. Despite the observed discrepancies with the experimental data, the thermodynamic function proposed by Sverjensky et al. [9] for $CaCl^+$ appears superior to that of Sterner et al. [7].
It could be argued that a new temperature function, more consistent with the experimental values, could have been used in this work. But, for the sake of consistency with the temperature function proposed by Sverjensky et al. [9] for the formation of $CaCl_2^0$, it was decided to use also the temperature function proposed by these authors for the formation of $CaCl^+$.

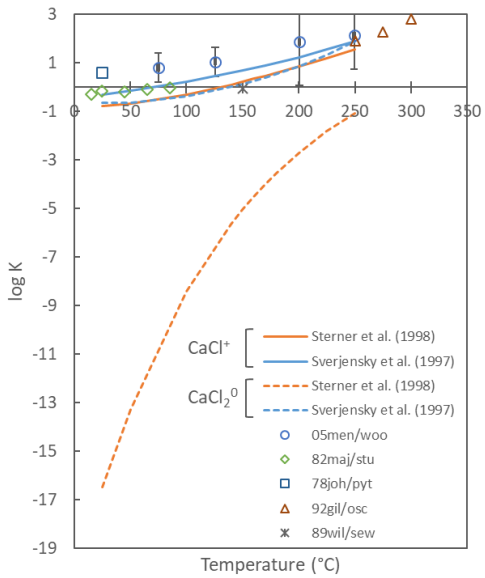

Figure 10 – Reaction constants K for the formation of the $CaCl^+$ and $CaCl_2^0$ aqueous species from Ca^{2+} and Cl^- as a function of temperature.

Sources cited in [10] for the formation constant of $CaCl^+$:
82maj/stu: [19]; 78joh/pyt: [20]; 92gil/osc: [21]; 89wil/sew: [22]

The identification of different solutes for the $CaCl_2$-H_2O system directly addresses the question of their distribution within the aqueous solution, depending on the total electrolyte concentration and on the temperature.
No experimental data could be found in the literature for the range of concentrations and temperatures considered in this work. Therefore, only the calculated aqueous speciation resulting from the model (Figure 11) is shown. It indicates the predominance of the Ca^{2+} (and Cl^-) aqueous species at low to moderate concentrations (*i.e.*, never above 9 M of total $CaCl_2$), mostly at low temperatures (below 150°C). Ca^{2+} is progressively replaced by $CaCl^+$, which

remains the predominant species over the whole range of concentrations and temperatures. This replacement occurs at lower concentrations as temperature increases.

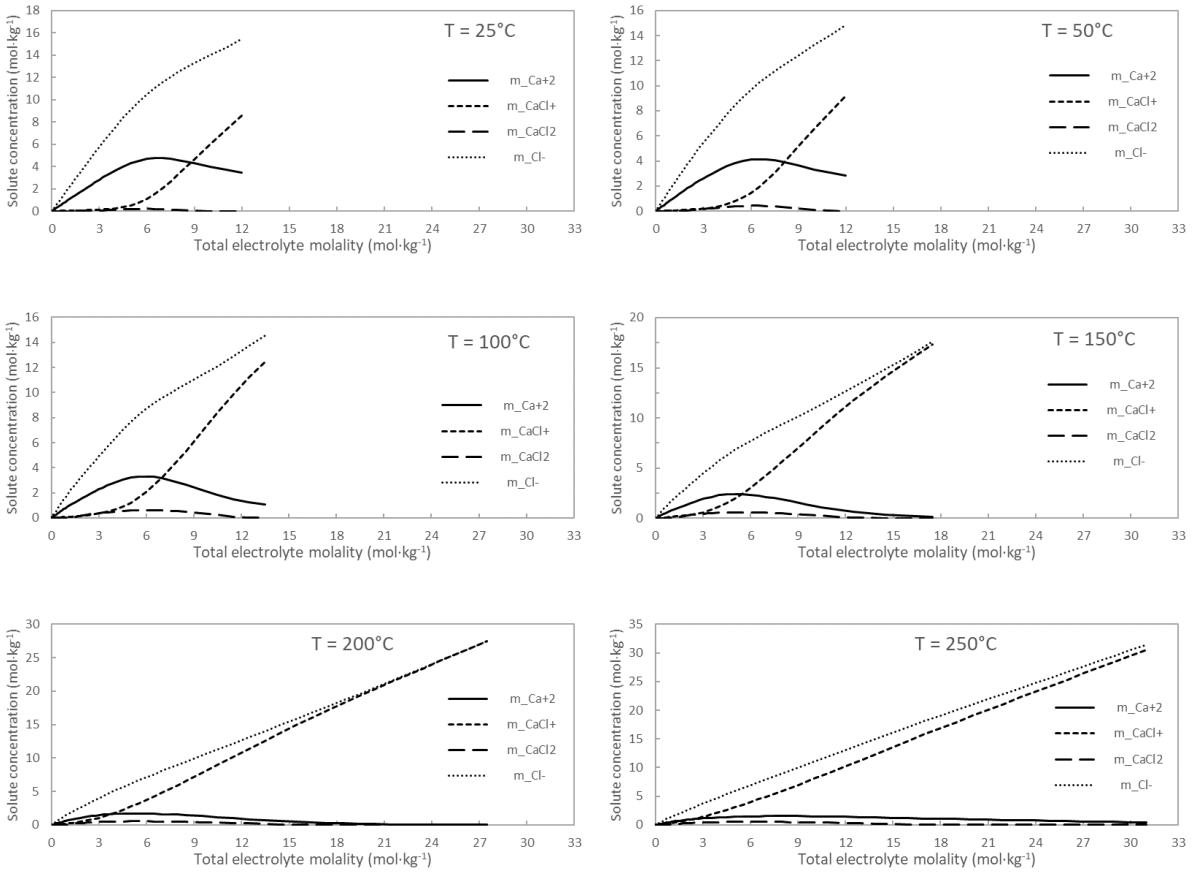

Figure 11 – Aqueous speciation of $CaCl_2$ aqueous solutions as a function of electrolyte concentration at various temperatures.

With this model, the $CaCl_2^0$ species always remains in the minority, which may explain its relative instability at the highest concentrations and temperatures. Given these low concentrations in $CaCl_2^0$, it could be envisaged to eliminate this species from the model. However, because one objective of this work was to combine consistently the HKF theory with the Pitzer equations, it was decided to keep the $CaCl_2^0$ species in the model.

Water vapor pressure above solutions saturated with CaCl2 salts vs. temperature

Comparing the calculated vapor pressure against the measured value along the salt-solution saturation curves [23] provides an additional criterion to check the quality of the model. In the case of the $CaCl_2$-H_2O chemical system, Li et al. [24] collected water vapor pressure data from the literature over a large range of temperatures. In Figure 12, the graphical comparison between the results of the model and the experimental data demonstrates once again the quality of the model in its temperature range of validity. In particular, the transition points between the different hydrates and the distinction between the polymorphs of the tetra-hydrate are well described (Figure 12-B).

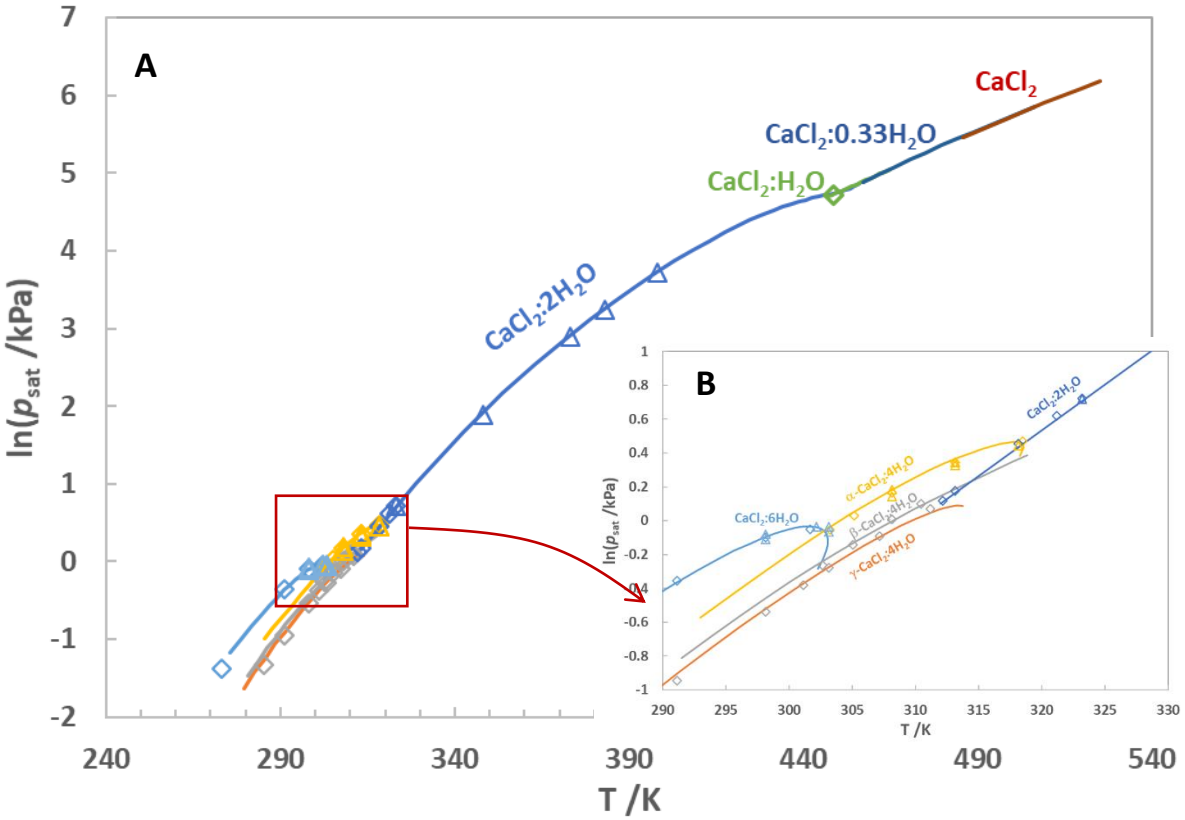

Figure 12 – Water vapor pressure above solutions saturated with $CaCl_2$ salts vs. temperature, A) over the whole temperature range (240-540K), and B) with a focus on the 298-325 K region where most hydrate transitions occur. Symbols represent experimental literature data (diamonds: [25]; triangles: [26]) and colored lines represent the model calculations (this work).

Calculated deviation for each binary and ternary system according to temperature conditions

Chemical system	Temperature (K)	$\sigma^{\$}$	N^{*}
Binary $CaCl_2$-H_2O	298.15	σ_Φ = 0.00942 (0.02448[§])	30
		σ_{cp} = 4.63877 (4.66758[§])	38
	323.15	σ_Φ = 0.04056	11
		σ_{cp} = 0.25677	9
	373.15	σ_Φ = 0.05331	11
	413.15	σ_Φ = 0.02252	17
	423.15	σ_Φ = 0.04449	11
	433.15	σ_Φ = 0.01651	17
	443.92	σ_Φ = 0.02170	36
	453.15	σ_Φ = 0.01074	15
	473.15	σ_Φ = 0.00753	74
	498.15	σ_Φ = 0.13913	79
	523.15	σ_Φ = 0.01227	92
Antarcticite	231 - 303	σ_s = 0.16939	34[#]
α-$CaCl_2.4H_2O$	285 - 318	σ_s = 0.01599	25[#]

β-$CaCl_2.4H_2O$	283 - 313	σ_s = 0.01409	20[#]
γ-$CaCl_2.4H_2O$	291 - 311	σ_s = 0.10917	17[#]
$CaCl_2.2H_2O$	263 - 453	σ_s = 0.01181	33[#]
$CaCl_2.H_2O$	446 - 463	σ_s = 0.00148	13[#]
$CaCl_2.0.33H_2O$	430 - 506	σ_s = 0.00636	18[#]
$CaCl_2$	485 - 538	σ_s = 0.02038	5[#]
Ternary HCl-$CaCl_2$-H_2O	298.15	σ_γ = 0.00435 (0.00222[§])	30
Ternary LiCl-$CaCl_2$-H_2O	298.15	σ_Φ = 0.11079 (0.11080[§])	161
Ternary $MgCl_2$-$CaCl_2$-H_2O	298.15	σ_Φ = 0.04965 (0.04981[§])	179
		σ_{cp} = 0.32352 (0.32351[§])	18
	323.15	σ_Φ = 0.05599	22
		σ_{cp} = 0.29637	18
	348.15	σ_{cp} = 0.27915	18
	373.15	σ_{cp} = 0.26745	18

[$] $\sigma_\Phi = \sqrt{\frac{\sum(\Phi^{exp}-\Phi^{calc})^2}{N}}$, deviation calculated for the osmotic coefficient; $\sigma_{cp} = \sqrt{\frac{\sum(c_p^{exp}-c_p^{calc})^2}{N}}$, deviation calculated for the heat capacity of the solution; $\sigma_s = \sqrt{\frac{\sum(\log IAP-\log K)^2}{N}}$, deviation calculated from saturation indices for salt-solution equilibria; $\sigma_\gamma = \sqrt{\frac{\sum\left(\log\left(\gamma_{HCl}^{\pm}\right)^{exp}-\log\left(\gamma_{HCl}^{\pm}\right)^{calc}\right)^2}{N}}$, deviation calculated for the mean activity coefficient of HCl

[*] Number of experimental data used for deviation calculations (and parameterization).

[§] Deviation calculated according to parameterization published by Lassin et al. [27]

[#] Values recommended by Pátek et al. [28]

Chemical system	Temperature (K)	Solid phase	σ[$]	N[*]
Ternary NaCl-$CaCl_2$-H_2O	291.15	Halite	σ_s = 0.09588	10
		Antarcticite	σ_s = 0.03347	4
	298.15	Halite	σ_s = 0.16983 (0.17787[§])	23
		Antarcticite	σ_s = 0.03249 (0.02735[§])	6
	313.15	Halite	σ_s = 0.29423	13
		α-$CaCl_2.4H_2O$	σ_s = 0.05480	3
	323.15	Halite	σ_s = 0.17640	31
		$CaCl_2.2H_2O$	σ_s = 0.03391	9
	348.15	Halite	σ_s = 0.11172	13
		$CaCl_2.2H_2O$	σ_s = 0.07620	2
	368.15-373.15	Halite	σ_s = 0.06153	35
		$CaCl_2.2H_2O$	σ_s = 0.05341	9
	398.15-303.15	Halite	σ_s = 0.06168	17
		$CaCl_2.2H_2O$	σ_s = 0.02426	4
Ternary HCl-$CaCl_2$-H_2O	298.15	Antarcticite	σ_s = 0.01811 (0.02242[§])	10
		α-$CaCl_2.4H_2O$	σ_s = 0.02318 (0.01425[§])	23
		β-$CaCl_2.4H_2O$	σ_s = 0.15553	6
		$CaCl_2.2H_2O$	σ_s = 0.01730 (0.02468[§])	9
Ternary KCl- $CaCl_2$-H_2O	298.15	Sylvite	σ_s = 0.03736 (0.03497[§])	11
		Antarcticite	σ_s = 0.02111 (0.01940[§])	5
	303.15	Sylvite	σ_s = 0.03572	24

		α-$CaCl_2.4H_2O$	σ_s = 0.02648	10
	308.15	Sylvite	σ_s = 0.05244	31
		α-$CaCl_2$:$4H_2O$	σ_s = 0.03690	7
	313.15 – 318.15	Sylvite	σ_s = 0.05585	20
		α-$CaCl_2.4H_2O$	σ_s = 0.04796	8
		$CaCl_2.2H_2O$	σ_s = 0.21453	6
	323.15 – 328.15	Sylvite	σ_s = 0.06649	33
		$CaCl_2.2H_2O$	σ_s = 0.05341	9
		$KCl.CaCl_2.2H_2O$	σ_s = 0.04245	12
	348.15	Sylvite	σ_s = 0.08566	24
		$CaCl_2$:$2H_2O$	σ_s = 0.19424	9
		KCl :$CaCl_2$:$2H_2O$	σ_s = 0.03619	12
	368.15 – 373.15	Sylvite	σ_s = 0.13768	25
		$CaCl_2.2H_2O$	σ_s = 0.05764	8
		$KCl.CaCl_2.2H_2O$	σ_s = 0.03977	3
		$KCl.CaCl_2$	σ_s = 0.11713	12
	423.15	Sylvite	σ_s = 0.03650	7
		$CaCl_2.2H_2O$	σ_s = 0.02932	2
		$KCl.CaCl_2$	σ_s = 0.07800	4
	473.15	Sylvite	σ_s = 0.01215	5
		$CaCl_2.H_2O$	σ_s = 0.07935	2
		$KCl.CaCl_2$	σ_s = 0.18351	6
	523.15	Sylvite	σ_s = 0.15626	3
		$CaCl_2.H_2O$	σ_s = 0.13229	1
		$KCl.CaCl_2$	σ_s = 0.57261	6
Ternary LiCl- $CaCl_2$-H_2O	273.15	$LiCl.2H_2O$	σ_s = 0.01133	5
		$LiCl.CaCl_2.5H_2O$	σ_s = 0.01845	4
		α-$CaCl_2.4H_2O$	σ_s = 0.02358	4
		Antarcticite	σ_s = 0.04927	10
	283.15	$LiCl.H_2O$	σ_s = 0.08711	6
		$LiCl.CaCl_2.5H_2O$	σ_s = 0.01841	7
		α-$CaCl_2.4H_2O$	σ_s = 0.02278	6
		Antarcticite	σ_s = 0.01479	9
	298.15	$LiCl.H_2O$	σ_s = 0.03903 (0.03344[§])	13
		$LiCl.CaCl_2.5H_2O$	σ_s = 0.01520 (0.03436[§])	9
		α-$CaCl_2.4H_2O$	σ_s = 0.02313 (0.01686[§])	15
		Antarcticite	σ_s = 0.02392 (0.01381[§])	9
	313.15	$LiCl.H_2O$	σ_s = 0.01749	6
		α-$CaCl_2.4H_2O$	σ_s = 0.07989	3
		$CaCl_2.2H_2O$	σ_s = 0.04513	7
	323.15	$LiCl.H_2O$	σ_s = 0.00833	6
		$CaCl_2.2H_2O$	σ_s = 0.02545	8
Ternary $MgCl_2$-$CaCl_2$-H_2O	298.15	Antarcticite	σ_s = 0.00470 (0.00902[§])	18
		α-$CaCl_2.4H_2O$	σ_s = 0.04667 (0.03907[§])	9
		Tachyhydrite	σ_s = 0.07569 (0.08376[§])	16
		Bischofite	σ_s = 0.04689 (0.03892[§])	13
	308.15	α-$CaCl_2.4H_2O$	σ_s = 0.44513	4
		Tachyhydrite	σ_s = 0.04170	9

	Bischofite	σ_s = 0.01462	6
323.15	$CaCl_2.2H_2O$	σ_s = 0.02445	5
	Tachyhydrite	σ_s = 0.07380	8
	Bischofite	σ_s = 0.01813	6
348.15	$CaCl_2.2H_2O$	σ_s = 0.05962	3
	Tachyhydrite	σ_s = 0.16185	11
	Bischofite	σ_s = 0.05943	5
383.15	$CaCl_2.2H_2O$	σ_s = 0.03785	3
	Tachyhydrite	σ_s = 0.43990	7
	$2CaCl_2.MgCl_2.6H_2O$	σ_s = 0.11429	4
	Bischofite	σ_s = 0.15732	2

Calculated aqueous speciation of the $CaCl_2$ electrolyte in HCl, LiCl, NaCl and $MgCl_2$ aqueous solutions at various concentrations and temperatures (25, 50 and 100°C)

The relative proportion (mol%.) of Ca^{2+}, $CaCl^+$ and $CaCl_2^0$ aqueous species is plotted as a function of total $CaCl_2$ concentration in aqueous mixtures containing either HCl, LiCl, NaCl or $MgCl_2$ electrolytes at specified concentrations. For 1:1 electrolytes, concentrations are: 0, 1, 3, 6 mol·kg^{-1}. For $MgCl_2$, concentrations are 0, 0.5, 1.5 and 3 mol·kg^{-1} in order to consider the same Cl contents as for 1:1 electrolytes.
Each electrolyte has its own specific influence on the aqueous speciation of $CaCl_2$.

HCl solutions (0, 1, 3 and 6 mol·kg^{-1}):

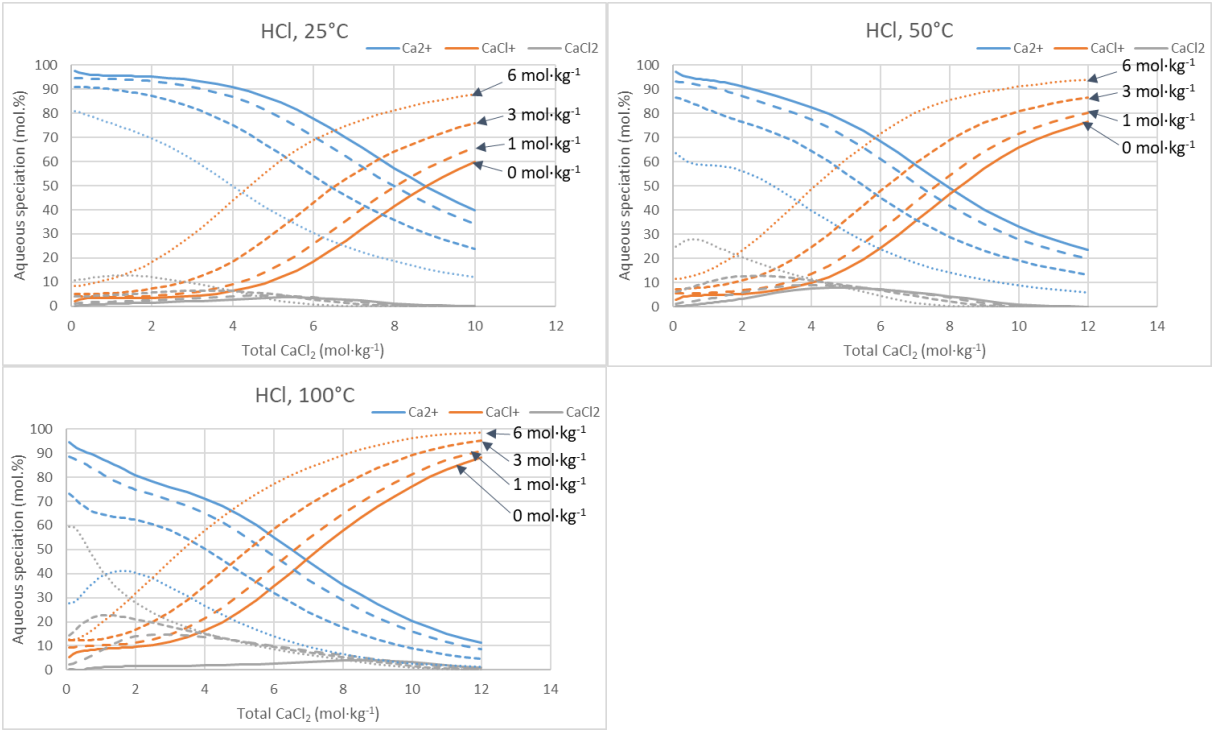

LiCl solutions (0, 1, 3 and 6 mol·kg^{-1}):

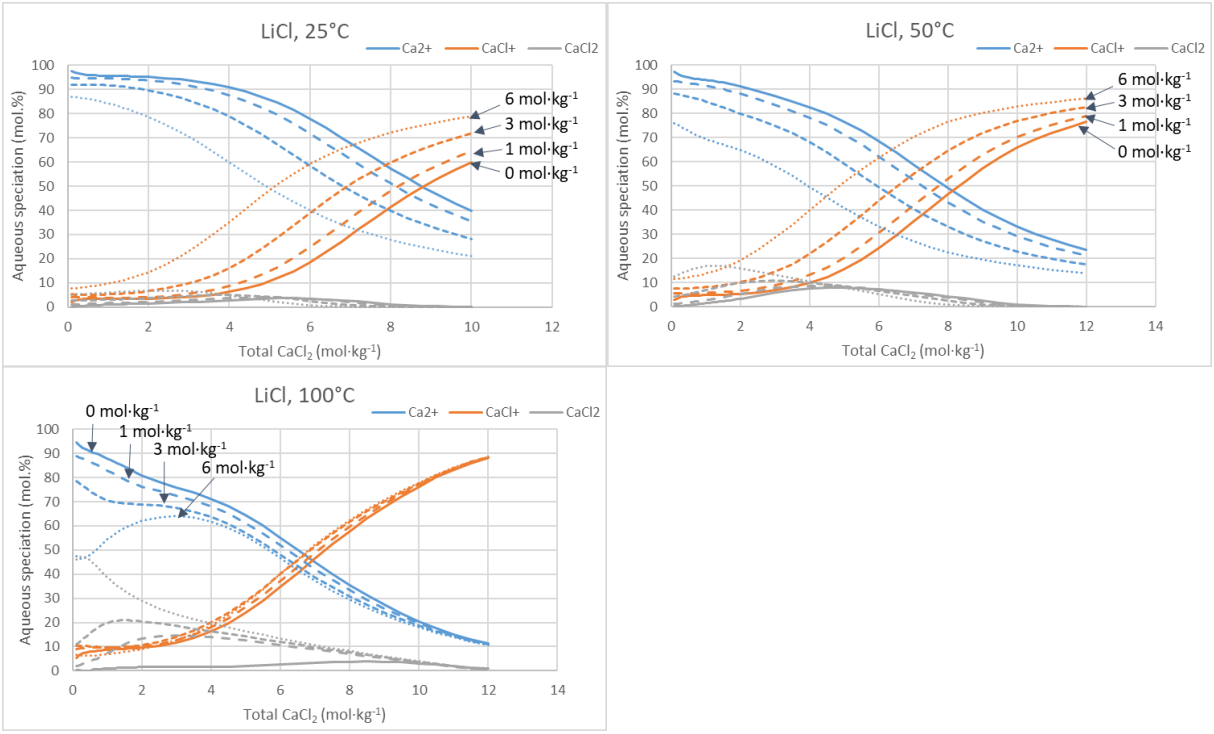

Note that the chemical model for the LiCl-H_2O system also considers partial dissociation [29], which in turn depends on the concentration of the $CaCl_2$ electrolyte:

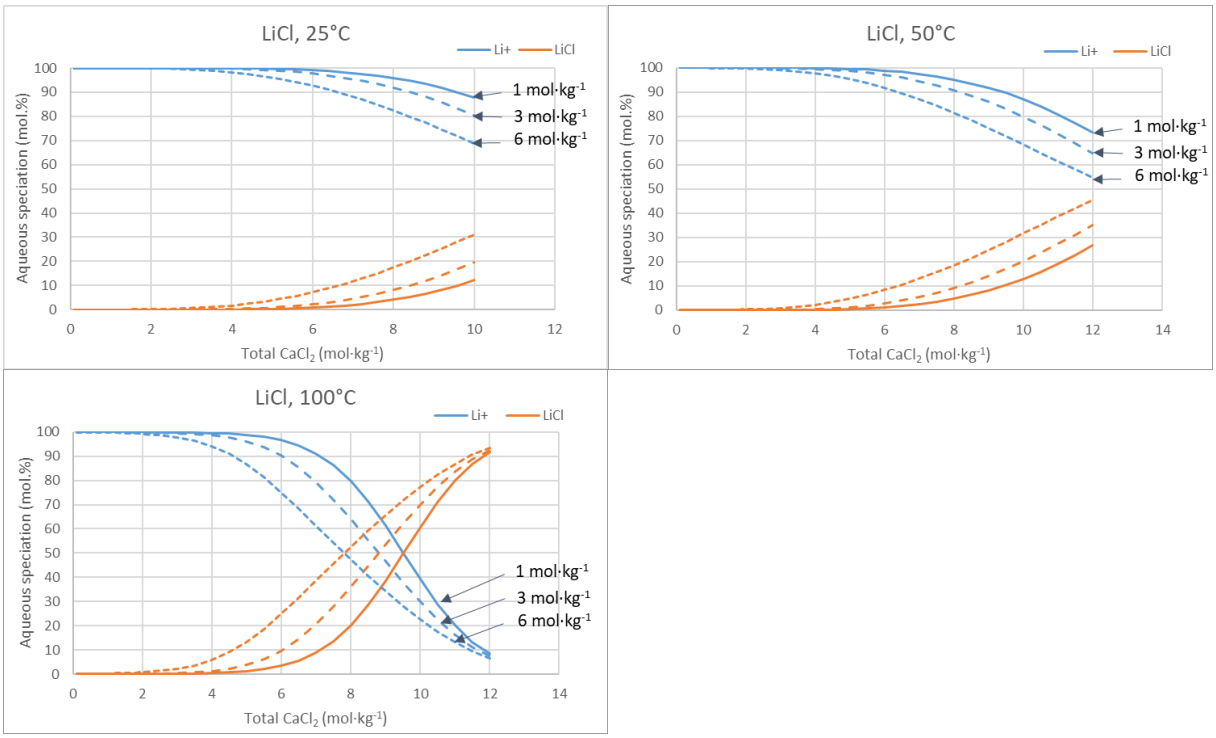

NaCl solutions (0, 1, 3 and 6 mol·kg^{-1}):

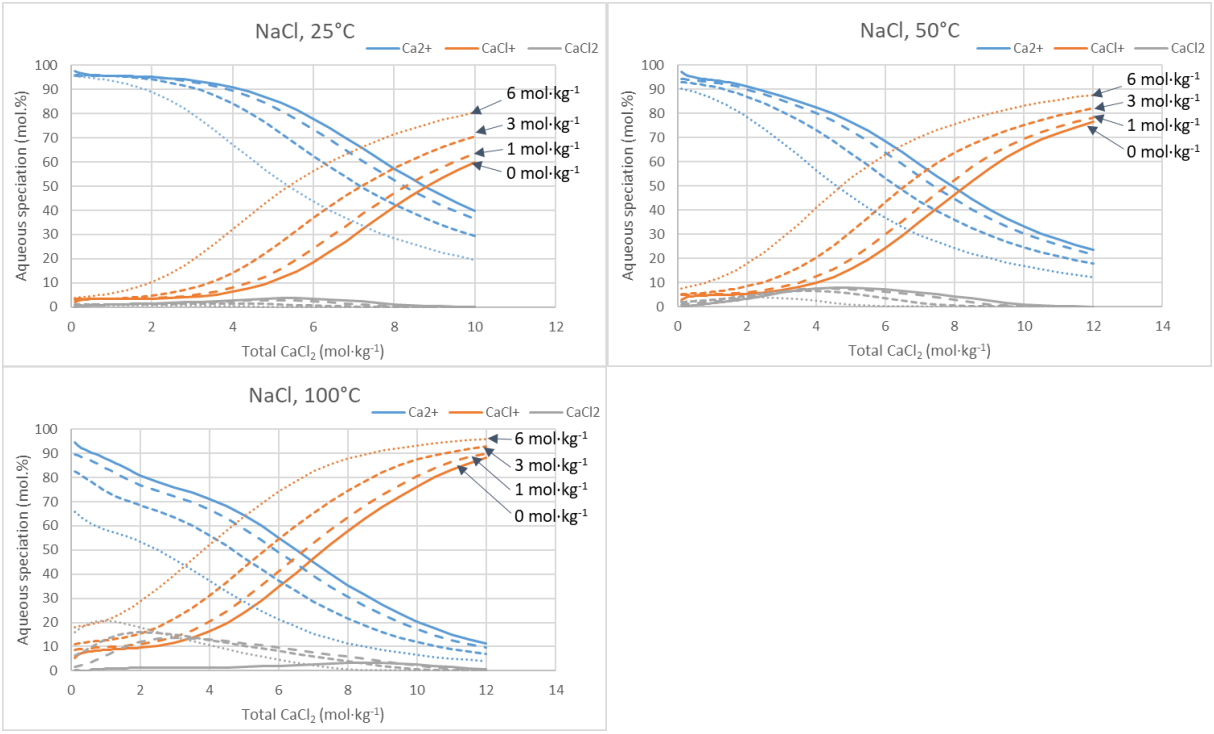

MgCl solutions (0, 0.5, 1.5 and 3 mol·kg^{-1}):

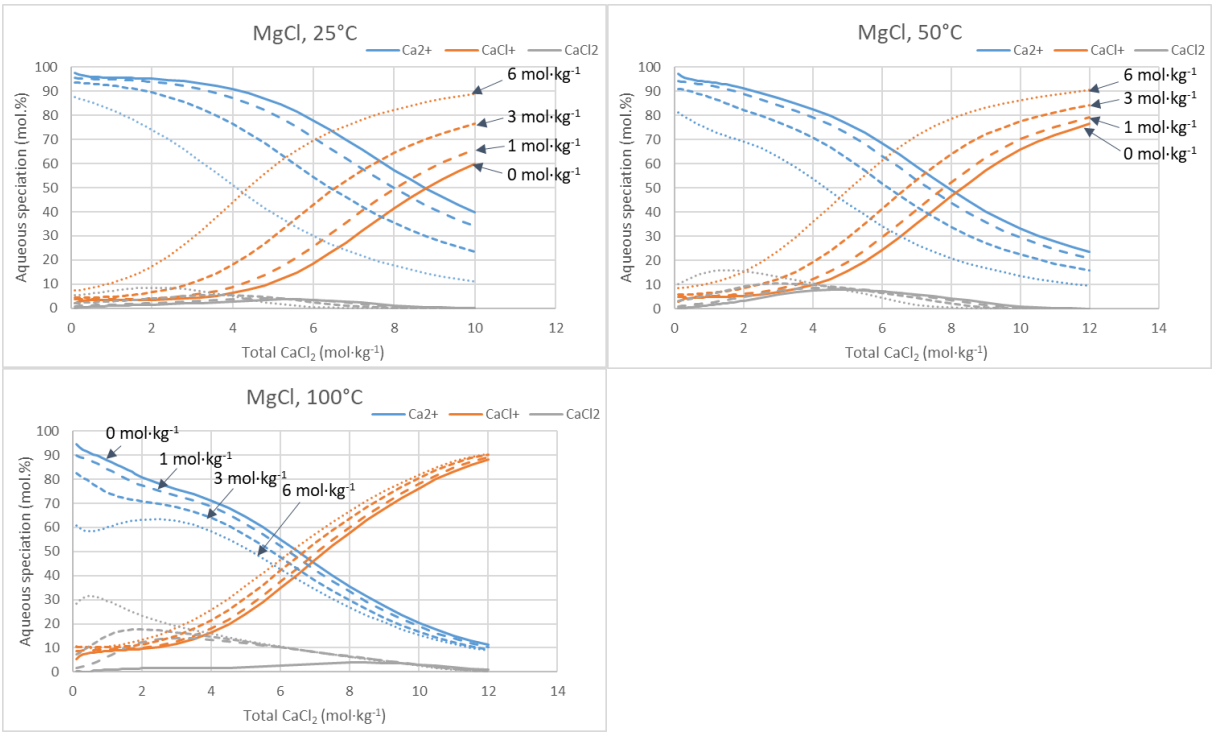

Phase diagrams and iso water activity curves in ternary aqueous mixtures at 25°C

Below are reported the figures modified from [27], according to the temperature-dependent model developed in the present study.

a- The LiCl-$CaCl_2$-H_2O system

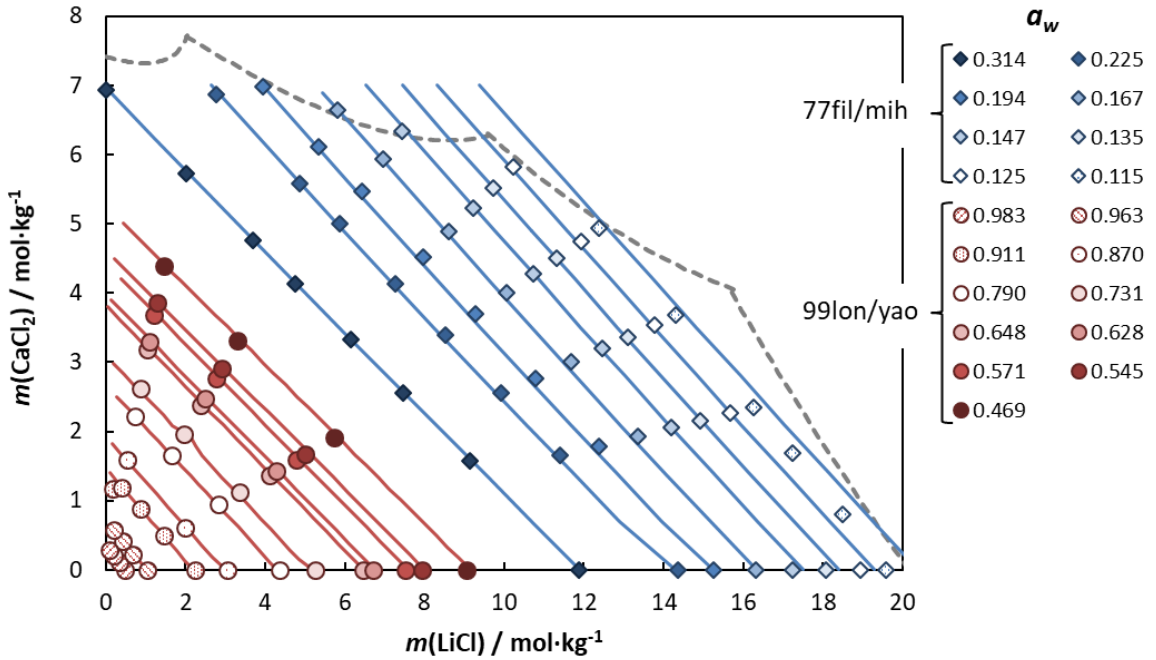

Figure 13 – Iso water activity curves in LiCl-$CaCl_2$ aqueous mixtures, at 25°C. Symbols: experimental data from [30] are represented by diamonds; those from [31] are represented by circles. The colors of the symbols are indicative of the water activity (see key). The solid lines represent the results of calculations for the same conditions. The dashed lines illustrate the solubility limits of the system.

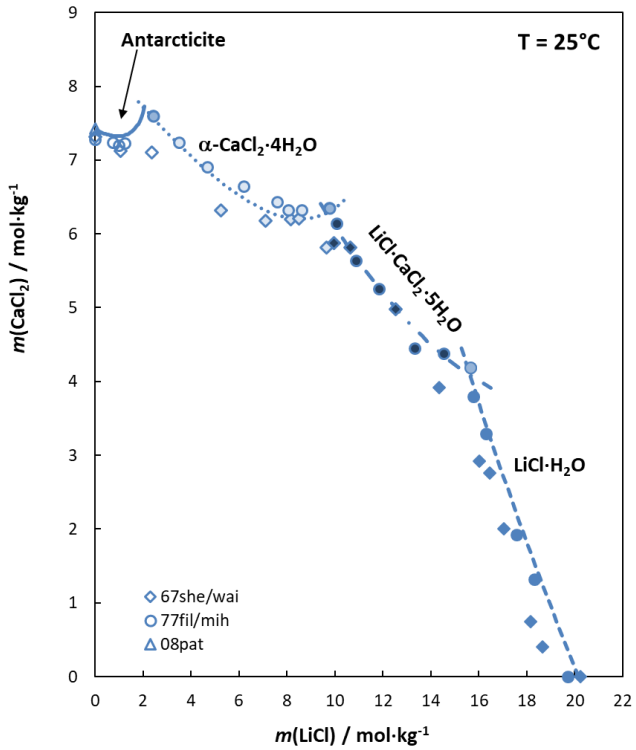

Figure 14 – Solubility diagram for the Li-Ca-Cl-H_2O system, at 25°C. Symbols: experimental data from [32] are represented by diamonds, those from [30] by circles, and the recommended antarcticite solubility of [28] by the solid black triangle (A). The solid black symbols represent antarcticite solubility; dark gray symbols represent $CaCl_2·4H_2O$ solubility; light gray symbols represent $LiCl·CaCl_2·5H_2O$ solubility; empty white symbols represent $LiCl·H_2O$ solubility. The lines represent model calculation results.

b- The NaCl-$CaCl_2$-H_2O system

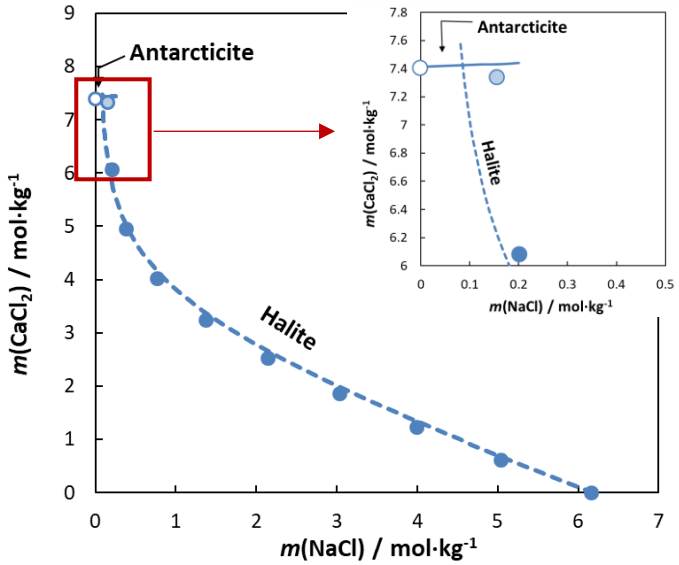

Figure 15 – Solubility diagram for the NaCl-$CaCl_2$-H_2O system, at 25°C. The symbols represent experimental data recommended by [33]. The solid black symbols represent halite solubility; the light gray symbols represent bischofite solubility. The lines represent calculation results (dashed line: halite; solid line: antarcticite).

c- The KCl-$CaCl_2$-H_2O system

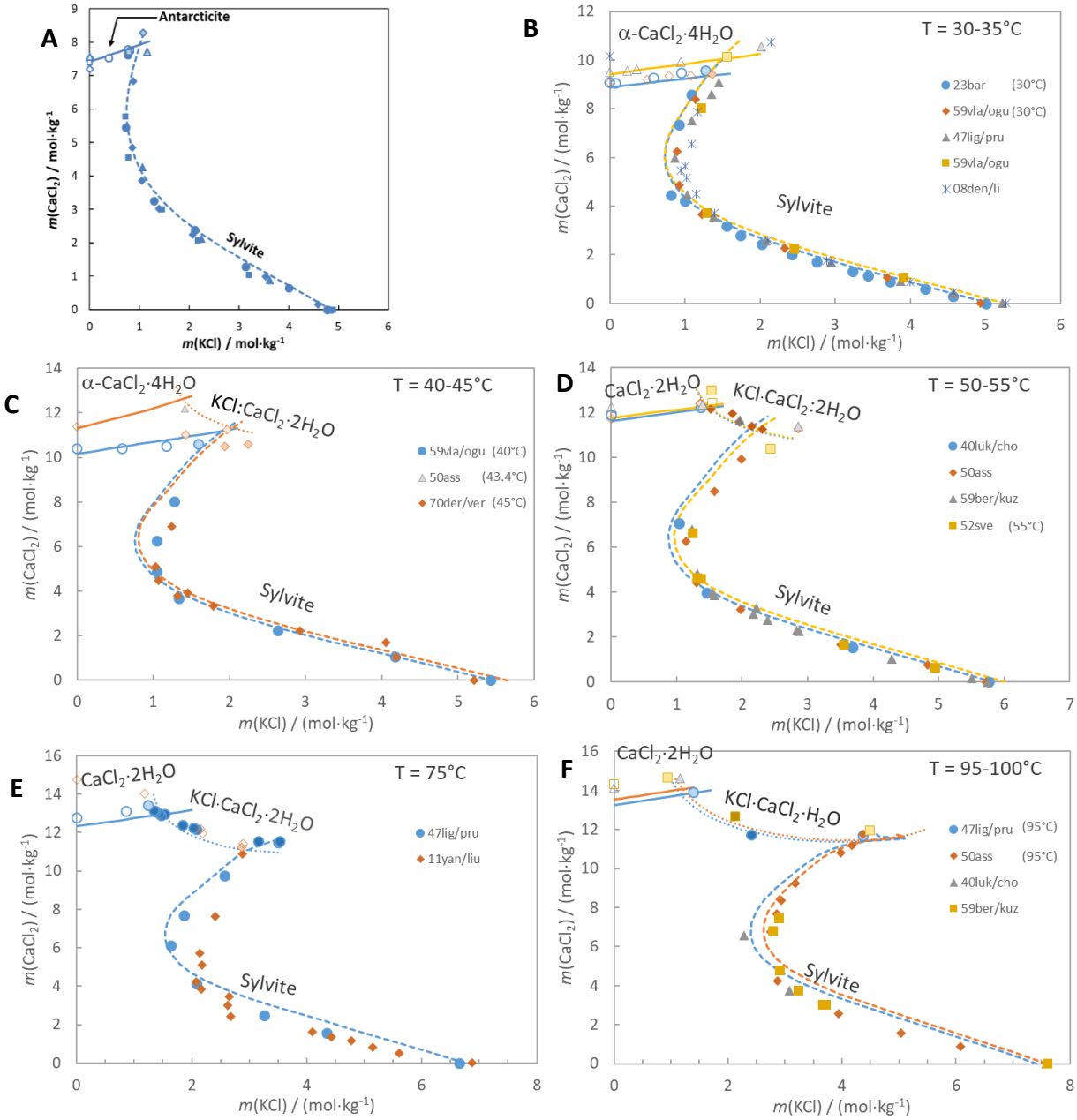

Figure 16 – Solubility diagrams for the KCl-$CaCl_2$- H_2O system, at 25°C (A): the symbols represent experimental data: diamonds, [34]; circles, [35]; triangles, [36]; squares, [37]. The solid dark blue symbols represent sylvite solubility, the empty white symbols represent antarcticite solubility, and solid light blue symbols represent the invariant points. The lines represent calculation results (dashed line: sylvite; solid line: antarcticite); at 30 and 35°C (B), 40 to 45°C (C), 50 and 55°C (D), 75°C (E), 95 and 100°C (F). For Figures B to F, symbols are experimental data collected and recommended by [33] and from [38] and solid and dashed lines are calculated values with our model.

d- The $MgCl_2$-$CaCl_2$-H_2O system

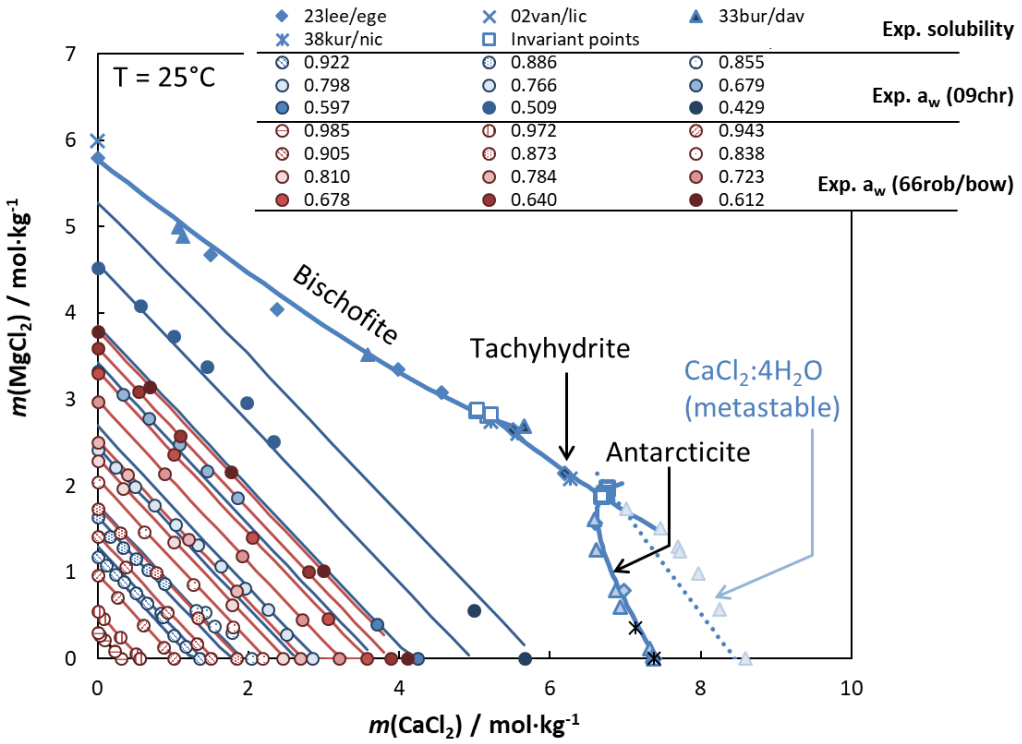

Figure 17 – Iso water activity curves in $CaCl_2$-$MgCl_2$ aqueous mixtures and solubility diagram, at 25°C. The symbols represent experimental data; the lines represent calculation results. The circles are iso-activity data representing the isopiestic measurements (in blue: [39]; in red [40]. Solubility data: diamonds, [37]; crosses, [41]; triangles, [42]; stars, [43]; empty squares, invariant points measured by the various authors. The solid blue symbols represent bischofite solubility; the dark blue symbols represent tachyhydrite solubility; the light blue symbols represent antarcticite solubility. Blue and red light lines: iso-water activity calculations. Heavy solid blue lines: calculated solubility of stable salts. Heavy doted blue line: calculated solubility of the metastable $CaCl_2 \cdot 4H_2O$ salt.

4.2 Applications of the thermodynamic model

4.2.1 CO_2 solubility in Na-Ca-Cl brines

Geothermal energy currently uses hot deep brines. The exploitation of these fluids can raise issues specifically due to their high salinity and the variations of temperature and pressure during their pumping. Among all the disorders, the potential degassing of fluids, including CO_2, are of main importance since it can trigger the precipitation of minerals in the facilities (production/injection wells, heat exchangers…) involving expensive maintenance works. To avoid these exploitation issues, geochemical modelling can help predicting the properties and the behaviour of such systems.

Following the development of the thermodynamic model presented in chapter 4.1, we investigated the solubility of CO_2 in such geochemical systems. In a first step, laboratory measurements were done to estimate the properties of saline chloride fluids (NaCl and $CaCl_2$) containing dissolved CO_2. Here we focus on CO_2 solubility for medium temperature brines up to 200°C.

In parallel to laboratory experiments, a modelling work was set-up to calculate these fluid properties, using the specific tool named PhreeSCALE (Lach et al., 2016; https://doi.org/10.1016/j.cageo.2016.03.016). The methodology relies on successive steps that include the estimation of Pitzer's interaction parameters for the binary and ternary systems and finally for the $CaCl_2$-NaCl-CO_2-H_2O systems. The model developed applies from 25°C up to 200°C.

These results were presented during the last European Geothermal Congress held in Berlin (17-21 October 2022) and are summarized in the following extended abstract referenced as:

Lassin A., Felipe dos Santos P., Ducousso M., Cézac P., André L. (2022). *Experimental measurements and modelling of thermodynamic properties of NaCl-$CaCl_2$ aqueous solutions up to high temperatures and CO_2 pressures.* **EGC 2022. Berlin. 17-21 October 2022.**

The publication is attached to this report as Appendix 4.

4.2.2 Density and heat capacity: comparison of experimental and calculated results

Thermophysical data of geothermal fluids like density or heat capacity are required for reliable geothermal site assessment and development (e.g. for exploration, well and pump design, and power plant layout). While the database for binary solutions made of water and one salt (often NaCl) is good, information for more complex and highly saline fluids (e.g. ternary solutions) is scarce.

In the first instance, GFZ performed laboratory measurements of fluid density on synthetic NaCl and $CaCl_2$ solutions. Different cation ratios were explored for total molalities up to 6 $mol \cdot kg^{-1}$. Pressure and temperature were ranging between 0.1 and 40 MPa and 20 and 80°C, respectively. An Anton Paar DMA4500M was used for density measurements at ambient pressure, whereas the DMA HP external density measuring cell measured density up to 700 bar and 200 °C (Figure 18).

Figure 18. - Density measurements. Left: Anton Paar DMA4500M for measurements at ambient pressure; right: DMA-HP.

About 700 new experimental points have been generated. First, these new data were compared with other experimental data from literature.

In the binary systems, at 25°C and 1 bar, the new acquisitions are consistent with published data. However, there are some small differences for the $CaCl_2$-H_2O system for molalities above 4 mol.kg^{-1} (Figure 19).
In the ternary system (Figure 20), at 25°C and 1 bar, the new acquisitions are consistent with literature data.

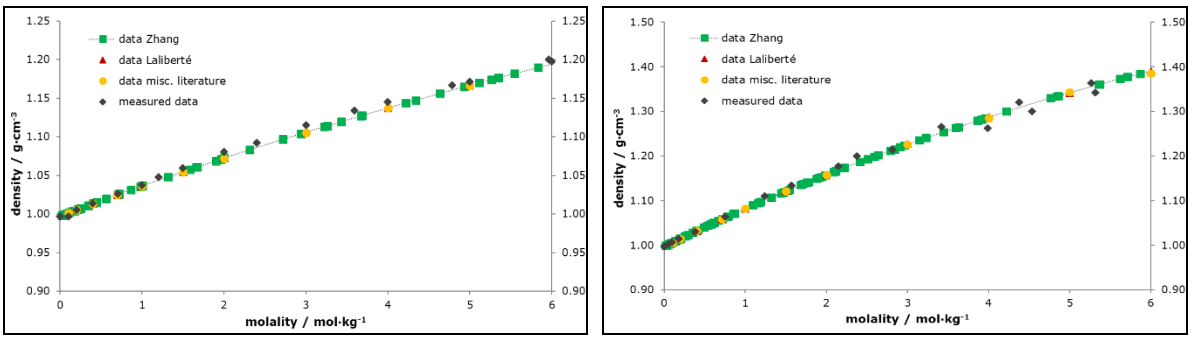

Figure 19. - Comparison of density measurements made in this study with experimental data from literature. Left: in the NaCl-H_2O system; right: in the $CaCl_2$-H_2O system.

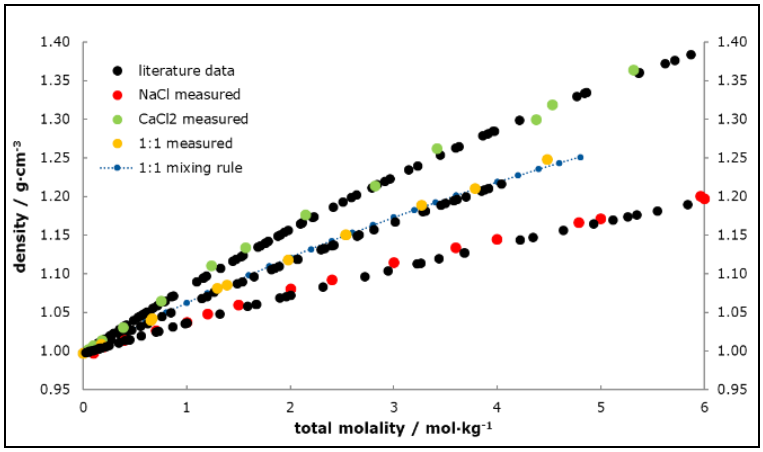

Figure 20. - Comparison of density measurements in the ternary NaCl-$CaCl_2$-H_2O system.

Then, the model of Lassin and André (2023) presented above for the NaCl-$CaCl_2$-H_2O system, based on the Pitzer equations and including the partial dissociation of the $CaCl_2$ electrolyte, is used to calculate density and heat capacities of the solutions investigated experimentally. The model is able to describe salt solubility in the NaCl-$CaCl_2$-H_2O system over the whole range of mixture ratios, at least up to 403 K (see chapter 4.1). We also observe a very good match for density (Figure 21) and heat capacity (Figure 22) calculations in NaCl solutions with errors lower than 2% (except when chloride concentration exceeds 9 mol·kg^{-1}). For the calcium chloride system, a good match is observed up to 3 mol·kg^{-1}.

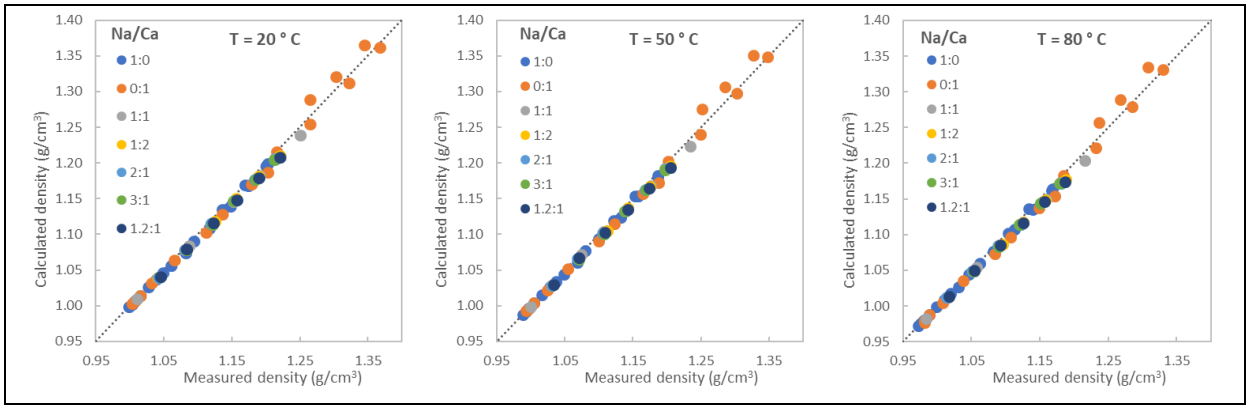

Figure 21. - Comparison between measured and calculated density in the NaCl-H_2O and $CaCl_2$-H_2O systems at three temperatures.

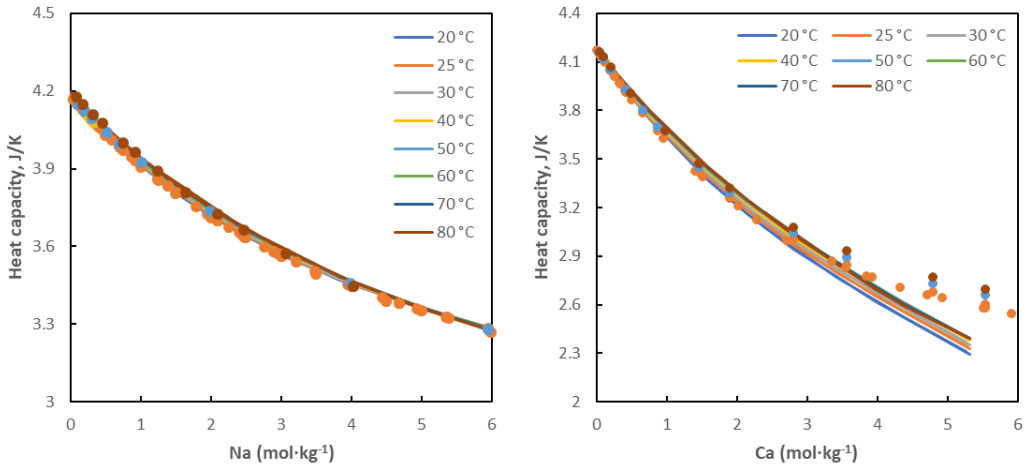

Figure 22. - Comparison between measured and calculated heat capacity in the NaCl-H_2O (left) and $CaCl_2$-H_2O (right) systems. Symbols are experimental data and solid lines are numerical results.

The model was further tested against literature heat capacity data for ternary NaCl-$CaCl_2$ aqueous mixtures, in the composition range that were targeted in the project. Some correspondences could be found with the systems studied by Saluja et al. (1995)[6]. The comparison between their experimental data and those calculated in the present study at 25 and 50°C (Figure 23) shows a reasonable match and a consistent evolution trend of the heat capacity with respect to the Na/Ca molar ratio.

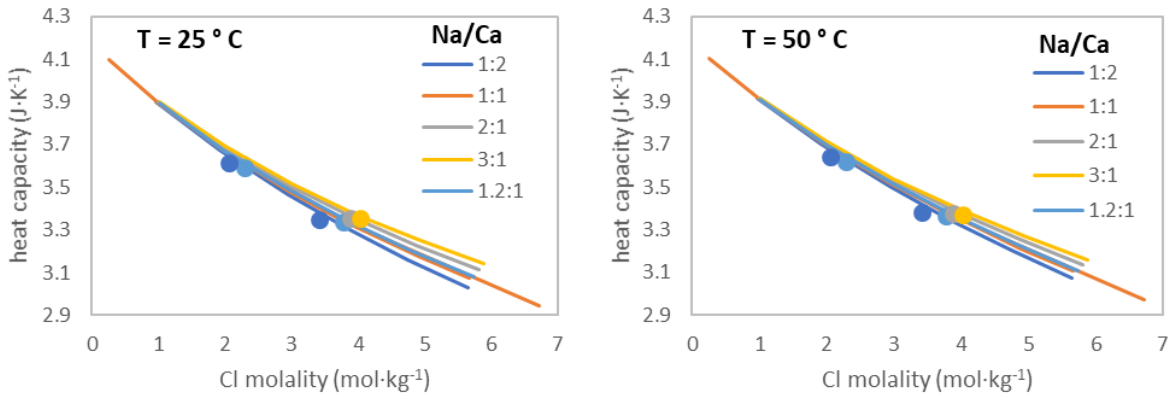

Figure 23. - Comparison between measured and calculated heat capacity in NaCl-$CaCl_2$ aqueous mixtures at 25°C (left) and 50°C (right). Symbols are literature experimental data from Saluja et al. (1995) and solid lines are numerical results.

[6] Saluja, P.P.S., Jobe, D.J., LeBlanc, J.C., Lemire, R.J. (1995) Apparent Molar Heat Capacities and Volumes of Mixed Electrolytes: [NaCl(aq) + CaCl2(aq)], [NaCl(aq) + MgCl2(aq)], and [CaCl2(aq) + MgCl2(aq)]. J. Chem. Eng. Data 40, 398–406. https://doi.org/10.1021/je00018a007

5 CONCLUSIONS

Overall, REFLECT Task 2.4 delivered a better understanding of the thermophysical properties of highly saline geothermal fluids by a combination of analytical data evaluation, improvement of measurement devices, laboratory measurements and numerical modelling. Most of the results have been disseminated to the general public at conferences and in scientific publications.

A new capillary viscometer is now available at GFZ to determine viscosity of arbitrarily saline fluids at pressures and temperatures of up to 50 MPa and 200 °C, respectively. Empirical correlations, e.g. for use in numerical models, to predict viscosity of NaCl aqueous solutions were evaluated against original data as a function of concentration and temperature. For the example of the Insheim, Germany geothermal fluid, measurements of density and viscosity were performed to decipher the effect of minor fluid constituents on these properties. It showed, that the measured data for density and viscosity of the solutions with lithium and/or strontium differ only slightly from those of the pure solution. For the given conditions, this indicates that when density and viscosity are determined and/or stated for fluids containing the main salts only, the error made is less than approximately 2 % with respect to the properties of the fluid encountered in situ.

Limiting conductivities, which are constants for distinct pressure and temperature conditions, were determined for the $NaHCO_3$ system at temperatures between 25 – 450 °C and a pressure of 25.5 MPa. So far, only values at room temperature were known for the limiting conductivity of $NaHCO_3$, whereby the new data agree very well with the literature data and reproduce electrical conductivities of $NaHCO_3$ solutions, measured within the framework of REFLECT, remarkably well.
Based on the new data set, a simple ternary fitting model was set-up that excellently reproduces electrical conductivities measured on a NaCl-$NaHCO_3$ system under similar experimental conditions. Therefore, future work should be aimed at systematically broaden the database with regard to both the limiting conductivities of important electrolytic components of hydrothermal brines at relevant pressure and temperature conditions and electrical properties of complex brines in general.

This report also details the developments of the geochemical model, especially the estimation of new Pitzer interaction parameters for the binary $CaCl_2$-H_2O system and for the ternary $CaCl_2$-MCl_x-H_2O (with M = Na, Ca, Mg, K, Li, and x = 1 or 2) systems. These parameters are valid between 25 °C and 200 °C. This model relies on the Helgeson-Kirkham-Flowers (HKF) for describing the standard thermodynamic properties of aqueous species and the Pitzer equations for describing their mutual interactions. It considers the aqueous speciation of the $CaCl_2$ electrolyte, according to the partial molar properties of the Ca^{2+}, $CaCl^+$, $CaCl_2^0$ and Cl^- aqueous species. This new model reproduces both recent measurements of density acquired during the REFLECT project but also literature data like osmotic coefficients and heat capacities. The model can also be used to simulate the solubility of CO_2 in such saline systems.

Geothermal operators will profit from the results of this task by an improved database of highly saline fluids as well as new modelling capabilities. This applies over the full value chain of geothermal site development, i.e. from exploration to operation, where complex fluid compositions and realistic reservoir conditions are of particular importance. The here obtained results contribute strongly in this regard and will stimulate follow-up investigations.

6 PUBLICATIONS AND CONFERENCES

Hoffert, U., Milsch, H. (2021). *Methods for measuring the density and viscosity of saline geothermal fluids under reservoir conditions*. **World Geothermal Congress 2020+1, Reykjavik, Iceland and online, Paper 13131.**

Kummerow J., Weinzierl W., Goldberg T., Giese R. (2022). *Thermoelectrical properties of salt solutions and monitoring of mineral precipitation by impedance spectroscopy.* **European Geothermal Congress 2022, Berlin, Germany, extended abstract.**

Lassin A., André L., Debure M. (2021). *An improved thermodynamic model based on Pitzer's equations to describe the chemical behaviour of complex chloride-type brines up to salt solubility and elevated temperatures, for geothermal and geological applications*. **Goldschmidt2021, 4-9 July 2021, Lyon, France and online.**

Lassin A., André L. (2023). *A revised description of the binary $CaCl_2$-H_2O chemical system up to solution-mineral equilibria and temperatures to 250°C using Pitzer equations. Extension to the multicomponent H^+-Li^+-Na^+-K^+-Mg^{2+}-Ca^{2+}//Cl^- aqueous system.* **Journal of Chemical Thermodynamics, 176, 106927, https://doi.org/10.1016/j.jct.2022.106927.**

Lassin A., Felipe dos Santos P., Ducousso M., Cézac P., André L. (2022). *Experimental measurements and modelling of thermodynamic properties of NaCl-$CaCl_2$ aqueous solutions up to high temperatures and CO_2 pressures.* **European Geothermal Congress 2022, Berlin, Germany, extended abstract.**

7 REFERENCES

References Section 2:

Falkenhagen, H. (1970): Theorie der Elektrolyte. S. Hirzel Verlag, Leipzig.

Out, D. J. P., Los, J. M. (1980): Viscosity of aqueous solutions of univalent electrolytes from 5 to 95°C. Journal of Solution Chemistry, 9 (1), 19-35. doi: 10.1007/BF00650134.

Zhang, H.-L., Han, S.-J. (1996): Viscosity and Density of Water + Sodium Chloride + Potassium Chloride Solutions at 298.15 K. J. Chem. Eng. Data, 41 (3), 516-520. doi: 10.1021/je9501402.

References Section 3:

Ho, P. C., Palmer, D. A., & Mesmer, R. E. (1994). Electrical conductivity measurements of aqueous sodium chloride solutions to 600 C and 300 MPa. Journal of solution chemistry, 23(9), 997-1018.

Kummerow, J., & Raab, S. (2015). Temperature dependence of electrical resistivity-Part I: Experimental investigations of hydrothermal fluids. Energy Procedia, 76, 240-246.

Kummerow, J., & Raab, S. (2015). Temperature dependence of electrical resistivity–part II: a new experimental set-up to study fluid-saturated rocks. Energy Procedia, 76, 247-255.

Kummerow, J., Raab, S., Schuessler, J. A., & Meyer, R. (2020). Non-reactive and reactive experiments to determine the electrical conductivities of aqueous geothermal solutions up to supercritical conditions. Journal of Volcanology and Geothermal Research, 391, 106388.

Quist, A. S., & Marshall, W. L. (1968). Electrical conductances of aqueous sodium chloride solutions from 0 to 800. degree. and at pressures to 4000 bars. The journal of physical chemistry, 72(2), 684-703.

Sinmyo, R., & Keppler, H. (2017). Electrical conductivity of NaCl-bearing aqueous fluids to 600 C and 1 GPa. Contributions to Mineralogy and Petrology, 172(1), 1-12.

Torres-Alvarado, I.S., Verma, M.P., Opondo, K., Nieva, D., Haklidir., F.T., Santoyo, E., Barragán, R.M., and Arellano, V. (2012). Estimates of geothermal reservoir fluid characteristics: GeoSys.Chem and WATCH. Revista Mexicana de Ciencias Geológicas, 29 (3), 713-724.

Watanabe, N., Yamaya, Y., Kitamura, K., & Mogi, T. (2021). Viscosity-dependent empirical formula for electrical conductivity of H2O-NaCl fluids at elevated temperatures and high salinity. Fluid Phase Equilibria, 549, 113187.

Zimmerman, G. H., Arcis, H., & Tremaine, P. R. (2012). Limiting conductivities and ion association constants of aqueous NaCl under hydrothermal conditions: experimental data and correlations. Journal of Chemical & Engineering Data, 57(9), 2415-2429.

References Section 4:

[1] K.S. Pitzer, Thermodynamics of electrolytes. I. Theoretical basis and general equations., J. Phys. Chem. 77 (1973) 268–277.

[2] K.S. Pitzer, Activity coefficients in electrolyte solutions., CRC Press. (1991) 542.

[3] A. Dinane, Thermodynamic Properties of NaCl-CsCl-LiCl(aq) at T =298.15 K: Water Activities, Osmotic and Activity Coefficients, J. Solution Chem. 36 (2007) 1421–1436. http://dx.doi.org/10.1007/s10953-007-9199-1.

[4] A. Lach, F. Boulahya, L. André, A. Lassin, M. Azaroual, J.P. Serin, P. Cézac, Thermal and volumetric properties of complex aqueous electrolyte solutions using the Pitzer formalism - The PhreeSCALE code, Comput. Geosci. 92 (2016) 58–69. doi:10.1016/j.cageo.2016.03.016.

[5] A. Lach, K. Ballerat-Busserolles, L. André, M. Simond, A. Lassin, P. Cézac, J.C. Neyt, J.P. Serin, Experimental Data and Modeling of Solution Density and Heat Capacity in the Na-K-Ca-Mg-Cl-H2O System up to 353.15 K and 5 mol·kg-1 Ionic Strength, J. Chem. Eng. Data. 62 (2017) 3561–3576. doi:10.1021/acs.jced.7b00553.

[6] D.L. Parkhurst, C.A.J. Appelo, Description of input and examples for PHREEQC version 3: a computer program for speciation, batch-reaction, one-dimensional transport, and inverse geochemical calculations, Reston, VA, 2013. http://pubs.er.usgs.gov/publication/tm6A43.

[7] S.M. Sterner, A.R. Felmy, C.S. Oakes, K.S. Pitzer, Correlation of thermodynamic data for aqueous electrolyte solutions to very high ionic strength using INSIGHT: Vapor saturated water activity in the system CaCl2-H2O to 250 °C and solid saturation, Symp. Thermophys. Prop. 19 (1998) 761–770.

[8] K.S. Pitzer, C.S. Oakes, Thermodynamics of calcium chloride in concentrated aqueous solutions and in crystals, J. Chem. Eng. Data. 39 (1994) 553–559.

[9] D.A. Sverjensky, E.L. Shock, H.C. Helgeson, Prediction of the thermodynamic properties of aqueous metal complexes to 1000°C and 5 kb., Geochim. Cosmochim. Acta. 61 (1997) 1359–1412.

[10] L.P. Méndez De Leo, R.H. Wood, Conductance Study of Association in Aqueous $CaCl_2$, $Ca(CH_3COO)_2$, and $Ca(CH_3COO)_2{\cdot}nCH_3COOH$ from 348 to 523 K at 10 MPa, J. Phys. Chem. B. 109 (2005) 14243–14250. doi:10.1021/jp051802p.

[11] R. Azougen, M. El Guendouzi, A. Rifai, J. Faridi, Water activities, activity coefficients and solubility in the binary and ternary aqueous solutions with LiCl + YCl_2 + H_2O with Y = Mg^{2+}; Ca^{2+}; or Ba^{2+}, Calphad. 34 (2010) 36–44. http://www.sciencedirect.com/science/article/B6TWC-4XRB1VD-1/2/b6bdb58303c41fe04e8d197162637b92.

[12] M.S. Gruszkiewicz, J.M. Simonson, Vapor pressures and isopiestic molalities of concentrated

$CaCl_{2(aq)}$, $CaBr_{2(aq)}$, and $NaCl_{(aq)}$ to T = 523 K, J. Chem. Thermodyn. 37 (2005) 906–930. http://www.sciencedirect.com/science/article/pii/S0021961405000030.

[13] H.F. Holmes, R.H. Busey, J.M. Simonson, R.E. Mesmer, $CaCl_{2(aq)}$ at elevated temperatures. Enthalpies of dilution, isopiestic molalities, and thermodynamic properties, J. Chem. Thermodyn. 26 (1994) 271–298. doi:10.1016/0021-9614(94)90005-1.

[14] G. Perron, A. Roux, J.E. Desnoyers, Heat capacities and volumes of NaCl, $MgCl_2$, $CaCl_2$, and $NiCl_2$ up to 6 molal in water, Can. J. Chem. 59 (1981) 3049–3054. doi:10.1139/v81-446.

[15] J. Ananthaswamy, G. Atkinson, Thermodynamics of Concentrated Electrolyte Mixtures. 5. A Review of the Thermodynamic Properties of Aqueous Calcium Chloride in the Temperature Range 273.15-373.15 K, J. Chem. Eng. Data. 30 (1985) 120–128. doi:10.1021/je00039a035.

[16] A. Lach, L. André, S. Guignot, C. Christov, P. Henocq, A. Lassin, A Pitzer Parametrization to Predict Solution Properties and Salt Solubility in the H-Na-K-Ca-Mg-NO_3-H_2O System at 298.15 K, J. Chem. Eng. Data. 63 (2018) 787–800. doi:10.1021/acs.jced.7b00953.

[17] J. Doherty, PEST. Model-independent parameter estimation. User manual: 5th Edition, (2004).

[18] C. Christov, N. Møller, Chemical equilibrium model of solution behavior and solubility in the H-Na-K-OH-Cl-HSO_4-SO_4-H_2O system to high concentration and temperature, Geochim. Cosmochim. Acta. 68 (2004) 1309–1331. http://www.sciencedirect.com/science/article/B6V66-4BVP5NN-C/2/b155b41e91cefdd87b7a43817c34582a.

[19] V. Majer, K. Štulík, A study of the stability of alkaline-earth metal complexes with fluoride and chloride ions at various temperatures by potentiometry with ion-selective electrodes, Talanta. 29 (1982) 145–148. doi:https://doi.org/10.1016/0039-9140(82)80039-8.

[20] K.S. Johnson, R.M. Pytkowicz, Ion association of Cl>-) with H>+), Na>+), K>+), Ca> 2+), and Mg> 2+) in aqueous solutions at 25 degrees C, Am. J. Sci. 278 (1978) 1428–1447.

[21] S.E. Gillespie, J.L. Oscarson, X. Chen, R.M. Izatt, C. Pando, Thermodynamic quantities for the interaction of Cl− with Mg2+, Ca2+ and H+ in aqueous solution from 250 to 325° C, J. Solution Chem. 21 (1992) 761–788.

[22] A.E. Williams-Jones, T.M. Seward, The stability of calcium chloride ion pairs in aqueous solutions at temperatures between 100 and 360°C, Geochim. Cosmochim. Acta. 53 (1989) 313–318. doi:http://dx.doi.org/10.1016/0016-7037(89)90383-9.

[23] D. Zeng, H. Zhou, W. Voigt, Thermodynamic consistency of solubility and vapor pressure of a binary saturated salt + water system: II. $CaCl_2$ + H_2O, Fluid Phase Equilib. 253 (2007) 1–11. http://www.sciencedirect.com/science/article/B6TG2-4MS3J8V-2/2/a4e0f8871723d150ecefef6c588b5fcd.

[24] D. Li, D. Zeng, X. Yin, H. Han, L. Guo, Y. Yao, Phase diagrams and thermochemical modeling of salt lake brine systems. II. NaCl+H_2O, KCl+H_2O, $MgCl_2$+H_2O and $CaCl_2$+H_2O systems, Calphad. 53 (2016) 78–89. doi:https://doi.org/10.1016/j.calphad.2016.03.007.

[25] A. Lannung, Dampfdruckmessungen des Systems Calciumchlorid–Wasser, Zeitschrift Für Anorg. Und Allg. Chemie. 228 (1936) 1–18. doi:https://doi.org/10.1002/zaac.19362280102.

[26] E.M. Collins, A.W.C. Menzies, A Comparative Method for Measuring Aqueous Vapor and Dissociation Pressures with Some of its Applications, J. Phys. Chem. 40 (1936) 379–397. doi:10.1021/j150372a010.

[27] A. Lassin, L. André, A. Lach, A.L. Thadée, P. Cézac, J.P. Serin, Solution properties and salt-solution equilibria in the H-Li-Na-K-Ca-Mg-Cl-H_2O system at 25 °C: A new thermodynamic model based

on Pitzer's equations, Calphad Comput. Coupling Phase Diagrams Thermochem. 61 (2018) 126–139. doi:10.1016/j.calphad.2018.03.005.

[28] J. Pátek, J. Klomfar, M. Součková, Solid−Liquid Equilibrium in the System of $CaCl_2$−H_2O with Special Regard to the Transition Points, J. Chem. Eng. Data. 53 (2008) 2260–2271. doi:10.1021/je800009w.

[29] A. Lassin, C. Christov, L. André, M. Azaroual, A thermodynamic model of aqueous electrolyte solution behavior and solid-liquid equilibrium in the Li-H-Na-K-Cl-OH-H_2O system to very high concentrations (40 molal) and from 0 to 250 °C, Am. J. Sci. 315 (2015) 204–256. doi:10.2475/03.2015.02.

[30] V.K. Filippov, K.N. Mihelbson, No Title, Zhurnal Neorg. Khimii. 22 (1977) 1689–1694.

[31] G.-M. Long, Y. Yao, F.-Q. Wang, R.-L. Wang, Isopiestic determination of activity coefficients of LiCl and $CaCl_2$ in LiCl–$CaCl_2$–H_2O system at 298.15 K, Wuli Huaxue Xuebao. 15 (1999) 956–960.

[32] V. Shewchuk, M. Waisfeld, No Title, Zhurnal Neorg. Khimii. 12 (1967) 1065–1069.

[33] A.B. Zdanovskii, E.F. Solov'eva, E.I. Lyakhovskaya, N.E. Shestakov, R.E. Shleimovich, L.M. Abutkova, Experimental solubility data on salt - water systems. Vol. 1, Three component systems, 2nd editio, "Chemistry" Publishing, Leningrad, 1973.

[34] A.G. Bergman, A.I. Kuznetsova, Diagramma rastvorimosti troinoi sistemy H_2O-KCl-$CaCl_2$ ot temperatury polnogo zamerzaniya do 300-gradusakh, Zhurnal Neorg. Khimii. 4 (1959) 194–204.

[35] M.M. Kolesnikov, S.D. Beskov, I.G. Druzhinin, No Title, Uchenyie Zap. Mosc. Obl. Pedagog. Instituta Im. Krupskoï. 193 (1968) 47.

[36] E.A. Rashkovskaya, E.I. Chernen'kaya, E.G. Bratach, No Title, Zhurnal Neorg. Khimii. 43 (1970) 2148.

[37] W.B. Lee, A.C. Egerton, LXXXIII.—Heterogeneous equilibria between the chlorides of calcium, magnesium, potassium, and their aqueous solutions. Part I, J. Chem. Soc. Trans. 123 (1923) 706–716.

[38] J. Yang, X. Liu, P.-P. Liang, Solubilities of salts in the ternary systems NaCl + $CaCl_2$ + H_2O and KCl + $CaCl_2$ + H_2O at 75°C, Russ. J. Phys. Chem. A. 85 (2011) 1149–1154. doi:10.1134/S0036024411070090.

[39] C. Christov, Isopiestic Determination of the Osmotic Coefficients of an Aqueous MgCl2 + CaCl2 Mixed Solution at (25 and 50)°C. Chemical Equilibrium Model of Solution Behavior and Solubility in the $MgCl_2$ + H_2O and $MgCl_2$ + $CaCl_2$ + H_2O Systems to High Concentration at (2, J. Chem. Eng. Data. 54 (2009) 627–635. http://pubs.acs.org/doi/abs/10.1021/je8005634.

[40] R.A. Robinson, V.E. Bower, Properties of aqueous mixtures of pure salts. Thermodynamics of the ternary system: water-calcium chloride-magnesium chloride at 25 C, J. Res. Natl. Bur. Stand. - A. Phys. Chem. 70A (1966) 305–311.

[41] J. Van't Hoff, Lichtenstein, No Title, Z. Phys. Chem. 39 (1902) 27.

[42] C.R. Bury, E.R.H. Davies, 178. The system magnesium chloride–lime–water, J. Chem. Soc. (1933) 701–705.

[43] N. Kurnakov, A. Nikolaev, Investigation of the system calcium chloride-magnesium chloride-water, IzV. AN SSSR. 2 (1938) 402–408.

8 APPENDIX

Preprints of the following publications are provided in the pdf-version of this report:

Hoffert, U., Milsch, H. (2021). *Methods for measuring the density and viscosity of saline geothermal fluids under reservoir conditions*. **World Geothermal Congress 2020+1, Reykjavik, Iceland and online, Paper 13131.**

Kummerow J., Weinzierl W., Goldberg T., Giese R. (2022). *Thermoelectrical properties of salt solutions and monitoring of mineral precipitation by impedance spectroscopy.* **European Geothermal Congress 2022, Berlin, Germany, extended abstract.**

Lassin A., André L. (2023). *A revised description of the binary $CaCl_2$-H_2O chemical system up to solution-mineral equilibria and temperatures to 250°C using Pitzer equations. Extension to the multicomponent H^+-Li^+-Na^+-K^+-Mg^{2+}-Ca^{2+}//Cl^- aqueous system.* **Journal of Chemical Thermodynamics, 176, 106927, https://doi.org/10.1016/j.jct.2022.106927.**

Lassin A., Felipe dos Santos P., Ducousso M., Cézac P., André L. (2022). *Experimental measurements and modelling of thermodynamic properties of NaCl-$CaCl_2$ aqueous solutions up to high temperatures and CO_2 pressures.* **European Geothermal Congress 2022, Berlin, Germany, extended abstract.**

8.1 Appendix 1

Hoffert, U., Milsch, H. (2021). *Methods for measuring the density and viscosity of saline geothermal fluids under reservoir conditions*. **World Geothermal Congress 2020+1, Reykjavik, Iceland and online, Paper 13131.**

Proceedings World Geothermal Congress 2020+1
Reykjavik, Iceland, April - October 2021

Methods for Measuring the Density and Viscosity of Saline Geothermal Fluids under Reservoir Conditions

Ulrike Hoffert and Harald Milsch

GFZ German Research Centre for Geosciences, Telegrafenberg, D-14473 Potsdam, Germany

hoffert@gfz-potsdam.de

Keywords: geothermal, fluids, density, viscosity, thermophysics

ABSTRACT

For the sustainable operation of a geothermal system, it is important to know the flow characteristics of the geothermal fluid as exactly as possible. Therefore, viscosity and density are important thermophysical parameters. In sedimentary basins, as prominent targets for geothermal energy exploitation, fluids are mostly highly saline and mainly consist of sodium chloride and calcium chloride. To obtain systematic knowledge about the viscosity and density of sodium chloride and calcium chloride solutions and mixtures of both salts, a laboratory study was conducted. For geothermal applications, salt solutions with different concentrations need to be measured at pressure and temperature conditions up to 200°C and 500 bar. For the viscosity measurement, a flow-through apparatus originally designed for rock-physical measurements was converted into a capillary viscometer. So far, measurements up to 125 bar and 90°C were conducted. Viscosity data of the salt solutions were obtained relative as deviation from pure water, used as the calibration agent for each temperature and pressure step. In this contribution, the general concept and the modifications of this apparatus are outlined. Density measurements are obtained by using an oscillating u-tube densitometer (DMA HP from Anton Paar). The results obtained so far are presented.

1. INTRODUCTION

In order to ensure a safe, economic and sustainable operation of geothermal plants, among others, the knowledge of the fluid properties as accurately as possible is required. Since the fluid is a key element in the geothermal cycle, the system has to be designed in accordance with its site-specific conditions. Viscosity describes the flow behavior and how quickly and effectively the fluid may be produced from the reservoir. The density implies the reservoir pressure and the prevalent stress in the subsurface.

This laboratory study is based on the research platform Groß Schönebeck operated by GFZ Potsdam in Northern Germany. In a depth of 4300 m, the fluid has a temperature of 150°C at about 450 bar (Huenges et al. 2002) and its value of total dissolved solids (TDS) is 265 g/L. During the operation, the fluid is exposed to changes in temperature and pressure. On its way out of the borehole, pressure decreases. In the above-ground facilities, temperature decreases. Before reinjection, the fluid temperature is about 70°C at 10 bar.

Sodium chloride and calcium chloride are the main solutes in fluids being found in the North East German Basin. Depending on the specific site, the ratio of the salts, their total molality within the fluid and the composition of other elements may differ. However, the physical properties of a geothermal fluid are determined by the main salts as those mentioned before.

Site specific differences in the salt concentrations result in varying density and viscosity of the fluids. Taking into account the changes in temperature and pressure, only estimating the fluid properties can have a severe impact on plant operation and may thereby also cause financial losses. An exact knowledge of the properties of the geothermal fluid as a function of temperature, pressure, and composition is crucial for an understanding of the parametric dependencies involved. Therefore, systematic investigations on model fluids have to be performed.

In an earlier publication, the results for atmospheric pressure and temperatures up to 80°C were presented (Hoffert and Milsch 2015). This study is aimed to extend the temperature and pressure range of the systematic measurements preferably up to reservoir conditions, i.e., 200°C and 500 bar.

2. MATERIALS AND METHODS

2.1 Sample preparation

In order to observe the actual influence of the salts on the properties of pure water, all measurements were performed with synthetically prepared brines. These solutions shall model possible geothermal fluids similar to those in the North German Basin. In addition, solutions were prepared with magnesium chloride in order to be able to distinguish the influence of the calcium chloride from that of divalent chlorides in general. The purity level of all three salts was above 99%. The reproducibility of the scale[1] is 0.1 mg which is equivalent to a deviation of less than 1‰ relative to the weighed quantities.

2.2 Measuring devices

2.2.1 Density

The density measurements were conducted with an Anton Paar DMA HP cell combined with a 100DX ISCO syringe pump. The device was calibrated with pure water and ethanol using the manufacturer's 'Excel Tool for Wide Range Adjustments'. Test

[1] KERN & SOHN GmbH. ABJ 220-4M

measurements with pure water showed a relative deviation from REFPROP[2] of 1% at maximum. The samples were stirred and heated up before injection to avoid the formation of air bubbles.

2.2.2 Viscosity

For measuring the viscosity of geothermal brines up to reservoir conditions encountered at the Groß Schönebeck site (150°C and 450 bar), a GFZ-built flow-through apparatus originally designed for rock-physical measurements was converted into a capillary viscometer (details about the original structure are described in Milsch et al 2008).

As shown in **Figure 1**, the apparatus consists of a vessel filled with oil, which is pressurized by a syringe pump (oil pump). The oil is heated by a thermostat. The sample fluid is pumped from a first pump (upstream) at a fixed flow rate through the capillary system, which is situated in the heated oil, to a second pump (downstream). The upstream pump regulates the flow rate, the downstream pump regulates the internal pressure of the capillary system. The actual measuring capillary consists of PEEK, is 1.6 m long and has an inner diameter of 130 µm. Several temperature sensors measure the temperature of the fluid and the oil. A differential pressure sensor records the pressure difference before and after the measuring capillary. The maximum temperature for this apparatus is 200°C. The maximum pressure depends on the equipped pumps and is currently 250 bar.

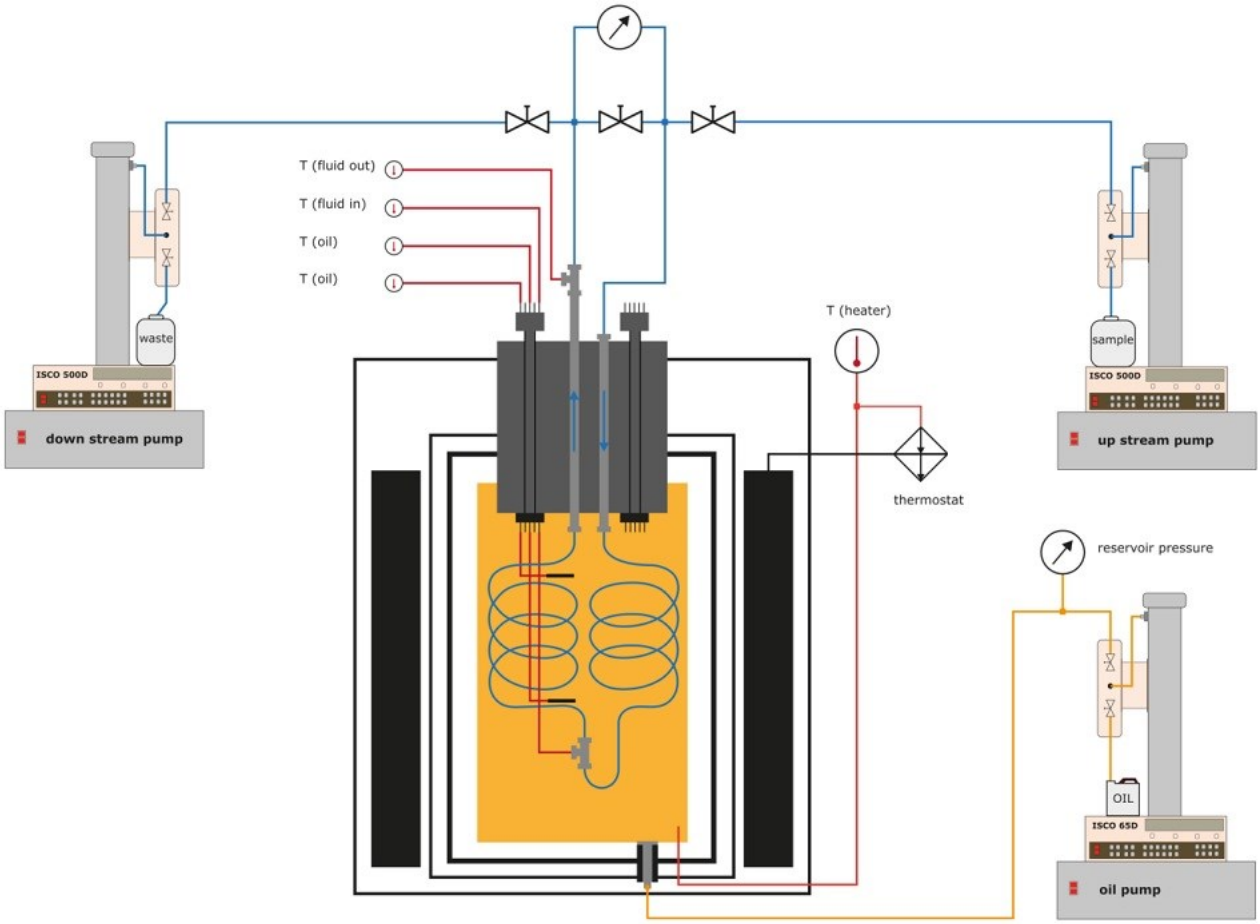

Figure 1: Schematic representation of the modified flow-through apparatus for measuring the viscosity up to reservoir conditions.

The viscosity is calculated using the equation of Hagen–Poiseuille:

$$\eta = \frac{\pi \cdot r^4 \cdot \Delta p}{8 \cdot l \cdot V} \tag{1}$$

where η, r, Δp, l and V are viscosity, inner radius of the capillary, pressure difference, length of the capillary, and fluid flow rate, respectively.

3. RESULTS AND DISCUSSION

3.1 Density

The temperature dependence at 100 bar and the pressure dependence at 50°C of the density data of the single salt solutions, containing only sodium chloride, calcium chloride and magnesium chloride, respectively, are shown in **Figure 2**. The density data

[2] NIST Reference Fluid Thermodynamic and Transport Properties Database (REFPROP)

of the 1:1 mixture (sodium chloride: calcium chloride and sodium chloride: magnesium chloride, respectively) compared to those of the pure salt solutions are shown depending on temperature at 100 bars in **Figure 3**. Indicated in the figure legends are the respective total molalities of the solutions related to the cations.

As expected, density decreases with higher temperatures and increases with higher pressures. The density data of the mixtures are systematically between those of the individual solutions.

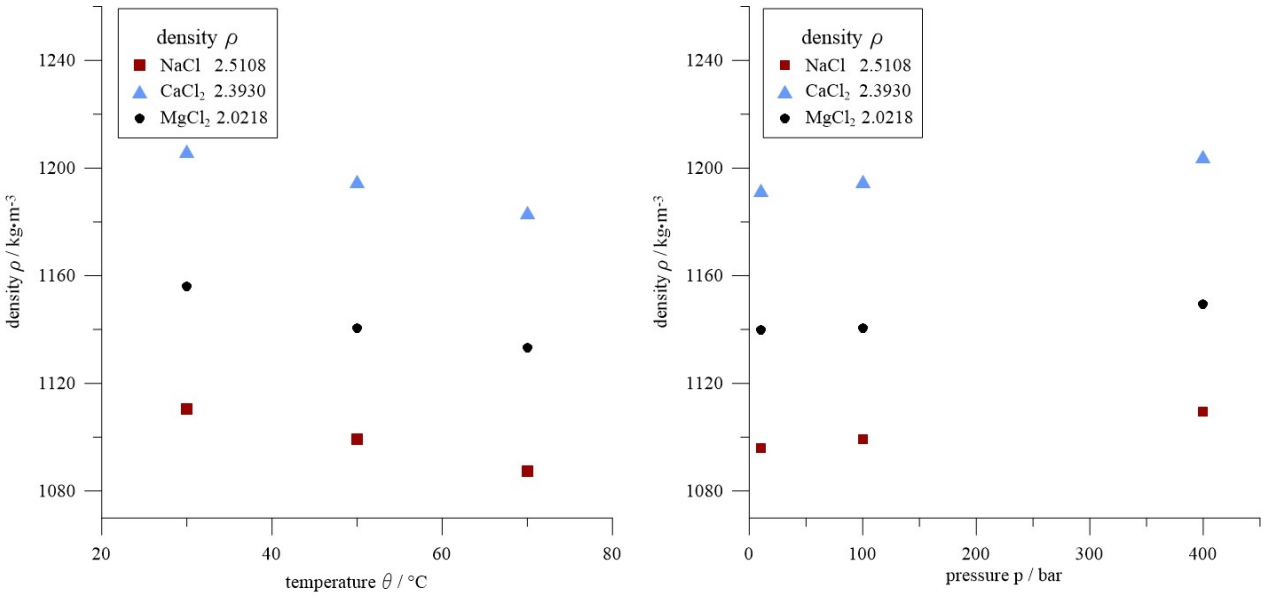

Figure 2: Measured density data of pure salt solutions of sodium chloride, calcium chloride and magnesium chloride in water; temperature dependence at 100 bar (*left*) and pressure dependence at 50°C (*right*). Numbers in the figure legends indicate the respective total molalities of the solutions related to the cations.

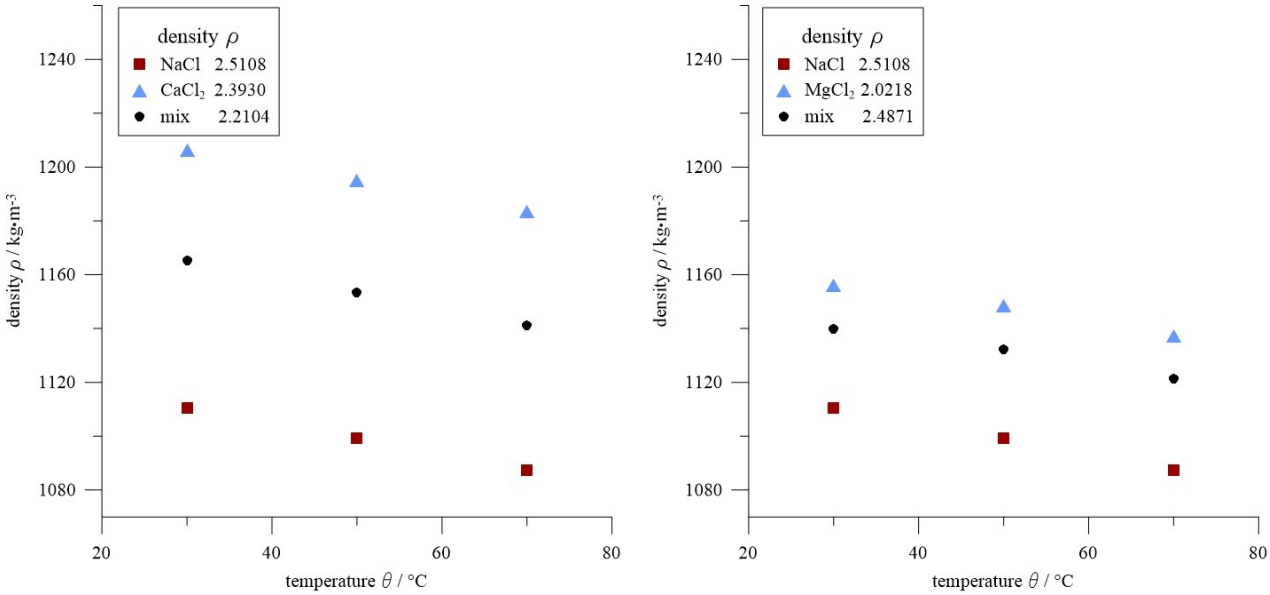

Figure 3: Measured density data of pure salt and mixed solutions of sodium chloride, calcium chloride and magnesium chloride in water; sodium chloride and calcium chloride (*left*) and sodium chloride and magnesium chloride (*right*) at 100 bar as a function of temperature. Numbers in the figure legends indicate the respective total molalities of the solutions related to the cations.

3.2 Viscosity

After the modification of the apparatus, systematic investigations with different capillary diameters and lengths as well as different flow rates were required. In addition, a sufficiently accurate determination of the fluid temperature within the measuring capillary had to be ensured. For measurements of pure water, the current structure (inner diameter: 130 µm and length: 1.6 m) allows an

accuracy better than about 2% as shown in **Figure 4** where the relative error of the viscosity data of pure water compared to REFPROP is shown for different pressure and flow conditions.

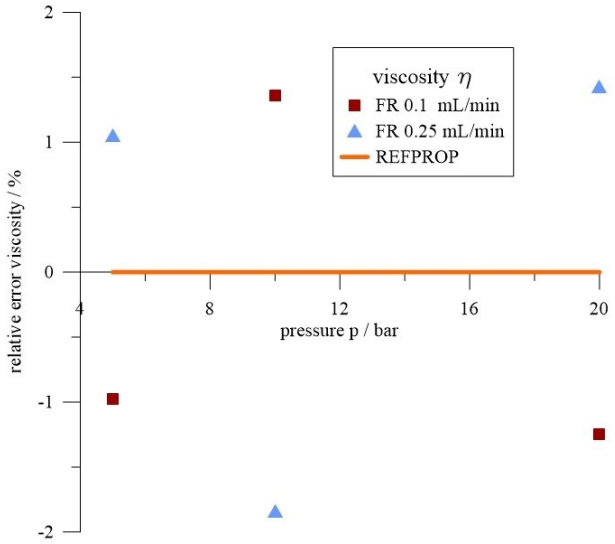

Figure 4: Relative error for viscosity measurements of pure water at room temperature, different pressures and flow rates, compared to REFPROP. FR in the legend indicates flow rate.

4. CONCLUSIONS

The present study provides new laboratory data for density of mixed solutions of sodium chloride, calcium chloride and magnesium chloride up to 70°C and 400 bar. A device for measuring the viscosity under reservoir conditions was presented.

In a previous publication, mixing rules were applied to the measured data in order to predict the properties of mixed solutions depending on their molality (Hoffert and Milsch 2015). Density and viscosity of mixed solutions ranging from 20°C to 80°C at atmospheric pressure were determined with high accuracy. The extension to higher pressures and temperatures is the subject of ongoing work.

Further modifications of the apparatus for viscosity measurements in order to further improve accuracy as well as to enable the simultaneous measurement of other properties such as electrical conductivity and sonic velocity is currently in planning and/or in the testing phase.

5. ACKNOWLEDGMENTS

The authors thank Tanja Ballerstedt for substantial technical support. The thermophysical laboratory and related research were made possible by a grant from the German Federal Ministry for the Environment, Nature Conservation, Building, and Nuclear Safety (BMUB; 0325217).

REFERENCES

Huenges et al.: The in-situ geothermal laboratory Groß Schönebeck – Learning to use low permeability aquifers for geothermal power, *Proceedings,* 27th Workshop on Geothermal Reservoir Engineering, Stanford University, Stanford, CA (2002).

Hoffert, U. and Milsch, H.: Experimental Investigations on the Thermophysical Properties of Synthetic Geothermal Fluids, *Proceedings*, World Geothermal Congress 2015 Melbourne, Australia (2015).

Milsch et al.: A new Apparatus for Long-term Petrophysical Investigations on Geothermal Reservoir Rocks at Simulated In-situ Conditions, *Transp Porous Med,* **74,** (2008), 73–85.

8.2 Appendix 2

Kummerow J., Weinzierl W., Goldberg T., Giese R. (2022). *Thermoelectrical properties of salt solutions and monitoring of mineral precipitation by impedance spectroscopy.* **European Geothermal Congress 2022, Berlin, Germany, extended abstract.**

Thermoelectrical properties of salt solutions and monitoring of mineral precipitation by impedance spectroscopy

Juliane Kummerow[1], Wolfgang Weinzierl[1], Tanya Goldberg[2], Ronny Giese[1]

[1] German Research Centre for Geosciences, GFZ, Telegrafenberg, 14473 Potsdam, Germany

[2] University of Applied Sciences Ruhr West, Duisburger Straße 100, 45479 Mülheim an der Ruhr

jule@gfz-potsdam.de

Keywords: geothermal fluids, calcite solubility, calcite scaling.

ABSTRACT

Calcite is one of the most abundant scaling minerals in geotechnical installations and the precise knowledge of the hydrochemical solution equilibria is key to predict its precipitation behaviour. In the framework of the EU-funded REFLECT project we perform solubility experiments in the H_2O-NaCl-CO_2 system to broaden the database for temperatures up to 210 °C. Here, we present preliminary results from a series of ongoing solubility measurements as a function of temperature and CO_2 partial pressure (0 – 50 bar) at various salinities ranging between 0 – 20 wt% NaCl. We use electrical conductivity measurements to monitor the progress in dissolution or precipitation from the solutions and to define equilibrium conditions. For this, we have developed a new 4-point electrode system, which was successfully tested at temperatures of up to 213 °C and a maximum system pressure of 70 bar.

1. INTRODUCTION

Scaling is one of the major obstacles for an economically efficient utilization of geothermal energy, as it often causes frequently and costly maintenance of both subsurface and surface installations including production and injection wells, pumps, and heat exchangers (e.g. Wanner et al., 2017, Köhl et al, 2020). Commonly, geothermal fluids contain a multitude of dissolved components such as salts, minerals and gases. However, changes in pressure and temperature during fluid extraction for geothermal energy and power production disturb the hydro-chemical equilibrium and may lead to mineral precipitation due to supersaturation, what in consequence can significantly reduce the flow rates of the geothermal system and rise the economic risk (e.g. Atkinson et al., 1991).

Calcite is one of the most abundant scaling minerals and can be found across a variety of geothermal production sites (Arnórsson, 1981; Haklidir and Balaban, 2019). Calcite is widespread in geothermal reservoir rocks, which is why in-situ formation waters are generally calcite saturated (Arnórsson, 1981). Carbonate scaling is mainly associated with $CO_{2(aq)}$ degassing from the geothermal fluid due to decompression and a subsequent increase in pH, which significantly reduces the solubility of carbonate minerals. Generally, the potential of calcite supersaturation is largely controlled by the initial temperature, the initial CO_2 partial pressure (pH), and salinity of the formation water, and is highest when pH and salinity are highest and temperature is lowest (Arnórsson, 1989). Accordingly, calcite scaling is rampant in low (80 – 120 °C) to medium (130 – 200 °C) temperature sites (Wanner et al., 2017; Quinao et al., 2017), but also causes serious problems in some high-temperature geothermal fields with temperatures of up to 250 °C (Li, 2017). Thus, precise knowledge of hydro-chemical solution equilibria provides an important tool that can be used to prevent unwanted mineral precipitation by adjusting operational production conditions.

Calcite solubilities in water and brines up to 6 M NaCl have been widely studied experimentally at temperatures below 100 °C (Kendall, 1912; Hastings et al., 1927; Miller, 1952; Yanatéva, 1955; Kindyakov et al., 1958; Weyl, 1959, 1966; MacDonald and North, 1974; Plummer et al., 1982, Wolf et al. 1989; Coto et al., 2012 and ref. in it), though a large number of the published data only cover ambient temperature and pressure conditions. Only limited experimental data are available for temperatures up to 300 °C and CO_2 pressures between 1 – 150 bar (Ellis, 1959, 1963; Segnit et al. 1962; Malinin and Kanukov, 1971; Bychkov et al. 2020), and there is a general lack for calcite solubility in high-salinity brines (> 6 wt% NaCl). As a consequence, large uncertainties in current model predictions arise. In order to better predict the scaling behavior of highly saline geothermal fluids in geotechnical installations, new solubility experiments were performed, focusing on fluids with salinities of 35 – 200 g/l NaCl, which are typical for most mid European geothermal sites. Here, we present first preliminary results from a series of ongoing systematic measurements targeting a temperature range of 24 – 210 °C at CO_2 pressures between 1 – 50 bar. We use in-

situ electrical impedance spectroscopy to define equilibrium conditions in the test solutions.

2. EXPERIMENTAL APPROACH

2.1 Development of a high-temperature conductivity probe

The solubility of calcite is highly influenced by the amount of carbonic acid present in the solution and already small fluctuations in pressure and temperature have an immediate effect on its pH. In order to keep system disturbances during the experiments to a minimum, the dissolution/precipitation process was continuously monitored by electrical conductometry. For this, a 4-point electrode system was developed, which had to be capable for electrical conductivity measurements at elevated temperature and pressure. The conductivity probe consists of a rod-like corpus made of PEEK, to which lower end two Ag/AgCl plates (current electrodes) are attached vis-a-vis and supernatant with a defined electrode spacing. Two additionally Ag/AgCl wires, serving as potential electrodes, are sealed into the corpus and placed between the current electrodes. An O-ring sealed adapter was designed for the dimensions of commercial high-pressure screw-in drivers, and is provided for the pressure-tight attachment in the lid of the autoclave. The conductivity probe was used up to 213 °C and a system pressure of 70 bar.

For conductivity measurements, an impedance spectrometer (Zahner-Zennium electrochemical work-station) was used to apply an AC voltage of 50 mV to the current electrodes. The conductance bridge provides the impedance, Z, and phase angle, φ, at distinct frequencies. The conductivity of the test solution, σ_{fl}, is given by

$$\sigma_{fl} = c/R, \qquad [1]$$

with R is the sample resistance, derived from

$$R = \cos\varphi \cdot Z, \qquad [2]$$

and c is the cell constant, which considers the geometry of the electrode layout. The cell constant of the conductivity probe was experimentally determined using distilled water, tap water, as well as 0.01 M and 0.1 M NaCl solutions at ambient conditions. Variations in the electrode spacing due to thermal expansion is regarded to be < 1 % at 200 °C, leading to an overall underestimation of σ_{fl} by 3% at maximum temperature.

2.2 Experimental equipment and procedure for the measurement of calcite solubilities

Solubility experiments at elevated temperature and pressure were conducted in two stainless steel batch reactors with a total capacity of 800 ml, which are lined with beakers made of Teflon or silica glass, respectively, to avoid corrosion. The test solutions were made of 670 g of solvent (degassed bi-distilled water or NaCl solutions at known concentrations) to which a sufficient excess of pure commercial calcite powder of

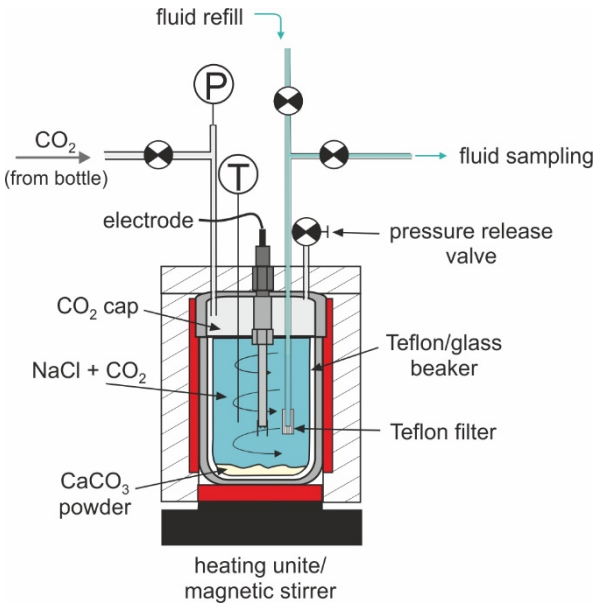

Figure 1: Schematic overview of the batch reactors.

20 g was added, thus a constant particle surface can be assumed over the entire course of the experiments. During the experiment, the solution was stirred by a magnetic stirrer at a continuous rate of 300 rpm.Experiments were performed between 24 – 210 °C and 1 – 50 bar pCO_2. A schematic overview of the set-up is shown in Figure 1.

For pressurization, both autoclaves were connected to a CO_2 bottle, whereby the system pressure was regulated via a pressure reducing valve at the bottle and metering valves at the autoclaves. Autoclave pressures were monitored by high- precision, dead-weight calibrated sensors with an accuracy of ± 0.2 bar. Before the experiment, CO_2 was flushed for approximately 15 - 20 min through the gas cap volume of the autoclaves to remove air from the vessels via open pressure release valves, which were closed afterwards to apply the desired pressure. For temperature control, the autoclaves were placed on heating plates /magnetic stirrers and jacketed with thermally-insulated heating sleeves, so that essentially the whole vessel including the gas cap was at constant temperature. The heating-sleeves were connected to controllers to keep the temperature constant ± 0.1 °C. The fluid temperatures were monitored by K-type thermocouples, placed in dead-ended and Teflon coated Hastelloy capillaries, which again were immersed directly in the tested solutions.

The achievement of equilibration between solution and calcite powder at the desired pressure and temperature conditions was determined via continuous electrical conductivity measurements. When changes in the electrical conductivity were less than 0.5 % for 12 hours, solubility equilibrium was assumed and fluid samples were extracted at system pressure and temperature through a PEEK capillary with attached 2 µm Teflon filter. To avoid contamination, the sampling capillary was flushed with about 10 ml of the produced fluid, which was poured away, before the proper sample was taken. Samples, taken at

temperatures below 150 °C, were discharged directly into a tube, containing a weighted amount of bi-distilled water to avoid precipitation, when the pressure was released to atmospheric conditions. In total, a maximum sample volume of ca. 280 cm^3 could be extracted from the vessel, before the electrodes became partially exposed. Several fluid samples could therefore be taken from the test solutions at different temperature and pressure levels, before the vessel had to be recharged.

Ca^{2+} concentration were determined via EDTA titration with the titration end point being color-indicated by Eriochrome Black T, whereby the determined $CaCO_3$ concentrations are based on the mean values of 5 individual titrations. Usually, the analytical uncertainty in the titration was less than 1 %.

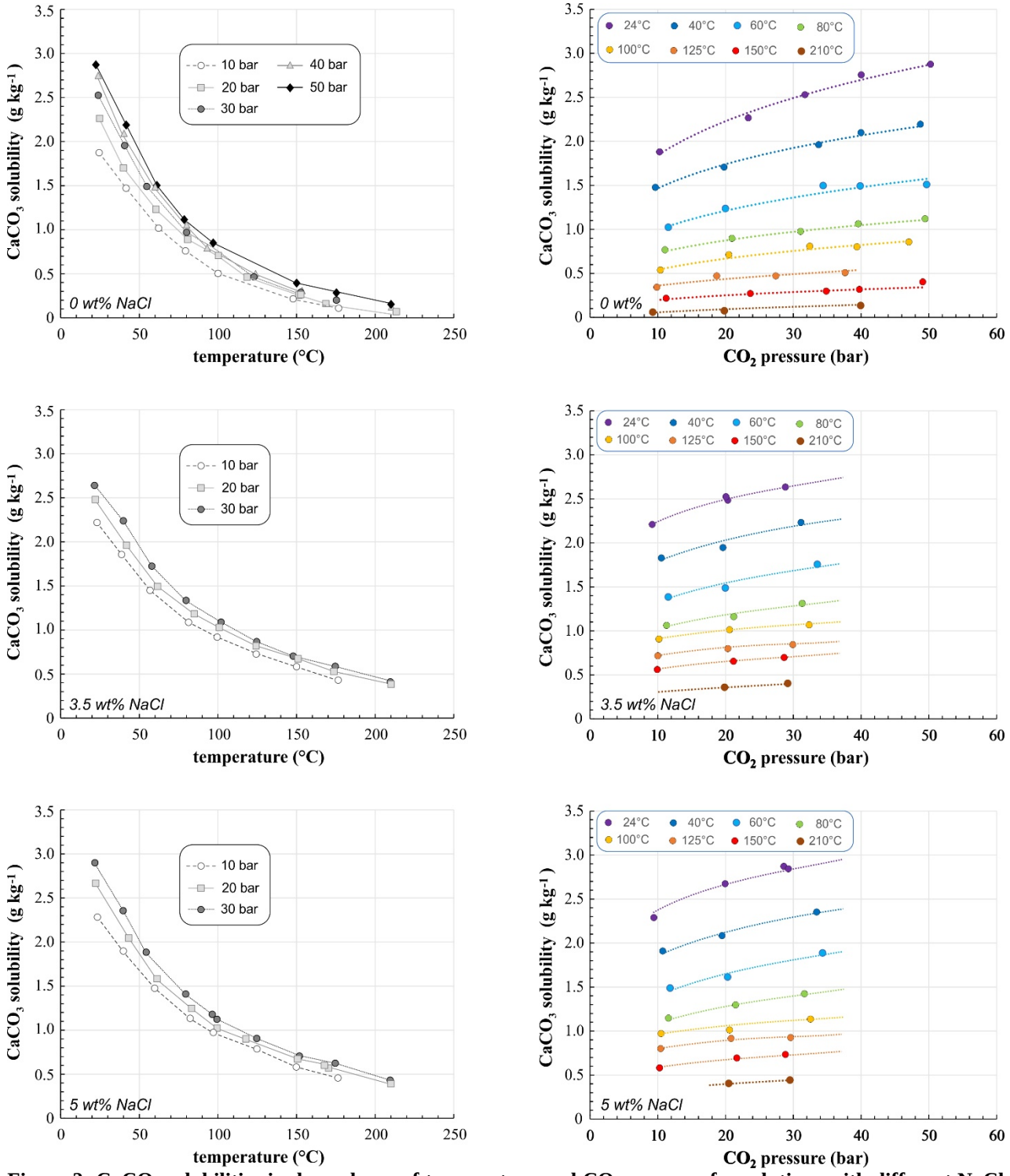

Figure 2: $CaCO_3$ solubilities in dependence of temperature and CO_2 pressure for solutions with different NaCl concentrations.

3. RESULTS AND CONCLUSION

So far, the solubility of calcite has been tested in pure water and NaCl solutions with concentrations of 3.5 wt% and 5 wt%. The measurements were conducted in a temperature range of 24 – 210 °C and covering pressures of 1 – 50 bar. Experiments with 10 wt% and 20 wt% NaCl solutions are ongoing.The preliminary results are plotted in Figure 2 as function of temperature and pCO_2, defined as the difference of the absolute pressure in the autoclave and the vapour pressure of water at the particular temperature. It can be seen that the solubility of calcite in all tested solvents decreases exponentially with increasing temperature and constant pressure, while the solubility increases with increasing pCO_2 at isothermal conditions. Where available, this is in agreement with data from previous studies (Miller, 1952; Ellis, 1959, 1963; Segnit, 1962; Bychkov et al., 2020). Figure 3 depicts the variation of calcite solubility in dependence of NaCl concentration for two temperatures. For comparison, data measured at 10 bar in this study were checked against data from Ellis (1963), which were determined at comparable pressure and temperature conditions. The agreement between the two datasets is reasonably satisfactory. Over the range of measured salinities, the solubility increases with the NaCl concentration in the solution.

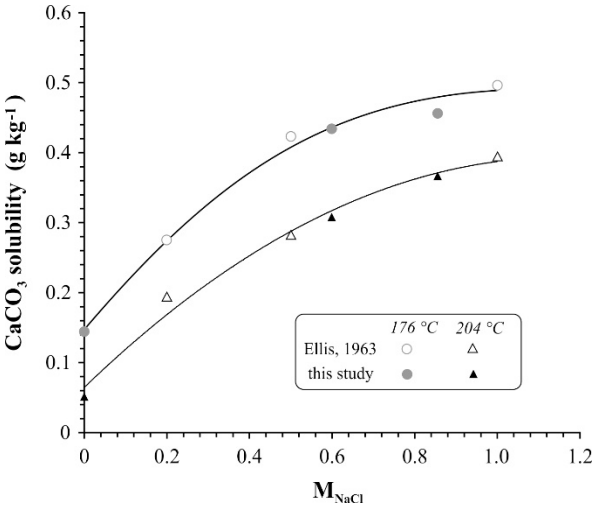

Figure 3: $CaCO_3$ solubility as function of the NaCl concentration at 176 °C, 204 °C and an approximate pressure of 10 bar. Open symbols are for literature data from Ellis, 1963. Solid symbols represent this study.

Precise knowledge of hydrochemical solution equilibria provides a tool that can be used to prevent unwanted mineral precipitation by adjusting operational production conditions. Thus, the new measurements carried out in this study contribute to a broadening of the existing experimental database with the final aim of calculating the solubility product and stability constants of aqueous calcium carbonate and bicarbonate complexes.

From the development of the specific conductivity over time and the titrated Ca^{2+} concentration, the course of the calcium concentration can be deduced, which shows a linear relationship and so that the measured conductivity can be used as a measure for the Ca^{2+} concentration (Baumann et al., 1985, Dreybrodt et al., 1996, Vosbeck, 2004)

REFERENCES

Arnórsson, S.: Mineral deposition from Icelandic geothermal waters, environmental and utilization problems, *J. Petroleum Technology*, **33 (1)**, (1981), 181-187.

Arnórsson, S.: Deposition of calcium carbonate minerals from geothermal waters — theoretical considerations, *Geothermics*, **18**, (1989), 33-39.

Atkinson, G., Oklahoma, U., Raju, K., Aramco, S., and Howell, R.D.: The thermodynamics of scale prediction, *SPE International Symposium on Oilfield Chemistry, Anaheim, California, February 1991*, SPE-21021-MS, (1991), 209-215

Baumann, J. Buhmann, D., Dreybrodt, W. and Schulz. H.D.: Calcite dissolution kinetics in porous media, *Chem. Geol.*, **53**, (1985), 219-228.

Benoit, W.R.: Carbonate scaling characteristics in Dixie Valley, Nevada geothermal wellbores, *Geothermics*, **18**, (1989), 41-48.

Bychkov, A.Yu., Bénézeth, P., Pokrovsky, O.S., Shvarov, Yu.V., Castillo, A. and Schott, J.: Experimental determination of calcite solubility and the stability of aqueous Ca- and Na-carbonate and -bicarbonate complexes at 100-160 °C and 1-50 bar pCO_2 using in situ pH measurements, *Geochim. Cosmochim. Acta*, **290**, (2020), 352-365.

Coto, B., Martos, C., Peña, J.L., R. Rodríguez, R. and Pastor, G.: Effects in the solubility of $CaCO_3$: Experimental study and model description, *Fluid Phase Equilibria*, **324**, (2012), 1-7.

Dreybrodt, W., Lauckner, J., Liu, Z., Svensson, U. and Buhmann, D.: The kinetics of the reaction $CO_2 + H_2O \longrightarrow H^+ + HCO_3^-$ as one of the rate limiting steps for the dissolution of calcite in the system H_2O-CO_2-$CaCO_3$, *Geochim. Cosmochim. Acta*, **60,** (1996), 3375-3381.

Ellis, A.J.: The solubility of calcite in carbon dioxide solutions, *Amer. J. Sci.*, **257**, (1959), 354-365.

Ellis, A.J.: The solubility of calcite in sodium chloride solutions at high temperature, *Amer. J. Sci.*, **261**, (1963), 259-267.

Haklidir, F.S.T. and Balaban, T.Ö.: A review of mineral precipitation and effective scale inhibition methods at geothermal power plants in West Anatolia (Turkey), *Geothermics*, **80**, (2019), 103-118.

Hastings, A.B., Murray; C.D. and Sendroy Jr., J.: Studies of the solubility of calcium salts. I. The solubility of calcium carbonate in salt solutions and biological fluids, *J. Biolog. Chem.*, **71 (3)**, (1927), 723-781.

Kendall, J.: The solubility of calcium carbonate in water, *T. Philos. Mag. Ser.*, **23 (6)**, (1912), 958-976.

Kindyakov, P.S., Khokhlova, A.V. and Lapchinskaya, L.L.: Solubility in the reciprocal system lithium carbonate-calcium hydrate-water., *Tr. Mosk. Inst. Tonkoi Khim. Tekhnol.*, **7**, (1958), 32-44.

Köhl, B., Grundy, J., Baumann, T.: Rippled Scales in a Geothermal Facility in the Bavarian Molasse Basin: A Key to Understand the Calcite Scaling Process. *Geotherm. Energy*, 8, (2020), 1–27.

Li, Y.: Calcite scaling potential of Kangding geothermal field, W-Sichuan plateau, China, *United Nation University - Geothermal training program 2017*, IS-108 Reykjavik, Iceland, (2017), Reports 2017 # 16.

MacDonald, R.W. and North, N.A.: The Effect of Pressure on the Solubility of $CaCO_3$, CaF_2, and $SrS0_4$ in Water, *Can. J. Chemistry*, **52 (18)**, (1974), 3181-3186.

Malinin, S.D. and Kanukov, A.B.: The solubility of calcite in homogeneous H_20-NaCl-CO_2 systems in the 200-600 °C temperature interval, *Geochem. Internat.*, **8**, (1971), 668-679.

Miller, J.P.: A portion of the system calcium carbonate–carbon dioxide–water, with geological implications, *Am. J. Sci.*, **250,** (1952), 161-203.

Plummer, L.N., and Busenberg, E.: The solubilities of calcite, aragonite and vaterite in CO_2-H_2O solutions between 0 and 90 °C, and evaluation of the aqueous model for the system $CaCO_3$-CO_2 - H_2O, *Geochim. Cosmochim. Acta*, **46,** (1982), 1301-1331.

Quinao, J.J., Buscarlet, E., and Siega, F.: Early identification and management of calcite deposition in the Ngatamariki geothermal field, New Zealand, *Proceedings of 42nd Workshop on Geothermal Reservoir Engineering 2017*, Stanford University, Stanford, USA, (2017), paper SGP-TR-212, 9 p.

Segnit, E.R., Holland, H.D., and Biscardi, C.J.: The solubility of calcite in aqueous solutions. I. The solubility of calcite in water between 75 degrees and 200 degrees at CO_2 pressures up to 60 atm, *Geochim. Cosmochim. Acta*, **26,** (1962), 1011-1040.

Vosbeck, K.: Experimentelle Bestimmung der Lösungskinetik synthetischer Calciumcarbonate und natürlicher Kalkgesteine, dissertation, *University of Bremen*, Germany, (2004), 111 p.

Wanner, C., Eichinger, F., Jahrfeld, T., and Diamond, L.W.: Causes of abundant calcite scaling in geothermal wells in the Bavarian Molasse Basin, Southern Germany, *Geothermics*, **70**, (2017), 324-338.

Weyl, P.K.: The change in solubility of calcium carbonate with temperature and carbon dioxide content, *Geochim. Cosmochim. Acta*, **17**, (1959), 214-225.

Weyl, P.K.: The solution behavior of carbonate materials in sea water, *EPR Publ.*, **428**, Shell Development Co., Houston, (1966), 59 p.

Wolf, M., Breitkopf, O. and Puk R.: Solubility of calcite in different electrolytes at temperatures between 10 and 60°C and at CO2 partial pressures of about 1 kPa, *Chem. Geol.*, **76**, (1989), 291–301.

Yanatéva, O.K.: Solubility in the system $CaCO_3$-$MgCO_3$-H_2O at different temperatures, *Zhurnal Neorganicheskoi Khimii*, **1**, (1955), 1473-1476.

Acknowledgements

We would like to acknowledge the machine shop of GFZ Potsdam and Mathias Kreplin for their support during the preparation of the experimental device in challenging times. The REFLECT project has received funding from the European Union's Horizon 2020 research and innovation programme under grant agreement n° 850626.

8.3 Appendix 3

Lassin A., André L. (2023). *A revised description of the binary $CaCl_2$-H_2O chemical system up to solution-mineral equilibria and temperatures to 250°C using Pitzer equations. Extension to the multicomponent H^+-Li^+-Na^+-K^+-Mg^{2+}-Ca^{2+}//Cl^- aqueous system.* **Journal of Chemical Thermodynamics, 176, 106927, https://doi.org/10.1016/j.jct.2022.106927.**

J. Chem. Thermodynamics 176 (2023) 106927

Contents lists available at ScienceDirect

The Journal of Chemical Thermodynamics

journal homepage: www.journals.elsevier.com/the-journal-of-chemical-thermodynamics

A revised description of the binary $CaCl_2$-H_2O chemical system up to solution-mineral equilibria and temperatures of 250 °C using Pitzer equations. Extension to the multicomponent HCl-LiCl-NaCl-KCl-$MgCl_2$-$CaCl_2$-H_2O system

Arnault Lassin [a,*], Laurent André [a,b]

[a] BRGM, 3 avenue Claude Guillemin, 45060 Orléans, France
[b] Université d'Orléans-CNRS/INSU-BRGM, UMR ISTO 7327, 45071 Orléans, France

ARTICLE INFO

Keywords:
Thermodynamic modeling
Aqueous electrolytes
Pitzer equations
HKF theory
Partial dissociation

ABSTRACT

Calcium chloride is a highly soluble chemical compound involved in variable amounts in many natural and industrial environments. The description of its chemical properties and mineral-solution equilibrium conditions must cover a wide range of temperatures and chemical compositions, including saline solutions. This article reports an improved model for the thermodynamic accurate description of the $CaCl_2$-H_2O chemical system according to the Pitzer formalism from 25 to 250 °C, over the whole concentration range between pure water and the solubility of salts (up to 30 M). It accounts for the aqueous speciation of the $CaCl_2$ electrolyte, according to the partial molar properties of the Ca^{2+}, $CaCl^+$, $CaCl_2^0$ and Cl^- aqueous species described by the HKF theory. The numerical stability, resulting from the lowered ionic strength in comparison to full dissociation, facilitates the development of temperature-dependent models for ternary systems containing the main major cations: H^+, Li^+, Na^+, K^+, and Mg^{2+}.

1. Introduction

Calcium chloride is a chemical compound involved in variable amounts in many natural and industrial environments. Due to its high solubility in water, its natural occurrences mostly concern saline deposits associated with hydrothermal systems [1]. Such deposits are often described as evaporites [2–4], whose deposition mechanisms have been widely studied in regard to secular variations in seawater chemistry or the formation of basinal brines [5–8]. These deposits can also result from the hydration of mantle rock minerals, like enstatite, when deep hot waters of marine origin flow within their porosity. Such water–rock interactions, which result in the transformation of primary mantle rocks into serpentinites, could be responsible for the formation of Salt Giants [3,9–12]. Such formations are characterized by the presence of relatively thick layers of tachyhydrite ($CaCl_2{\cdot}(MgCl_2)_2{\cdot}12H_2O$), a very soluble salt that is not stable in the current most arid environments in the world. The $CaCl_2$-rich hot waters associated with these hydrothermal systems are often recorded in fluid inclusions, which are used to investigate the past conditions of temperature, pressure and chemistry [13,14]. In some specific contexts of the Earth's deep crust, where temperatures and pressures are relatively high (above 350 °C and 200 bars), the hydrolysis of $CaCl_2$ is thought to be responsible for the generation of significant amounts of HCl [15]. In other specific environments located in Proterozoic sedimentary basins, $CaCl_2$-rich brines may be responsible for the alteration of monazite minerals contained in high-grade uranium deposits [16].

Industrial applications of calcium chloride, including thermal processes, are numerous [1,17,18] because of the combination of its hygroscopic character, heat of hydration, the low to medium melting points of its hydrates and its low material costs. Beyond the conventional applications like deicing, dust control and road stabilization, the physical and chemical properties of aqueous $CaCl_2$ and its solid hydrates are useful for phase change material, desiccants, heat pumps and refrigeration, and thermal energy storage [19–21]. $CaCl_2$ can also be used to tune the crystallinity of some minerals, like $Mg(OH)_2$, which is produced for specific applications for instance as a flame retardant filler [22]. Mixed with other chemical compounds, it is also used as a coagulant to prevent silica scaling in the surface installation of geothermal plants

* Corresponding author.
E-mail address: a.lassin@brgm.fr (A. Lassin).

https://doi.org/10.1016/j.jct.2022.106927
Received 7 January 2022; Received in revised form 21 September 2022; Accepted 22 September 2022
Available online 26 September 2022

[23,24], or in wells where geothermal fluids undergo significant temperature variations during ascent in the production well and during reinjection. For all the aforementioned applications, the supply of $CaCl_2$ in its various forms is provided by sufficient production based on the refining of natural brines [25], the reaction of calcium hydroxide with ammonium chloride in Solvay soda production, and the reaction of hydrochloric acid with calcium carbonate [18].

In addition, depending on the chemical composition of the pore brine in a reservoir rock targeted for CO_2 geological storage, $CaCl_2$ may influence the solubility of the gas [26–29].

Due to the variety of uses and occurrences of $CaCl_2$ in natural and industrial environments with, in some instances, environmental and economic issues, it is necessary to have a reliable description of its chemical properties and solid–gas-solution equilibrium conditions over a wide range of temperatures and chemical compositions, including saline solutions. In this context, the objective of this work was to improve the thermodynamic description of the $CaCl_2$-H_2O chemical system according to a combined Pitzer-HKF formalism from 0 to 250 °C, over the whole concentration range between pure water and the solubility of salts, and to extend its application to ternary systems containing the main major cations: H^+, Li^+, Na^+, K^+, and Mg^{2+}.

2. Theoretical background and methodology

Despite important advances previously made by numerous researchers, the $CaCl_2$-H_2O system still needs improvement. For instance, the model of Li et al. [30] based on the Pitzer-Simonson-Clegg equations, is able to describe reliably the solution properties and solid–liquid equilibria over a wide range of temperatures and concentrations of binary aqueous chloride systems, including $CaCl_2$. Yet, the description of more complex systems is still necessary, and should rely on thermodynamic models implemented in modelling tools that can be used by a large scientific community. The Pitzer equations belong to these models as they are implemented in several geochemical and reactive transport simulation tools [31–33], and as they were often used to calculate the properties of the $CaCl_2$-H_2O system as described hereafter. In the original philosophy of the Pitzer approach [34,35], aqueous electrolytes are assumed to be fully dissociated and mutual influences between solutes are described by specific interaction parameters that affect ion activity coefficients rather than by aqueous complexation constants. This helped to improve the description of a number of saline aqueous systems up to salinities of c.a. 6 mol·kg^{-1}. In order to extend the range of concentrations to higher values and to consider pH-sensitive chemical systems and weak electrolytes, it was found necessary to introduce the possibility of considering partial dissociation or aqueous complex formation [36–38]. The corresponding Pitzer equations are summarized in the Supplementary materials (Appendix 1). Other options proposed to extend the description of solution properties to higher concentrations included the use of additional ionic strength-dependent specific interaction parameters [39–42], and a mole fraction description of the concentrations [43]. However, considering partial dissociation has advantages that led us to select this option. Indeed, describing the formation of aqueous complexes is inherently consistent with the Debye-Hückel theory, which applies to dilute aqueous solutions. Thus, considering partial dissociation brings consistency as a continuum between concentrated and dilute systems where the effects of ionic strength dominate the ion-specific interactions. In addition, when partial dissociation is taken into account, the number of "free" water molecules remaining in the brine is larger than in the full dissociation case and, thus, the aqueous solution "status" can be maintained up to higher concentrations. At the same time, the ionic strength of the brine increases less when partial dissociation is considered, which contributes to stabilizing the solvation of the Pitzer equations. Moreover, solution properties like density, heat capacity and enthalpy should be better described when considering the contribution of the various complexes or ion pairs, the standard properties of which differ from the simple weighted sum of the fully dissociated species. Despite these advantages, one must acknowledge that this option also has significant drawbacks due to the semi-empirical character of the Pitzer equations. In particular, increasing the variety of aqueous species increases the number of specific interaction parameters to consider when parameterizing the Pitzer equations. The risk is generating an exponentially growing dataset of interaction parameters, which poses an open question. In addition, the use of aqueous complexation constants determined for dilute solutions to constrain the estimation of specific interaction parameters for higher concentrations may be tricky. In some cases, a value different from that determined for dilute solutions, and thus with a questionable physical meaning, had to be proposed, as previously done by Møller [44] for the $CaSO_4^0$ ion pair, and as illustrated in the following.

The $CaCl_2$-H_2O chemical system is concerned by these evolutions of the Pitzer equations since the solubility of antarcticite ($CaCl_2$:$6H_2O$) is 7.3 mol·kg^{-1} at 25 °C, and that of the stable salt ($CaCl_{2,cr}$) at 250 °C is about 30.8 mol·kg^{-1} according to Pitzer and Oakes [45]. This led Sterner et al. [46] to revise the previous thermodynamic models developed in particular by Møller [44] and Greenberg and Møller [47]. Sterner et al. [46] proposed 4 models based on the different evolutions of the Pitzer equations: (*i*) the basic Pitzer equation, (*ii*) the Pitzer equation augmented by an ionic strength-dependent third virial contribution, (*iii*) the Pitzer equation together with equilibria involving the formation of $CaCl^+$ and $CaCl_2^0$, and (*iv*) the simultaneous combination of all of the above.

Unsurprisingly, the two first models of Sterner et al. [46] could not satisfactorily describe the osmotic coefficient data over the whole range of temperatures and concentrations. Models (*iii*) and (*iv*) did much better with an advantage for model (*iv*) because of its greater numerical stability, especially at high temperatures and concentrations. Interestingly, the authors considered a limited number of temperature-dependent interaction parameters for their models based on the partial dissociation hypothesis. Indeed, only 9 parameters per temperature were necessary in model (*iii*), namely the aqueous complex formation constants of $CaCl^+$ and $CaCl_2^0$ from Ca^{2+} and Cl^-, the binary interaction parameters $\beta^{(0)}$, $\beta^{(1)}$, C^{ϕ} for the Ca^{2+}-Cl^- and $CaCl^+$-Cl^- ion pairs and the mutual binary interaction λ for the $CaCl_2$ aqueous complex. In model (*iv*), the C_1^{Φ} parameter was added to account for the ionic strength-dependent term of the interaction between Ca^{2+} and Cl^-, and between $CaCl^+$ and Cl^-. Then, the temperature variation of each interaction parameter or formation constant was fitted with 3 coefficient temperature functions.

More recently, Lach et al. [48] proposed a new set of interaction parameters to include experimental solution heat capacity data as additional constraints to the optimization procedure. However, the concentration of $CaCl_2$ was limited to 7 mol·kg^{-1} and temperatures were comprised between 0 and 75 °C. Because of this limited concentration range, the authors could describe both the osmotic coefficient and solution heat capacity of $CaCl_2$ aqueous solutions by considering full dissociation of the electrolyte. Then Lassin et al. [49] introduced the $CaCl_2^0$ ion pair to extend the description of the osmotic coefficient data at 25 °C beyond the solubility limit of antarcticite, in the metastability domain of the aqueous solution (up to 11 mol·kg^{-1}). This made it possible to determine new interaction parameters for describing solution properties (activity coefficients and water activity) and salt solubilities in the multicomponent H-Li-Na-K-Ca-Mg-Cl-H_2O system, but at 25 °C only.

Considering partial dissociation is actually constrained by the standard partial thermodynamic properties of the solutes, which depend on temperature and pressure. A convenient way to describe such a dependency is to use an equation of state that relates the standard partial molar volume of the aqueous species to the temperature and the pressure. In the present work, the robust, well-known and well-documented revised-HKF theory is applied [50–52]. The combined use of the revised HKF-theory and of the Pitzer equations has been previously described in the literature and proved to be a powerful approach able to cover very

large conditions of temperatures and concentrations [53–57]. The geochemical calculation code used in the present work is PHREESCALE [48,58], which is an evolution of PhreeqC [31], software that is widely used in the geochemical modelling community.

The general description of the model development performed in the present work is extensively detailed in the Supplementary materials (Appendix 2). Regardless of the formation constants of the aqueous complexes which were set according to [59], 12 specific interaction parameters were found necessary to reproduce the osmotic coefficient data, each parameter being variable with temperature (in Kelvin) according to the following expression (equation (1)) implemented in PhreeSCALE:

$$Y(T) = a_1 + a_2T + a_3T^2 + a_4T^3 + a_5/T + a_6\ln(T) \quad (1)$$

For all Y parameters, which are presented in Table 1, the a_4 coefficient was set to 0. The number of digits of the parameters reported in Table 1 is very large but, at the highest concentrations and temperatures, the computation is very unstable and truncations may lead to failures.

The formation and individual standard properties of the aqueous complexes, $CaCl^+$ and $CaCl_2^0$, are given in Table 2. The formation properties (e.g. log K, the logarithm of the thermodynamic constant of any reaction) depend on temperature according to equation (2):

$$log\ K = A + BT + C/T + D\ log(T) + E/T^2 \quad (2)$$

with T in Kelvin.

log K are used to calculate the aqueous speciation while the individual standard properties (HKF parameters) are used to calculate the thermal and volumetric properties of the solutes and, then, of the aqueous solution [58].

Once solution properties are described satisfactorily over the whole range of temperatures and concentrations, including the liquid–vapor equilibrium at saturation with the stable salts [30,62], the solubility product of these salts can be deduced from the calculated ion activity product of the corresponding dissolution reaction. The temperature function coefficients obtained this way are reported in Table 3.

After the binary $CaCl_2$-H_2O system has been fully parameterized, the study can focus on the ternary systems (i.e. with an additional cation among Li, Na, K and Mg) using the same methodology. However, much fewer solution properties have been measured in mixed systems and the most abundant information in the literature comes from solubility measurements. The temperature range of available data varies with the system. Most of these data could be reproduced satisfactorily using cation-cation (θ) and cation-cation–anion (ψ) interaction parameters (Table 1) and solubility products of salts (Table 3).

3. Results and discussion

a. The binary $CaCl_2$-H_2O system.

- *Osmotic coefficient*

Osmotic coefficients calculated over the whole range of

Table 1
Temperature-dependent Pitzer interaction parameters estimated in this work (unless indicated otherwise) to describe the $CaCl_2$-H_2O binary system and the HCl-$CaCl_2$-H_2O, LiCl-$CaCl_2$-H_2O, NaCl-$CaCl_2$-H_2O, KCl-$CaCl_2$-H_2O, and $MgCl_2$-$CaCl_2$-H_2O ternary systems.[a,b]

Parameter		a_1	a_2	a_3	a_5	a_6
$CaCl_2$-H_2O system		0 < T < 250 °C				
$\beta^{(0)}$	Ca^{2+}-Cl^-	2.64951	−7.76412E-3	8.55745E-06	−240.83888	0
$\beta^{(0)}$	$CaCl^+$-Cl^-	1.69861	−5.11886E-3	3.94991E-06	1.01651	0
$\beta^{(1)}$	Ca^{2+}-Cl^-	9.78521	−9.136031E-3	0	−1572.72024	0
$\beta^{(1)}$	$CaCl^+$-Cl^-	−1.30849	7.491923E-3	0	0	0
C^ϕ	Ca^{2+}-Cl^-	4.43923E-2	−1.97602E-4	2.08590E-07	9.89356E-1	0
C^ϕ	$CaCl^+$-Cl^-	−7.74506E-2	2.64517E-4	−2.28284E-07	−2.51838E-1	0
λ	$CaCl_2^0$-Cl^-	3.43665	−1.36667E-2	1.37988E-05	1.29783	0
λ	$CaCl_2^0$-Ca^{2+}	7.25380E-1	−2.98981E-3	2.08541E-06	−6.19108E-2	0
λ	$CaCl_2^0$-$CaCl^+$	−310.67494	−1.19739E-1	3.23404E-05	7337.89850	56.017375
θ	Ca^{2+}-$CaCl^+$	−16.66512	4.71423E-2	−4.34747E-05	1925.51497	0
μ	$CaCl_2^0$-$CaCl_2^0$-$CaCl_2^0$	2.9	0	0	0	0
ζ	$CaCl_2^0$-$CaCl^+$-Cl^-	−0.21759	−7.72569E-4	1.60629E-06	100.84472	0
HCl-$CaCl_2$-H_2O system		25 °C	Consistent with the HCl-H_2O parameters from [60]			
θ [c]	H^+-Ca^{2+}	9.68627E-2	0	0	0	0
θ	H^+-$CaCl^+$	7.50E-03	0	0	0	0
ψ	H^+-Ca^{2+}-Cl^-	−1.01797E-03	0	0	0	0
ψ	H^+-$CaCl^+$-Cl^-	−1.80E-03	0	0	0	0
LiCl-$CaCl_2$-H_2O system		10 < T < 50 °C	Consistent with the LiCl-H_2O parameters from [61]			
θ	Li^+-Ca^{2+}	0.02578	0	0	0	0
θ	Li^+-$CaCl^+$	−0.07	0	0	0	0
ψ	Li^+-Ca^{2+}-Cl^-	0	0	0	0	0
ψ	Li^+-$CaCl^+$-Cl^-	5.04638	−1.76648E-2	2.04973E-05	−475.1255	0
NaCl-$CaCl_2$-H_2O system		18 < T < 130 °C	Consistent with the NaCl-H_2O parameters from [44]			
θ [c]	Na^+-Ca^{2+}	0.05	0	0	0	0
θ	Na^+-$CaCl^+$	−0.05	0	0	0	0
ψ	Na^+-Ca^{2+}-Cl^-	5.6136E-2	−4.1646E-4	6.7532E-07	0	0
ψ	Na^+-$CaCl^+$-Cl^-	6.3123E-2	−4.7242E-4	7.6190E-07	0	0
KCl-$CaCl_2$-H_2O system		18 < T < 200 °C	Consistent with the KCl-H_2O parameters from [47]			
θ [c]	K^+-Ca^{2+}	0.1156	0	0	0	0
θ	K^+-$CaCl^+$	2.28922	−2.56619E-3	0	−582.8673	0
ψ	K^+-Ca^{2+}-Cl^-	7.23166	−2.1006E-2	2.0230E-05	−839.19018	0
ψ	K^+-$CaCl^+$-Cl^-	−0.19453	2.24792E-4	0	44.60541	0
$MgCl_2$-$CaCl_2$-H_2O system		25 < T < 110 °C	Consistent with the $MgCl_2$-H_2O parameters from [48]			
θ	Mg^{2+}-Ca^{2+}	0.05	0	0	0	0
θ	Mg^{2+}-$CaCl^+$	7.0589E-3	1.200E-5	0	0	0
ψ	Mg^{2+}-Ca^{2+}-Cl^-	1.84775E-1	−6.15313E-4	0	0	0
ψ	Mg^{2+}-$CaCl^+$-Cl^-	−2.62484E-1	1.47044E-3	−2.0487E-06	0	0

[a] : the coefficient a_4, of the temperature dependence function given in the text (equation (1)), is set to 0 for all interaction parameters.
[b] :ternary interaction parameters involving the $CaCl_2^0$ aqueous species were all set to 0 and are not reported in this table (see text for more details).
[c] : valid up to 250 °C.

Table 2
Formation reaction (log K, Equation (2)) and individual properties (HKF parameters*) of the aqueous complexes of the $CaCl_2$-H_2O system.

Reaction	A	B	C	D	E
$Ca^{2+} + Cl^- = CaCl^+$	784.30407	1.29811E-1	−43492.573	−285.72525	2,630,012
$Ca^{2+} + 2Cl^- = CaCl_2^0$	1562.1171	2.55796E-1	−85801.168	−569.81877	5,221,187.6

Species	**a_1**	**a_2**	**a_3**	**a_4**	**c_1**	**c_2**	**ω**
Source: [59]							
Ca^{2+}	−0.81E-1	−30.34E+2	22.16	−10.37E+4	37.66	−10.55E+4	5.17E+5
Cl^-	1.687	20.09E+2	23.28	−11.91E+4	−18.41	−23.91E+4	6.09E+5
$CaCl^+$	1.13587	−4.8103E+2	25.9195	−11.4282E+4	87.3782	2.1928E+4	2.0343E+5
$CaCl_2^0$	2.602	30.99E+2	11.85	−12.91E+4	100.25	13.69E+4	−0.159E+5

*: a_1 ($J{\cdot}mol^{-1}{\cdot}bar^{-1}$); a_2 ($J{\cdot}mol^{-1}$); a_3 ($J{\cdot}K{\cdot}mol^{-1}{\cdot}bar^{-1}$); a_4 ($J{\cdot}K{\cdot}mol^{-1}$); c_1 ($\cdot mol^{-1}{\cdot}K^{-1}$); c_2 ($J{\cdot}K{\cdot}mol^{-1}$); ω ($J{\cdot}mol^{-1}$).

Table 3
Solubility products (log K, Eq. (2))[a] of the various salts estimated in this work.

Salt and dissolution reaction	A	B·10^3	C	E	T range (°C)
Antarcticite $CaCl_2{\cdot}6H_2O = CaCl^+ + Cl^- + 6H_2O$	29.9618	−39.6182	−4331.89	0	0–30
α-$CaCl_2{\cdot}4H_2O$ (ghiaraite) $CaCl_2{\cdot}4H_2O = CaCl^+ + Cl^- + 4H_2O$	−21.2256	41.7284	4099.02	0	25–46
β-$CaCl_2{\cdot}4H_2O$ $CaCl_2{\cdot}4H_2O = CaCl^+ + Cl^- + 4H_2O$	7.43447	−7.72095	0	0	25–43
γ-$CaCl_2{\cdot}4H_2O$ $CaCl_2{\cdot}4H_2O = CaCl^+ + Cl^- + 4H_2O$	−8.0835	17.6240	2385.79	0	25–40
$CaCl_2{\cdot}2H_2O$ (sinjarite) $CaCl_2{\cdot}2H_2O = CaCl^+ + Cl^- + 2H_2O$	25.5584	−27.4357	−5833.03	812,151	20–177
$CaCl_2{\cdot}H_2O$ $CaCl_2{\cdot}H_2O = CaCl^+ + Cl^- + H_2O$	13.53563	−18.64790	0	0	175–190
$CaCl_2{\cdot}1/3H_2O$ $CaCl_2{\cdot}0{\cdot}.33H_2O = CaCl^+ + Cl^- + 0{\cdot}.33H_2O$	15.12605	−20.80292	0	0	190–233
$CaCl_2$ $CaCl_2 = CaCl^+ + Cl^-$	16.52931	−23.03200	0	0	225-250[b]
$LiCl{\cdot}CaCl_2{\cdot}5H_2O$ $LiCl{\cdot}CaCl_2{\cdot}5H_2O = Li^+ + Ca^{2+} + 3Cl^- + 5H_2O$	51.8798	−0.08461	−4919.4	0	≤ 25
Tachyhydrite $CaCl_2(MgCl_2)_2{:}12H_2O = CaCl^+ + 2\,Mg^{2+} + 5Cl^{--} + 12H_2O$	80.0289	−0.12865	−7611.7	0	25–110
$(CaCl_2)_2MgCl_2{:}6H_2O$ $(CaCl_2)_2MgCl_2{:}6H_2O = 2CaCl^+ + Mg^{2+} + 4Cl^- + 6H_2O$	15.90	0	0	0	110
$KCl{:}CaCl_2{:}2H_2O$ $KCl{:}CaCl_2{:}2H_2O = K^+ + CaCl^+ + 2Cl^- + 2H_2O$	13.60481	−0.01934	0	0	45–95
$KCl{:}CaCl_2{:}H_2O$ $KCl{:}CaCl_2{:}H_2O = K^+ + CaCl^+ + 2Cl^- + H_2O$	14.493	−0.02000			95–110
$KCl{:}CaCl_2$ $KCl{:}CaCl_2 = K^+ + CaCl^+ + 2Cl^-$	17.15829	−0.02548	0	0	≥110

[a] : the D coefficient was found to be always 0.
[b] : temperature region actually not correctly described by the model.

concentrations comprised between pure water and saturation with respect to solid salt, from 25 to 250 °C, are compared to experimental values in Fig. 1. Very good agreement was found both at low and high concentrations over the whole temperature range. However, some discrepancies can be observed between the model and the values recommended by Pitzer and Oakes [45], at 50, 100 and 150 °C. We note that the values recommended at 150 °C are superimposed on the experimental values measured later by Gruszkiewicz and Simonson [63] at 140 °C, the latter being correctly described by the model.

At higher temperatures (i.e., 160, 180 and 225 °C) the model also closely matches the experimental values obtained by Gruszkiewicz and Simonson [63], which were not used in the optimization procedure as is explained in Appendix 2 (Supplementary materials).

At 25 °C, the values recommended by Pitzer and Oakes [45] are consistent with those recently measured by Azougen et al. [64], which are also consistent with the critically selected experimental data and smoothed values recommended by Rard and Clegg [65].

These observations suggest that the values recommended by Pitzer and Oakes [45] at 50, 100 and 150 °C should be considered with caution and that new experimental data should be acquired to fix this issue.

- *Thermal properties*

The set of interaction parameters developed in this work is temperature dependent. This means that thermal properties of the aqueous solutions can be calculated with PhreeSCALE and compared to experimental data.

Perron et al. [67] measured apparent heat capacities at 25 °C and Ananthaswamy and Atkinson [68] report experimental measurements of heat capacities and apparent enthalpies of $CaCl_2$ aqueous solution at 25 and 50 °C. Saluja et al. [69] and Gao et al. [70] measured heat capacities for $CaCl_2$ concentrations up to 6 M and temperatures up to 100 °C.

Literature and calculated values of heat capacity can be compared in Fig. 2. Heat capacity is correctly described up to 4 M and between 25 and 100 °C. Out of this range, significant discrepancies appear. Furthermore, despite the order of magnitude being correct, the apparent enthalpy is systematically underestimated by the model, by a factor of about 1/3 (not shown).

Many parameters can explain these discrepancies. Indeed, the solution heat capacity depends on the standard partial molar heat capacity of the solutes, the aqueous speciation and the apparent heat capacity. The apparent enthalpy and the apparent heat capacity depend on

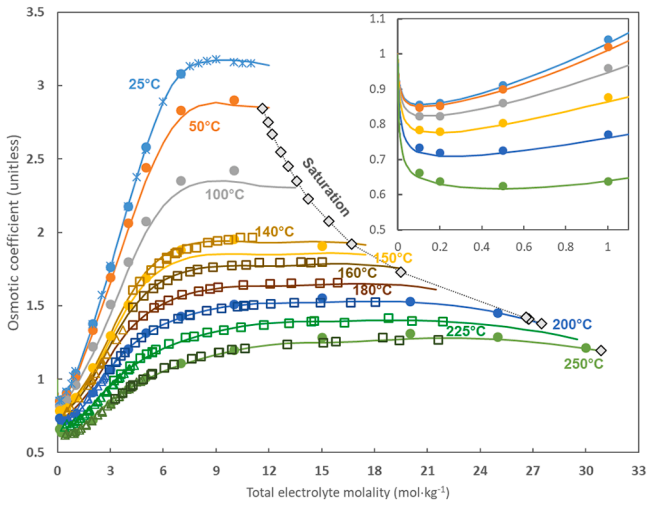

Fig. 1. Osmotic coefficient of $CaCl_2$ aqueous solutions as a function of electrolyte concentration, over the temperature range 25–250 °C. Symbols represent experimental data; filled circles and diamonds: [45]; stars: [64]; squares: [63]; triangles: [66]. Lines represent calculated values (this work).

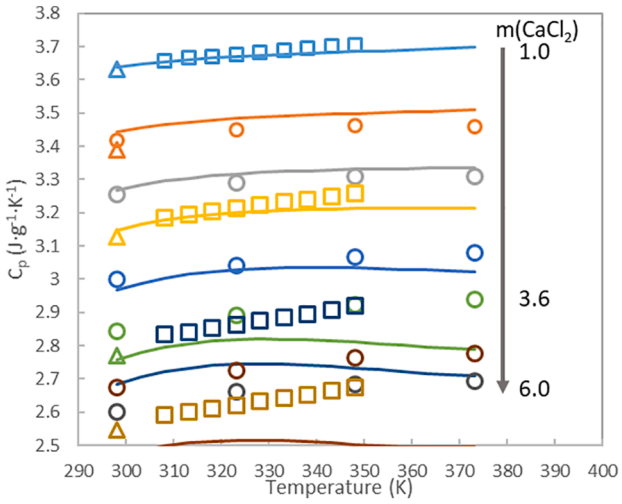

Fig. 2. Heat capacity of $CaCl_2$ aqueous solutions as a function of temperature for different electrolyte concentrations between 1 and 6 M. Symbols represent experimental data [67,69,70] and lines represent the model (this work).

derivatives of the excess Gibbs energy with respect to temperature, which also depend on the aqueous speciation [71]. Any of these contributions can be a source of error that is difficult to evaluate. The standard partial molar heat capacity of the $CaCl^+$ and $CaCl_2^0$ aqueous species were estimated by Sverjensky et al. [59], using empirical equations. No experimental data is available to check the aqueous speciation calculated in the present work, especially at high salinity. The experimental apparent enthalpy data are available on a narrow range of temperatures and concentrations. Thus, they can only have a small weight on the parameter estimation procedure, compared to the much more numerous osmotic coefficient data. This indicates that there is still room for further improvements of the model.

- *Aqueous speciation*

The identification of different solutes for the $CaCl_2$-H_2O system directly addresses the question of their distribution within the aqueous solution, depending on the total electrolyte concentration and on the temperature. Details are given in the Supplementary materials (Appendix 3, including Fig. A3-3). Results indicate the predominance of the Ca^{2+} (and Cl^-) aqueous species at low to moderate concentrations (i.e., never above 9 M of total $CaCl_2$), mostly at low temperatures (below 150 °C). Ca^{2+} is progressively replaced by $CaCl^+$, which remains the predominant species over the whole range of concentrations and temperatures. This replacement occurs at lower concentrations as temperature increases.

With this model, the $CaCl_2^0$ species always remains in the minority, which may explain its relative instability at the highest concentrations and temperatures.

- *Salt solubility*

Solubility calculations were performed in the binary $CaCl_2$-H_2O system as a function of temperature to provide additional insights into the reliability of the model. This was done in two steps. First, the ionic activity products were calculated at the saturation points defined according to the smoothed recommended values of Pátek et al. [72] who worked extensively on the collection and critical selection of existing solubility data. These ionic activity products were then used to fit temperature-dependent solubility products for each $CaCl_2{\cdot}nH_2O$ solid salt (with n = 0, 1/3, 1, 2, 4, 6) in their respective temperature domain of stability. Finally solid-aqueous solution equilibrium calculations were performed to check the ability of the model to reproduce the $CaCl_2$-H_2O phase diagram.

Because $CaCl^+$ is the major aqueous species in the saturation domain, it is more relevant to write the dissolution reactions of salts with respect to this species, instead of Ca^{2+}. Indeed, especially at high temperature and very high total electrolyte concentration, Ca^{2+} becomes a trace species, which brings instability to the mineral-solution equilibrium calculations. It was found that a simple Van't Hoff approximation could be applied for most hydrates to fit the temperature dependence of the solubility product in the temperature range of interest. The corresponding coefficients are reported in Table 3. The log K values at 25 °C for antarcticite ($CaCl_2{\cdot}6H_2O$), α-$CaCl_2{\cdot}4H_2O$ (or ghiaraite) and $CaCl_2{\cdot}2H_2O$ (or sinjarite) compare very well with those proposed by Lassin et al. [49], which are 3.915, 5.27, and 7.35, respectively.

Results of the solubility calculations as a function of temperature are plotted in Fig. 3. Very good agreement was achieved for the hydrates containing 6 down to 1/3 water molecules, i.e. from 20 °C to 230 °C. Above this, discrepancies can be observed between the recommended

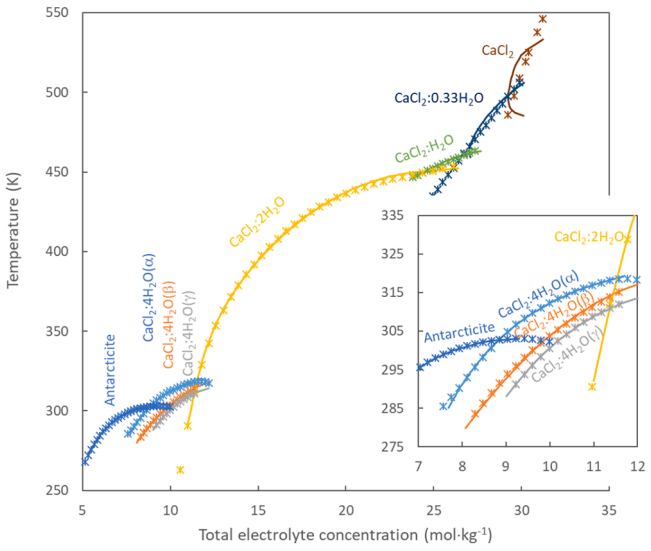

Fig. 3. Solubility of $CaCl_2$ hydrates as a function of temperature. Stars represent the smoothed recommended values of Pátek et al. [72] and lines represent the model calculations (this work).

and the calculated solubility of $CaCl_2$.

An additional criterion is used in the literature to check the quality of the model. It is based on the vapor pressure above solutions saturated with $CaCl_2$ salts as a function of temperature. Details are given in the Supplementary materials (Appendix 4) and results confirm the quality of the model in its temperature range of validity.

Finally, the model developed in this work is able to describe most of the available experimental osmotic coefficient data very satisfactorily, which makes it almost unique in the literature. In addition, it describes the solubility of the various hydrates up to a temperature of 230 °C and a total electrolyte concentration of 29.5 mol·kg^{-1}. However, the model presents several weaknesses regarding its ability to describe derived solution properties like heat capacity and enthalpy. Furthermore, the aqueous speciation calculated at high concentrations and temperatures can be questionable as the presence of larger amounts of the $CaCl_2^0$ aqueous species could be expected.

Further verifications and developments are conducted in the next sections based on the description of aqueous solution properties (like isopiestic properties) and solid-solution equilibria in ternary systems, which were previously studied at 25 °C by Lassin et al. [49] who did not consider the $CaCl^+$ aqueous species in their model. New results are presented below, and the updated and temperature-dependent interaction parameters and solubility products are given in Table 1 and Table 3, respectively. Note that, because the $CaCl_2^0$ aqueous species remains minor in the $CaCl_2$-H_2O binary system for every conditions of temperature and concentration, it was found that the specific ternary interaction parameters involving this species (namely, λ, ζ, η and μ parameters) could be set to 0 for all the ternary systems studied in this work. Thus, to save space, they are not reported in Table 1.

b. The HCl-$CaCl_2$-H_2O system.

For this ternary system, experimental data are available at 25 °C only. Modeling results are compared to these published data in Fig. 4 for the mean activity coefficient of aqueous HCl, and in Fig. 5 for the solubility of calcium chloride hydrates as a function of HCl concentration. With a new σ value of 0.00435 instead of 0.00222 (see the Supplementary materials, Appendix 5), it appears that the mean activity coefficient of HCl is slightly better described by the previous model of Lassin et al. [49], despite 4 ternary interaction parameters, instead of 2, being used in the new model. The solubility of antarcticite is better described by the new model (new σ = 0.01811 compared with 0.02242)

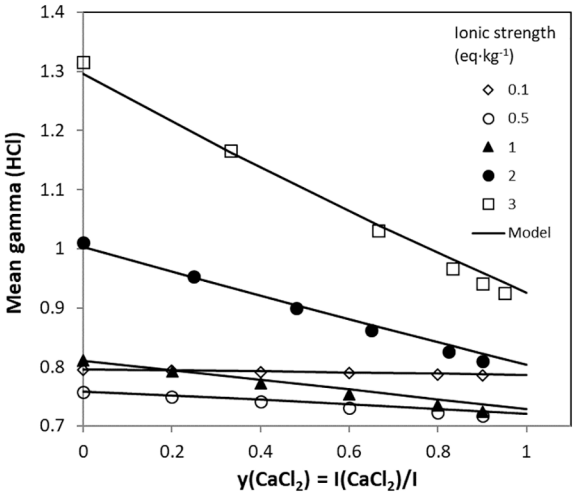

Fig. 4. Mean activity coefficient of HCl in HCl-$CaCl_2$ aqueous mixtures at 25 °C, as a function of $CaCl_2$ ionic strength fraction, y($CaCl_2$), for ionic strengths comprised between 0.1 and 3.0 eq kg^{-1}. The symbols represent experimental measurements from [73]; the lines represent modeling results.

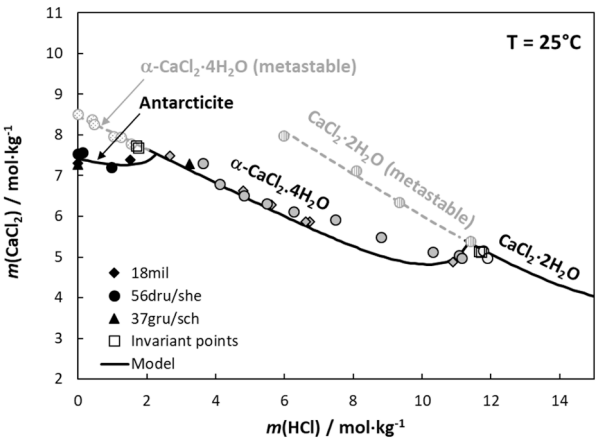

Fig. 5. Solubility diagram for the HCl-$CaCl_2$-H_2O system, at 25 °C. Symbols: experimental data, with circles from [74], diamonds from [75], and triangles from [76]. The black symbols represent antarcticite solubility, the dark gray symbols represent $CaCl_2$·$4H_2O$ solubility, and the light gray symbols represent $CaCl_2$·$2H_2O$ solubility. The solid symbols represent stable minerals while the dotted or hatched symbols designate metastable minerals. The empty squares indicate the invariant points identified by [75] and [76]. The lines represent the solubilities of the stable salts (solid lines) and of the metastable salts (dashed lines) according to model calculations.

like that of the di-hydrate (new σ = 0.01730 compared with 0.02468), whereas that of the tetra-hydrate is better described by the previous model (new σ = 0.02318 compared with 0.01425), especially at high HCl contents. It should be noted that the solubility product of the salts is now constrained by the recommended values of Pátek et al. [72], which was not the case in the previous model.

It must be highlighted here that the aqueous speciation of the $CaCl_2$ electrolyte is affected by the chemical composition of the brine mixture and temperatures. Indeed, the speciation in the ternary HCl-$CaCl_2$-H_2O systems but also in all the other systems presented hereafter (i.e. MCl_n-$CaCl_2$-H_2O with M = Li, Na, K, Mg) differs from the one presented for the binary $CaCl_2$-H_2O system in Fig. A3-3 (Appendix 3, Supplementary materials). This speciation is graphically presented for each system in the Supplementary materials (Appendix 6). Together with what follows, it illustrates that the proposed model is able to describe satisfactorily the solution properties and solution-solid equilibria while considering the chemical complexity of the aqueous mixtures.

c. The LiCl-$CaCl_2$-H_2O system.

Only three interaction parameters were needed to describe this system, namely $\theta(Li^+/Ca^{2+})$, $\theta(Li^+/CaCl^+)$, and $\psi(Li^+/CaCl^+/Cl^-)$. This represents a simplification with respect to our previous 25 °C model, which required 6 non-zero interaction parameters [49]. The results are close to those obtained previously. Thus, they are plotted in the Supplementary materials (Appendix 7), Fig. A7-5 for isowater activity data and in Fig. A7-6 for solubility at 25 °C. Nevertheless, the new model is apparently less accurate for the solubility of antarcticite (new σ = 0.02392 compared with 0.01381). This can be explained by the fact that the solubility of this mineral now takes into account the value recommended by Pátek et al. [72]. For other salts, the new model is either equivalent (for α-$CaCl_2$·$4H_2O$ and LiCl·H_2O; new σ = 0.02313 and 0.03903 compared with 0.01686 and 0.03344, respectively) or slightly better (for the double salt LiCl·$CaCl_2$·$5H_2O$; new σ = 0.01520 compared with 0.03436). Note that the new log K(25 °C) value for this salt is 10.155, which compares well with the value of 10.27 estimated in the previous study, and with the value of 10.60 that was proposed by Christov et al. [77].

Only two sets of solubility data were found for temperatures above 25 °C, namely 40 and 50 °C [78,79]. In addition, Xu et al. [80] recently

produced vapor–liquid equilibrium data for LiCl-$CaCl_2$ aqueous mixtures, from 50 to 150 °C. The latter set of data covers the whole range of mixture fractions from the binary LiCl to the binary $CaCl_2$ brines, for total Cl concentrations comprised between 15 and 20 mol·kg^{-1}. Unfortunately, a preliminary test showed a strong inconsistency between the experimental vapor pressure at equilibrium with the binary LiCl brines and the values calculated with our model. As our LiCl-H_2O model had been thoroughly tested up to 250 °C against large sets of solution properties and solid–liquid equilibrium data [61], it is beyond the scope of this study to perform further verifications. Thus, it was decided to leave these data aside. Yet, it is worth mentioning that the calculated vapor pressures above the binary $CaCl_2$ brine are consistent with the experimental data of Xu et al. [80].

Nevertheless, good agreement was achieved between experimental solubility data and the model at 40 and 50 °C (Fig. 6-C,D) using constant θ parameters for Li^+/Ca^{2+} and $Li^+/CaCl^+$ interactions and a temperature-variable $Li^+/CaCl^+/Cl^-$ interaction parameter ψ (Table 1). At 40 °C (Fig. 6-C), calculations suggest that, in the region of low LiCl concentrations, the experimental data of Blidin [78] describe the metastable solubility of the β-$CaCl_2$·4H_2O solid salt rather than the stable solubility of the α-$CaCl_2$·4H_2O salt.

In addition, Wang et al. [81] and Zeng et al. [79] also produced solubility data at 0 and 10 °C, respectively. Fig. 6-A,B shows the possible extension of our model below 25 °C, down to 0 °C. Note that, at these temperatures, the authors did not specify the polymorph of the calcium chloride tetrahydrate that was formed during their experiment. Calculations suggest that the α polymorph is the possible candidate. However, at 0 °C, in the narrow range of LiCl concentrations comprised between 11 and 14 M, the model correctly describes the solubility of α-$CaCl_2$·4H_2O and LiCl·$CaCl_2$·5H_2O but as metastable phases. Indeed, in this region, the calculated stability of antarcticite appears exaggerated compared to the experimental data of Wang et al. [81]. To reproduce the solubility of the LiCl:$CaCl_2$:5H_2O double salt that is also observed at 25 °C (Fig. A7-6, Appendix 7, Supplementary materials), a temperature dependence of its solubility product was proposed (Table 3).

d. The NaCl-$CaCl_2$-H_2O system.

As for the previous ternary system, results for this chemical system at 25 °C are plotted in Fig. A7-7 (Appendix 7, Supplementary materials), showing a very good match between calculated and experimental data. At this temperature, the new model is equivalent to the previous one for the solubility of antarcticite (new $\sigma = 0.03249$ compared with 0.02735) and of halite (new $\sigma = 0.16983$ compared with 0.17787).

Solubility data between 18 and 130 °C were found in the literature (Fig. 7), mostly in the collections of Zdanovskii et al. [82], Linke [83] and Silcock [84], but also in more recent works by Yang et al. [85]. However, while most of the data collected by Zdanovskii et al. [82] are fairly consistent for each temperature, those from Yang et al. [85] at 75 °C show very different behavior (Fig. 7-C). Because of the very large stability domain of the $CaCl_2$:2H_2O salt, in comparison with the observations made by all the other authors, and at different temperatures, these data were excluded from the optimization procedure.

The results shown in Fig. 7 were obtained by using constant $\theta(Na^+/Ca^{2+})$ and $\theta(Na^+/CaCl^+)$, and temperature-variable $\psi(Na^+/Ca^{2+}/Cl^-)$ and $\psi(Na^+/CaCl^+/Cl^-)$ parameters.

Experimental heat capacity data were also found in the literature. Saluja et al. [69] measured heat capacities of mixtures for ionic strengths comprised between 3 and 5 eq·kg^{-1}, temperatures between 25 and 100 °C, and a pressure of 0.6 MPa. These data could not be used as constraints for the optimization procedure of the model, but can be used for checking as illustrated in Fig. 8.

The comparison of calculated heat capacity with experimental values shows that the data points are distributed below the first bisector. A number of them accumulate along this line, which represents equality of calculated and experimental values. Moreover, the quasi vertical distribution of the points suggests that the heat capacity may be independent of the mixture composition in some specific conditions only. As this is questionable, we conclude that some experimental issues may have occurred during the work of Saluja et al. [86] and, therefore, new experimental data are need for further verifications.

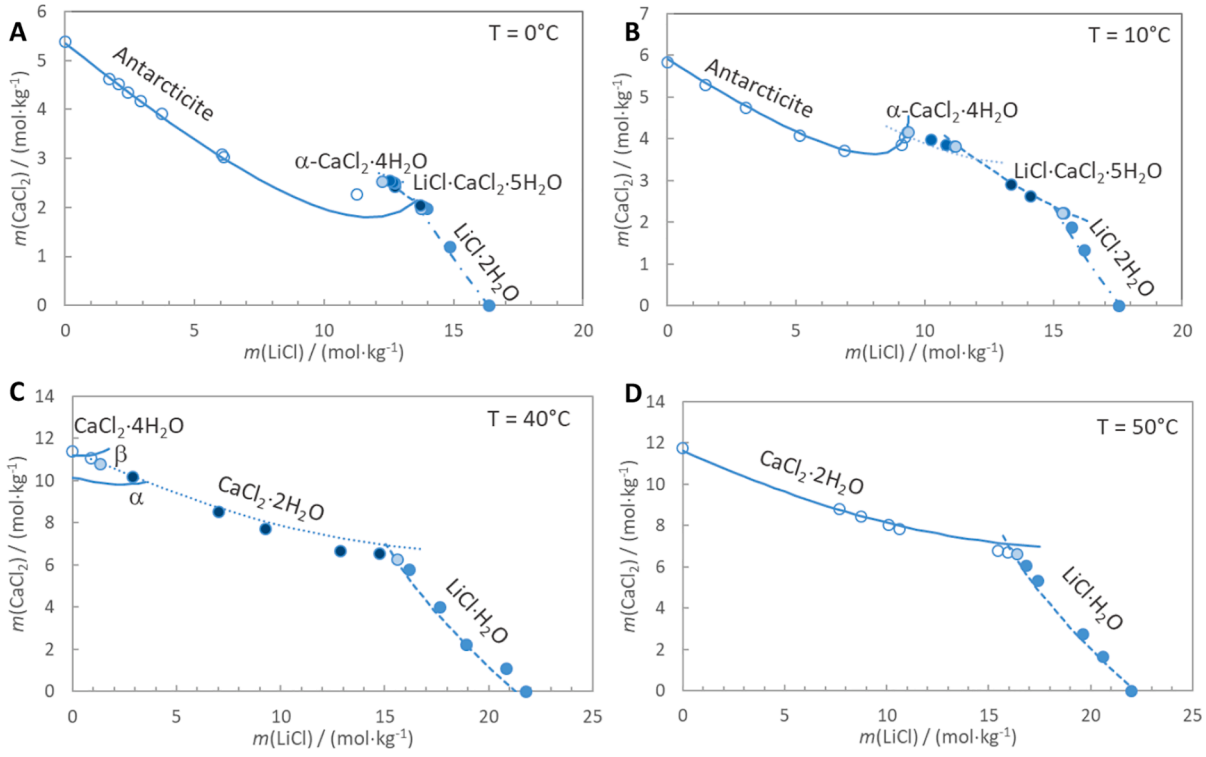

Fig. 6. Solubility diagrams in the LiCl-$CaCl_2$-H_2O system at 0 °C (A), 10 °C (B), 40 °C (C) and 50 °C (D). Symbols: experimental data from [78], [79] and [81]; lines: calculated values with our model.

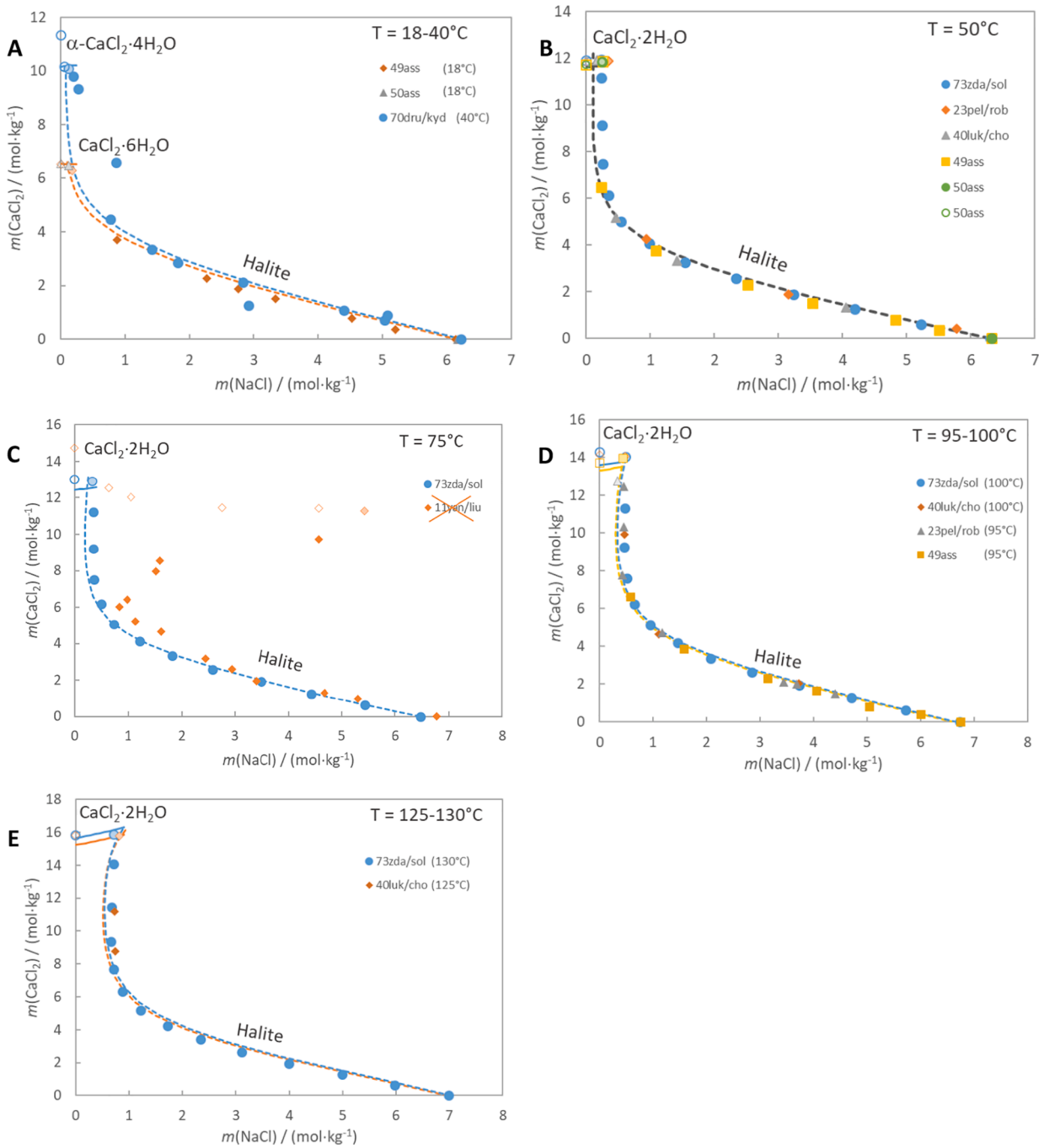

Fig. 7. Solubility diagrams in the NaCl-$CaCl_2$-H_2O system at 18 and 40 °C (A), 50 °C (B), 75 °C (C), 95 and 100 °C (D) and 125 and 130 °C (E). Symbols: experimental data collected and recommended by [82] and from [85]; lines: values calculated with our model.

e. The KCl-$CaCl_2$-H_2O system.

Here again, results for this chemical system at 25 °C are plotted in Fig. A7-8 (Appendix 7, Supplementary materials), showing a very good match between calculated and experimental data. At this specific temperature, the new model is equivalent to the previous one for the solubility of antarcticite (new σ = 0.02111 compared with 0.01940) and of sylvite (new σ = 0.03736 compared with 0.03497).

Solubility data between 18 and 250 °C were found in the literature (Fig. 9), mostly in the collections of Zdanovskii et al. [82], Linke [83] and Silcock [84], as for the previous chemical system. Yang et al. [85] also produced solubility data at 75 °C. Contrary to the NaCl-$CaCl_2$-H_2O system, double salts can form but their identification seems to be challenging. Indeed, among the various authors reported by Zdanovskii et al. [82], Lightfoot and Prutton [87,88] reported the 2KCl:$CaCl_2$:2H_2O hydrated double salt at 75 and 95 °C while Assarsson [89] and Sveshnikova [90,91] reported the KCl:$CaCl_2$ anhydrous double salt for temperatures between 37.8, 43.4, 50 and 95 °C. In addition, Bergman and Kuznetsova [92] observed two polymorphs of this anhydrous double salt, the α being stable between 50 and 150 °C, and the β being stable above these temperatures. Other authors cited in Zdanovskii et al. [82] did not identify any double salts, but various hydrates of the simple $CaCl_2$ salt, instead [93,94]. Yang et al. [85] did not observe any double salt at 75 °C either.

These contradictory observations in fact give some freedom for the model development because several options for the mineralogical

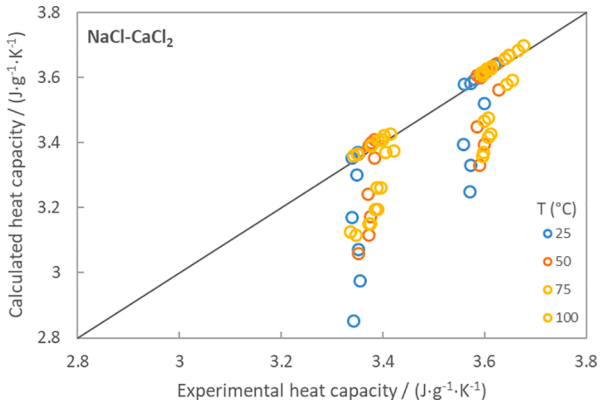

Fig. 8. Calculated vs experimental heat capacity of NaCl-$CaCl_2$ aqueous mixtures, at various temperatures and for ionic strengths comprised between 3 and 5 eq·kg^{-1}. Experimental data of [86].

control of the chemical composition of the saturated solution can be tested. Finally, it was found that temperature variation had to be implemented for three interaction parameters and that three double salts were necessary to fully describe the solubility diagrams of the KCl-$CaCl_2$-H_2O system from 18 to 200 °C, as shown in Fig. 9 and Fig. A7-8 (Appendix 7, Supplementary Materials). The three interaction parameters are $\theta(K^+/CaCl^+)$, $\psi(K^+/Ca^{2+}/Cl^-)$ and $\psi(K^+/CaCl^+/Cl^-)$.

The three double salts are KCl:$CaCl_2$:$2H_2O$, KCl:$CaCl_2$:H_2O and KCl:$CaCl_2$, which are stable between 40 and 95 °C, 95 and 100 °C, and above 100 °C, respectively. They were determined according to the slope and the curvature of the solubility line given by their chemical composition, which better described the experimental data point than any other chemical composition (among those proposed by the various authors cited above).

Fig. 9-A shows that the model can extend to temperatures lower than 25 °C and illustrates that it can help discriminate between experimental data sets. More specifically, the data from Mazzetti (1929, cited in Zdanovskii et al. [82]) should be discarded from the recommended values.

At high temperatures (Fig. 9-G), the new thermodynamic model can be applied up to salt solubility and 200 °C, except in the region where the less hydrated $CaCl_2$ salts are stable. At even higher temperatures, the model becomes unstable and it cannot be used to describe salt solubility. It could however be used at these temperatures for describing solution properties of moderate salinity.

f. The $MgCl_2$-$CaCl_2$-H_2O system.

Both isopiestic and solubility data at 25 °C were correctly described over the whole range of compositions, as shown in Fig. A7-9 (Appendix 7, Supplementary materials). The solubility product of tachyhydrite had to be slightly revised in order to fit the corresponding solubility data points. The revised value is 16.42 (see Table 3), which compares quite well with the previous value of 17.05 proposed by Christov [95]. The consequence is that the new model better describes the solubility of tachyhydrite (new σ = 0.07569 compared with 0.08376). The solubility of antarcticite is also improved (new σ = 0.00470 compared with 0.00902) whereas for other salts, the new model is either equivalent (for α-$CaCl_2$·$4H_2O$ and bischofite: new σ = 0.04667 and 0.04689 compared with 0.03907 and 0.03892, respectively).

For this system, solubility data can be found in the literature up to 110 °C, essentially in the collections of Zdanovskii et al. [82], Linke [83] and Silcock [84]. This chemical system is characterized by an extended region where the solubility is controlled by tachyhydrite at all temperatures (Fig. 10). At 110 °C, however, an additional double salt appears in the solubility diagram. Its chemical composition is $2CaCl_2$:$MgCl_2$:$6H_2O$.

To describe the solid–liquid equilibria of this chemical system (Fig. 10), the temperature variability of the three interaction parameters $\theta(Mg^{2+}/CaCl^+)$, $\psi(Mg^{2+}/Ca^{2+}/Cl^-)$ and $\psi(Mg^{2+}/CaCl^+/Cl^-)$ had to be implemented. It was not possible to define a temperature function for the $2CaCl_2$:$MgCl_2$:$6H_2O$ since it was observed for one temperature only. Its solubility product determined at 110 °C is reported in Table 3.

Solution data were also found in the literature: Saluja et al. [86] provided the heat capacity of $MgCl_2$-$CaCl_2$ aqueous mixtures for ionic strengths comprised between 2.7 and 4.8 eq·kg^{-1}, temperatures between 25 and 100 °C, and a pressure of 0.6 MPa. In addition, Christov [95] performed isopiestic measurements for $MgCl_2$-$CaCl_2$ aqueous mixtures of ionic strengths between 3.7 and 5.9 eq·kg^{-1}, at 50 °C. The chemical compositions of these aqueous mixtures are far from the solubility limits of the system. They do not bring strong constraints to the optimization procedure of the model and, consequently, they were used only for checking as illustrated in Fig. 11. Here, contrary to the NaCl-$CaCl_2$-H_2O system, all the heat capacity data points line up along the first bisector and thus indicate a good match between calculated and experimental values (Fig. 11-A). As expected, the calculated isopiestic lines also fit the experimental data points (Fig. 11-B).

4. Conclusion

A new thermodynamic model has been developed in the framework of the combined HKF-Pitzer equations in order to describe solution properties and phase diagrams of aqueous chloride systems bearing calcium, up to elevated temperatures. This model accounts for the aqueous speciation of the $CaCl_2$ electrolyte, according to the standard partial molar properties of the Ca^{2+}, $CaCl^+$, $CaCl_2^0$ and Cl^- aqueous species described by the HKF theory.

As a result, the $CaCl^+$ aqueous complex and the Cl^- anion are the

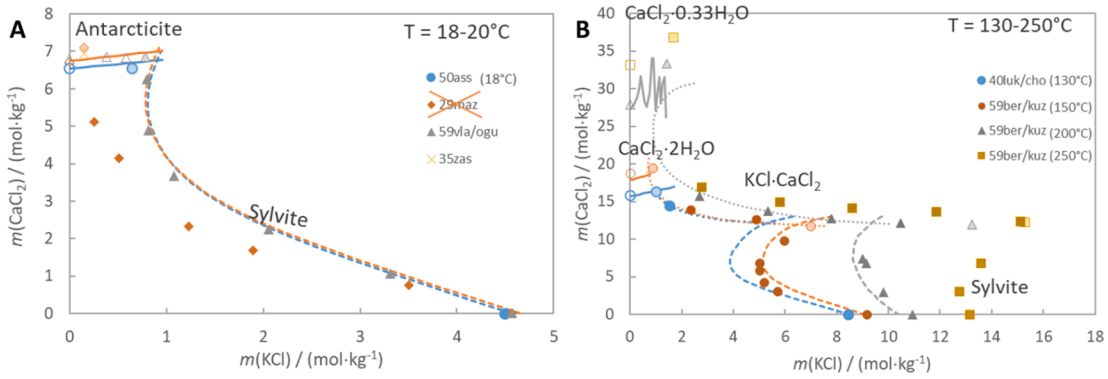

Fig. 9. Solubility diagrams in the KCl-$CaCl_2$-H_2O system at 18 and 20 °C (A), and 130 to 250 °C (B). Symbols: experimental data collected and recommended by [82] and from [85]; lines: calculated values with our model.

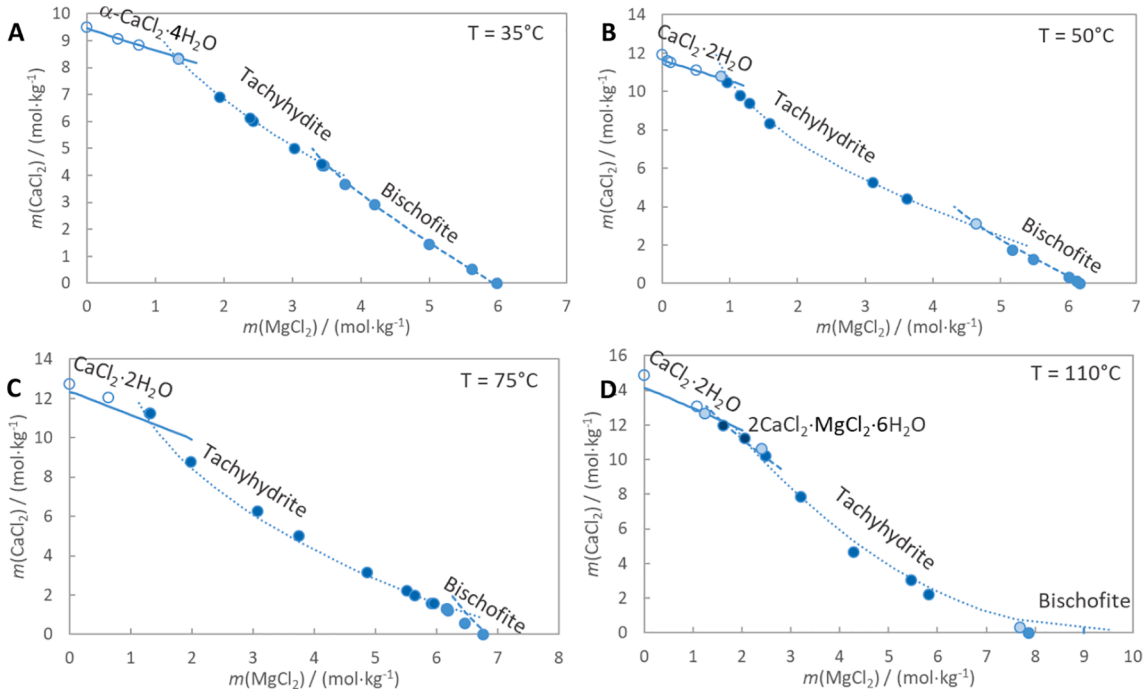

Fig. 10. Solubility diagrams in the $MgCl_2$-$CaCl_2$-H_2O system at 35 °C (A), 50 °C (B), 75 °C (C), and 110 °C (D). Symbols: experimental data collected by [82] and [83]; lines: calculated values with our model.

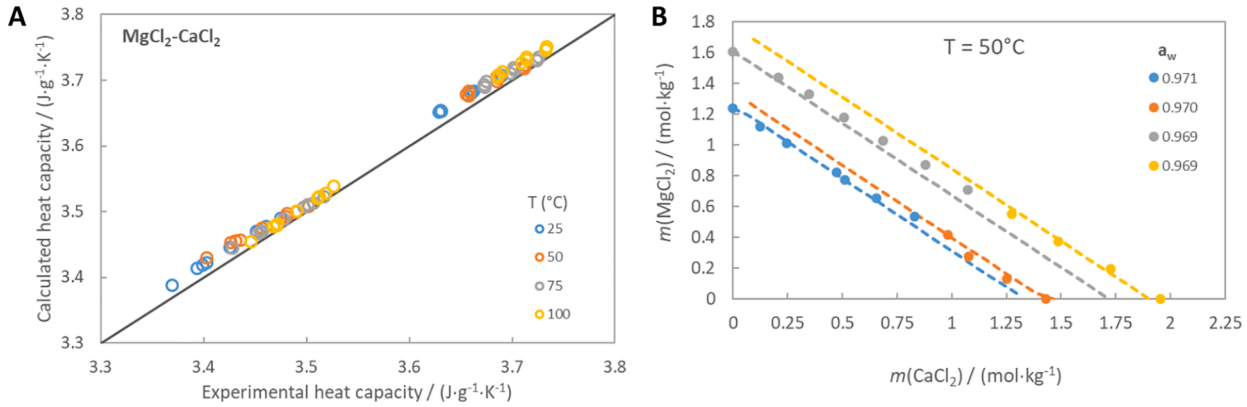

Fig. 11. Calculated vs experimental heat capacity of $MgCl_2$-$CaCl_2$ aqueous mixtures, at various temperatures and for ionic strengths comprised between 3 and 5 eq·kg^{-1} (A), and isopiestic data (B). Experimental heat capacities are taken from [86] and isopiestic measurements from [95].

main species of the $CaCl_2$ electrolyte in most of the investigated conditions of temperature and chemical composition of the system. Despite the complexity induced by partial dissociation, the number of additional ternary interaction parameters needed for describing the chemical behavior of ternary systems remains reasonably limited.

The model applies up to 250 °C in the binary $CaCl_2$ aqueous systems. It can also apply to ternary systems containing other major alkaline and alkaline earth cations, namely Li, Na, K and Mg, up to temperatures generally above 100 °C. The model becomes unstable for ternary systems and temperatures above 200 °C at high concentrations (close to the solubility limits). Therefore, it needs improvements, but at this time and to our knowledge it is the only model with such capabilities that can be used with a free geochemical code like PhreeSCALE. As such, it extends the range of application to hydrothermal environments in the domain of geosciences, or to specific industrial issues dealing with chloride brines like the geological storage of CO_2 in deep saline aquifers.

CRediT authorship contribution statement

Arnault Lassin: Data curation, Writing – original draft. **Laurent André:** Supervision, Validation, Writing – review & editing.

Declaration of Competing Interest

The authors declare that they have no known competing financial interests or personal relationships that could have appeared to influence the work reported in this paper.

Data availability

All the data used in this article are available in the literature

Acknowledgements

This project has received funding from the European Union's

Horizon 2020 research and innovation programme under grant agreement No 850626 (REFLECT Project). The authors cordially thank Sally Ferguson (Alba Traductions) for polishing the English version. The authors are grateful to two anonymous reviewers who helped significantly improve the final manuscript.

Appendix A. Supplementary data

Supplementary data to this article can be found online at https://doi.org/10.1016/j.jct.2022.106927.

References

[1] D.E. Garrett, Handbook of lithium and natural calcium chloride. Their Deposits, Processing, Uses and Properties, Elsevier Academic Press, 2004.
[2] M. Bąbel, B.C. Schreiber, 9.17 - Geochemistry of Evaporites and Evolution of Seawater, in: H.D. Holland, K.K.B.T.-T. on G. (Second E. Turekian (Eds.), Elsevier, Oxford, 2014: pp. 483–560. doi:https://doi.org/10.1016/B978-0-08-095975-7.00718-X.
[3] J.K. Warren, Evaporites through time: Tectonic, climatic and eustatic controls in marine and nonmarine deposits, Earth-Sci. Rev. 98 (2010) 217–268, https://doi.org/10.1016/j.earscirev.2009.11.004.
[4] M. El Tabakh, C. Utha-Aroon, B.C. Schreiber, Sedimentology of the Cretaceous Maha Sarakham evaporites in the Khorat Plateau of northeastern Thailand, Sed. Geol. 123 (1999) 31–62.
[5] T. Lowenstein, F. Risacher, Closed Basin Brine Evolution and the Influence of Ca–Cl Inflow Waters: Death Valley and Bristol Dry Lake California, Qaidam Basin, China, and Salar de Atacama, Chile, Aquat Geochem. 15 (2009) 71–94, https://doi.org/10.1007/s10498-008-9046-z.
[6] T.K. Lowenstein, L.A. Hardie, M.N. Timofeeff, R.V. Demicco, Secular variation in seawater chemistry and the origin of calcium chloride basinal brines, Geology 31 (2003) 857–860.
[7] L.A. Hardie, Secular variation in seawater chemistry: An explanation for the coupled secular variation in the mineralogies of marine limestones and potash evaporites over the past 600 my, Geology 24 (1996) 279–283.
[8] L.A. Hardie, The roles of rifting and hydrothermal $CaCl_2$ brines in the origin of potash evaporites; an hypothesis, Am. J. Sci. 290 (1990) 43–106.
[9] M. Debure, A. Lassin, N.C. Marty, F. Claret, A. Virgone, S. Calassou, E.C. Gaucher, Thermodynamic evidence of giant salt deposit formation by serpentinization: an alternative mechanism to solar evaporation, Sci. Rep. 9 (2019) 11720, https://doi.org/10.1038/s41598-019-48138-9.
[10] V. Scribano, S. Carbone, F.C. Manuella, M. Hovland, H. Rueslåtten, H.-K. Johnsen, Origin of salt giants in abyssal serpentinite systems, Int. J. Earth Sci. 1–14 (2017).
[11] V. Scribano, S. Carbone, F. Manuella, V. Scribano, S. Carbone, F.C. Manuella, Tracking the Serpentinite Feet of the Mediterranean Salt Giant, Geosciences. 8 (2018) 352, https://doi.org/10.3390/geosciences8090352.
[12] P. Szatmari, C.M. de Lima, G. Fontaneta, N. de Melo Lima, E. Zambonato, M. R. Menezes, J. Bahniuk, S.L. Coelho, M. Figueiredo, C.P. Florencio, Petrography, geochemistry and origin of South Atlantic evaporites: The Brazilian side, Mar. Pet. Geol. 127 (2021), 104805.
[13] G. Xu, Fluid inclusions with NaCl–$CaCl_2$–H_2O composition from the Cloncurry hydrothermal system, NW Queensland, Australia, Lithos 53 (2000) 21–35.
[14] D.A. Vanko, R.J. Bodnar, S.M. Sterner, Synthetic fluid inclusions: VIII. Vapor-saturated halite solubility in part of the system NaCl-$CaCl_2$-H_2O, with application to fluid inclusions from oceanic hydrothermal systems, Geochim. Cosmochim. Acta 52 (1988) 2451–2456.
[15] J.L. Bischoff, R.J. Rosenbauer, R.O. Fournier, The generation of HCl in the system $CaCl_2$-H_2O: Vapor-liquid relations from 380–500 C, Geochim. Cosmochim. Acta 60 (1996) 7–16.
[16] A. Richard, J.-M. Montel, R. Leborgne, C. Peiffert, M. Cuney, M. Cathelineau, Monazite Alteration in H_2O–HCl–NaCl–$CaCl_2$ Fluids at 150 °C and psat: Implications for Uranium Deposits, Minerals 5 (2015) 693–706.
[17] K.E. N'Tsoukpoe, H.U. Rammelberg, A.F. Lele, K. Korhammer, B.A. Watts, T. Schmidt, W.K.L. Ruck, A review on the use of calcium chloride in applied thermal engineering, Appl. Therm. Eng. 75 (2015) 513–531, https://doi.org/10.1016/j.applthermaleng.2014.09.047.
[18] L.M. Vrana, Calcium Chloride, Kirk-Othmer Encycl. Chem. Technol. (2001), https://doi.org/10.1002/0471238961.0301120318050904.a01.pub2.
[19] A.D. Pathak, I. Tranca, S.V. Nedea, H.A. Zondag, C.C.M. Rindt, D.M.J. Smeulders, First-principles study of chemical mixtures of $CaCl_2$ and $MgCl_2$ hydrates for optimized seasonal heat storage, J. Phys. Chem. C 121 (2017) 20576–20590.
[20] A. Jabbari-Hichri, S. Bennici, A. Auroux, Enhancing the heat storage density of silica–alumina by addition of hygroscopic salts ($CaCl_2$, $Ba(OH)_2$, and $LiNO_3$), Sol. Energy Mater. Sol. Cells 140 (2015) 351–360.
[21] D. Zhu, H. Wu, S. Wang, Experimental study on composite silica gel supported $CaCl_2$ sorbent for low grade heat storage, Int. J. Therm. Sci. 45 (2006) 804–813.
[22] Q.L. Wu, L. Xiang, Y. Jin, Influence of $CaCl_2$ on the hydrothermal modification of $Mg(OH)_2$, Powder Technol. 165 (2006) 100–104.
[23] S. Vitolo, M.L. Cialdella, Silica separation from reinjection brines at Monte Amiata geothermal plants, Italy, Geothermics. 23 (1994) 257–266.
[24] M. Badruk, I. Matsunaga, Experimental results of silica removal from simulated solutions of geothermal brine of Kizildere field, Turkey, Geothermics 30 (2001) 561–570.
[25] B. Lindal, The production of chemicals from brine and seawater using geothermal energy, Geothermics. 2 (1970) 910–917.
[26] J. Lara Cruz, E. Neyrolles, F. Contamine, P. Cézac, Experimental Study of Carbon Dioxide Solubility in Sodium Chloride and Calcium Chloride Brines at 333.15 and 453.15 K for Pressures up to 40 MPa, J. Chem. Eng. Data 66 (2021) 249–261, https://doi.org/10.1021/acs.jced.0c00592.
[27] D. Tong, J.P.M. Trusler, D. Vega-Maza, Solubility of CO_2 in Aqueous Solutions of $CaCl_2$ or $MgCl_2$ and in a Synthetic Formation Brine at Temperatures up to 423 K and Pressures up to 40 MPa, J. Chem. Eng. Data 58 (2013) 2116–2124, https://doi.org/10.1021/je400396s.
[28] H. Messabeb, F. Contamine, P. Cézac, J.P. Serin, C. Pouget, E.C. Gaucher, Experimental measurement of CO_2 solubility in aqueous $CaCl_2$ solution at temperature from 323.15 to 423.15 K and pressure up to 20 MPa using the conductometric titration, J. Chem. Eng. Data 62 (2017) 4228–4234.
[29] M. Poulain, H. Messabeb, A. Lach, F. Contamine, P. Cézac, J.P. Serin, J.C. Dupin, H. Martinez, Experimental Measurements of Carbon Dioxide Solubility in Na-Ca-K-Cl Solutions at High Temperatures and Pressures up to 20 MPa, J. Chem. Eng. Data 64 (2019) 2497–2503, https://doi.org/10.1021/acs.jced.9b00023.
[30] D. Li, D. Zeng, X. Yin, H. Han, L. Guo, Y. Yao, Phase diagrams and thermochemical modeling of salt lake brine systems. II. NaCl+H_2O, KCl+H_2O, $MgCl_2$+H_2O and $CaCl_2$+H_2O systems, Calphad. 53 (2016) 78–89. doi: https://doi.org/10.1016/j.calphad.2016.03.007.
[31] D.L. Parkhurst, C.A.J. Appelo, Description of input and examples for PHREEQC version 3: a computer program for speciation, batch-reaction, one-dimensional transport, and inverse geochemical calculations, Reston, VA, 2013. http://pubs.er.usgs.gov/publication/tm6A43.
[32] T. Xu, N. Spycher, E. Sonnenthal, G. Zhang, L. Zheng, K. Pruess, TOUGHREACT Version 2.0: A simulator for subsurface reactive transport under non-isothermal multiphase flow conditions, Comput. Geosci. 37 (2011) 763–774, https://doi.org/10.1016/j.cageo.2010.10.007.
[33] C.M. Bethke, S. Yeakel, The Geochemist's Workbench Release 10.0: GWB Essentials Guide, Aqueous Solut. LLC, Champagin, IL, 149p. (2014).
[34] K.S. Pitzer, Thermodynamics of electrolytes. I. Theoretical basis and general equations, J. Phys. Chem. 77 (1973) 268–277.
[35] K.S. Pitzer, J.J. Kim, Thermodynamics of electrolytes. IV. Activity and osmotic coefficients for mixed electrolytes, J. Am. Chem. Soc. 96 (1974) 5701–5707.
[36] A.R. Felmy, J.H. Weare, The prediction of borate mineral equilibria in natural waters: Application to Searles Lake, California, Geochim. Cosmochim. Acta 50 (1986) 2771–2783. http://www.sciencedirect.com/science/article/B6V66-488Y44N-18S/1/38105d1eba0746a14d946286bd690c73.
[37] K.S. Pitzer, L.F. Silvester, Thermodynamics of electrolytes. VI. Weak electrolytes including H3PO4, J. Solution Chem. 5 (1976) 269–278.
[38] C.E. Harvie, N. Møller, J.H. Weare, The prediction of mineral solubilities in natural waters: The Na-K-Mg-Ca-H-Cl-SO_4-OH-HCO_3-CO_3-CO_2-H_2O system to high ionic strengths at 25°C, Geochim. Cosmochim. Acta 48 (1984) 723–751. http://www.sciencedirect.com/science/article/B6V66-48C8HRC-KV/2/9c5c161390a75bc649a798c3f173b26f.
[39] S.L. Clegg, K.S. Pitzer, Thermodynamics of multicomponent, miscible, ionic solutions: generalized equations for symmetrical electrolytes, J. Phys. Chem. 96 (1992) 3513–3520, https://doi.org/10.1021/j100187a061.
[40] S.L. Clegg, K.S. Pitzer, P. Brimblecombe, Thermodynamics of Multicomponent, Miscible, Ionic Solutions. 2. Mixtures Including Unsymmetrical Electrolytes, J. Phys. Chem. 96 (1992) 9470–9479. doi:10.1021/j100202a074.
[41] C. Christov, Thermodynamics of formation of double salts and mixed crystals from aqueous solutions, J. Chem. Thermodyn. 37 (2005) 1036–1060. http://www.sciencedirect.com/science/article/B6WHM-4FM3X02-1/2/4f6c08d9cc44293d420e360e55d1e306.
[42] V.K. Filippov, N.A. Charykov, N.D. Solechnik, Thermodynamics of the Systems Ni // Cl, SO_4-H_2O and Co // Cl, SO_4-H_2O at 25°C, J. Appl. Chem. USSR. 58 (1985) 1811–1814.
[43] S.V. Petrenko, K.S. Pitzer, Thermodynamics of aqueous NaOH over the complete composition range and to 523 K and 400 MPa, J. Phys. Chem. B 101 (1997) 3589–3595.
[44] N. Møller, The prediction of mineral solubilities in natural waters: A chemical equilibrium model for the Na-Ca-Cl-SO_4-H_2O system, to high temperature and concentration, Geochim. Cosmochim. Acta 52 (1988) 821–837, https://doi.org/10.1016/0016-7037(88)90354-7.
[45] K.S. Pitzer, C.S. Oakes, Thermodynamics of calcium chloride in concentrated aqueous solutions and in crystals, J. Chem. Eng. Data 39 (1994) 553–559.
[46] S.M. Sterner, A.R. Felmy, C.S. Oakes, K.S. Pitzer, Correlation of thermodynamic data for aqueous electrolyte solutions to very high ionic strength using INSIGHT: Vapor saturated water activity in the system CaCl2-H2O to 250 °C and solid saturation, Symp. Thermophys. Prop. 19 (1998) 761–770.
[47] J.P. Greenberg, N. Møller, The prediction of mineral solubilities in natural waters: A chemical equilibrium model for the Na-K-Ca-Cl-SO_4-H_2O system to high concentration from 0 to 250°C, Geochim. Cosmochim. Acta 53 (1989) 2503–2518, https://doi.org/10.1016/0016-7037(89)90124-5.
[48] A. Lach, K. Ballerat-Busserolles, L. André, M. Simond, A. Lassin, P. Cézac, J.C. Neyt, J.P. Serin, Experimental Data and Modeling of Solution Density and Heat Capacity in the Na-K-Ca-Mg-Cl-H_2O System up to 353.15 K and 5 mol·kg-1 Ionic Strength, J. Chem. Eng. Data 62 (2017) 3561–3576, https://doi.org/10.1021/acs.jced.7b00553.

[49] A. Lassin, L. André, A. Lach, A.L. Thadée, P. Cézac, J.P. Serin, Solution properties and salt-solution equilibria in the H-Li-Na-K-Ca-Mg-Cl-H_2O system at 25 °C: A new thermodynamic model based on Pitzer's equations, CALPHAD: Comput. Coupling Phase Diagrams Thermochem. 61 (2018) 126–139, https://doi.org/10.1016/j.calphad.2018.03.005.

[50] H.C. Helgeson, D.H. Kirkham, G.C. Flowers, Theoretical prediction of the thermodynamic behavior of aqueous electrolytes at high pressures and temperatures: IV. Calculation of activity coefficients, osmotic coefficients, and apparent molal and standard and relative partial molal properties to 600°C, Am. J. Sci. 281 (1981) 1249–1516.

[51] J.C. Tanger, H.C. Helgeson, Calculation of the thermodynamic and transport properties of aqueous species at high pressures and temperatures: Revised equations of state for the standard partial molal properties of ions and electrolytes, Am. J. Sci. 288 (1988) 19–98.

[52] J.W. Johnson, E.H. Oelkers, H.C. Helgeson, SUPCRT92: a software package for calculating the standard molal thermodynamic properties of minerals, gases, and aqueous species from 1 to 5000 bars and 0° to 1000°C, Comput. Geosci. 18 (1992) 899–947.

[53] C. Hervé, S. Ye, L. Bernard, A. Jacques, X. Pierre, Calculation of CO_2, CH_4 and H_2S solubilities in aqueous electrolyte solution at high pressure and high temperature, J. Therm. Sci. 6 (1997) 251–259.

[54] N.N. Akinfiev, M.V. Mironenko, S.A. Grant, Thermodynamic properties of NaCl solutions at subzero temperatures, J. Solution Chem. 30 (2001) 1065–1080, https://doi.org/10.1023/A:1014445917207.

[55] P.F. dos Santos, L. Andre, M. Ducousso, A. Lassin, F. Contamine, A. Lach, M. Parmentier, P. Cézac, An improved model for CO2 solubility in aqueous Na^+–Cl^-–SO_4^{2-} systems up to 473.15 K and 40 MPa, Chem. Geol. 582 (2021), 120443.

[56] A.W. Hakin, J. Lian Liu, K. Erickson, J.-V. Munoz, Apparent molar heat capacities and apparent molar volumes of $Pr(ClO_4)_{3(aq)}$, $Gd(ClO_4)_{3(aq)}$, $Ho(ClO_4)_{3(aq)}$, and $Tm(ClO_4)_{3(aq)}$ at T=(288.15, 298.15, 313.15, and 328.15) K and p=0.1 MPa, J. Chem. Thermodyn. 36 (2004) 773–786, https://doi.org/10.1016/j.jct.2004.02.004.

[57] M.M. Lencka, R.E. Riman, Thermodynamic modeling of hydrothermal synthesis of ceramic powders, Chem. Mater. 5 (1993) 61–70.

[58] A. Lach, F. Boulahya, L. André, A. Lassin, M. Azaroual, J.P. Serin, P. Cézac, Thermal and volumetric properties of complex aqueous electrolyte solutions using the Pitzer formalism – The PhreeSCALE code, Comput. Geosci. 92 (2016) 58–69, https://doi.org/10.1016/j.cageo.2016.03.016.

[59] D.A. Sverjensky, E.L. Shock, H.C. Helgeson, Prediction of the thermodynamic properties of aqueous metal complexes to 1000°C and 5 kb, Geochim. Cosmochim. Acta 61 (1997) 1359–1412.

[60] C. Christov, N. Møller, A chemical equilibrium model of solution behavior and solubility in the H-Na-K-Ca-OH-Cl-HSO_4-SO_4-H_2O system to high concentration and temperature, Geochim. Cosmochim. Acta 68 (2004) 3717–3739. http://www.sciencedirect.com/science/article/B6V66-4D5NKMD-8/2/89ea28788f535121249a01bb71cac712.

[61] A. Lassin, C. Christov, L. André, M. Azaroual, A thermodynamic model of aqueous electrolyte solution behavior and solid-liquid equilibrium in the Li-H-Na-K-Cl-OH-H_2O system to very high concentrations (40 molal) and from 0 to 250 °C, Am. J. Sci. 315 (2015) 204–256, https://doi.org/10.2475/03.2015.02.

[62] D. Zeng, H. Zhou, W. Voigt, Thermodynamic consistency of solubility and vapor pressure of a binary saturated salt + water system: II. $CaCl_2$ + H_2O, Fluid Phase Equilib. 253 (2007) 1–11. http://www.sciencedirect.com/science/article/B6TG2-4MS3J8V-2/2/a4e0f8871723d150ecefef6c588b5fcd.

[63] M.S. Gruszkiewicz, J.M. Simonson, Vapor pressures and isopiestic molalities of concentrated $CaCl_{2(aq)}$, $CaBr_{2(aq)}$, and $NaCl_{(aq)}$ to T = 523 K, J. Chem. Thermodyn. 37 (2005) 906–930. http://www.sciencedirect.com/science/article/pii/S0021961405000030.

[64] R. Azougen, M. El Guendouzi, A. Rifai, J. Faridi, Water activities, activity coefficients and solubility in the binary and ternary aqueous solutions with LiCl + YCl_2 + H_2O with Y = Mg^{2+}; Ca^{2+}; or Ba^{2+}, Calphad 34 (2010) 36–44. http://www.sciencedirect.com/science/article/B6TWC-4XRB1VD-1/2/b6bdb58303c41fe04e8d197162637b92.

[65] J.A. Rard, S.L. Clegg, Critical Evaluation of the Thermodynamic Properties of Aqueous Calcium Chloride. 1. Osmotic and Activity Coefficients of 0–10.77 $mol.kg^{-1}$ Aqueous Calcium Chloride Solutions at 298.15 K and Correlation with Extended Pitzer Ion-Interaction Models, J. Chem. Eng. Data 42 (1997) 819–849, https://doi.org/10.1021/je9700582.

[66] H.F. Holmes, R.H. Busey, J.M. Simonson, R.E. Mesmer, $CaCl_{2(aq)}$ at elevated temperatures. Enthalpies of dilution, isopiestic molalities, and thermodynamic properties, J. Chem. Thermodyn. 26 (1994) 271–298, https://doi.org/10.1016/0021-9614(94)90005-1.

[67] G. Perron, A. Roux, J.E. Desnoyers, Heat capacities and volumes of NaCl, $MgCl_2$, $CaCl_2$, and $NiCl_2$ up to 6 molal in water, Can. J. Chem. 59 (1981) 3049–3054, https://doi.org/10.1139/v81-446.

[68] J. Ananthaswamy, G. Atkinson, Thermodynamics of Concentrated Electrolyte Mixtures. 5. A Review of the Thermodynamic Properties of Aqueous Calcium Chloride in the Temperature Range 273.15-373.15 K, J. Chem. Eng. Data 30 (1985) 120–128, https://doi.org/10.1021/je00039a035.

[69] P.P.S. Saluja, D.J. Jobe, J.C. LeBlanc, R.J. Lemire, Apparent Molar Heat Capacities and Volumes of Mixed Electrolytes: [$NaCl_{(aq)}$ + $CaCl_{2(aq)}$], [$NaCl_{(aq)}$ + $MgCl_{2(aq)}$], and [$CaCl_{2(aq)}$ + $MgCl_{2(aq)}$], J. Chem. Eng. Data 40 (1995) 398–406, https://doi.org/10.1021/je00018a007.

[70] N. Gao, G. Chen, Y. Jiang, Y. He, Isobaric heat capacity of potential liquid desiccant solutions containing calcium chloride and its mixtures, HVAC&R Res. 20 (2014) 328–331, https://doi.org/10.1080/10789669.2014.888907.

[71] K.S. Pitzer, Activity coefficients in electrolyte solutions, CRC Press. (1991) 542.

[72] J. Pátek, J. Klomfar, M. Součková, Solid−Liquid Equilibrium in the System of $CaCl_2$−H_2O with Special Regard to the Transition Points, J. Chem. Eng. Data 53 (2008) 2260–2271, https://doi.org/10.1021/je800009w.

[73] K.H. Khoo, C.-Y. Chan, T.-K. Lim, Thermodynamics of electrolyte solutions. The system HCl+$CaCl_2$+H_2O at 298.15 K, J. Solution Chem. 6 (1977) 651–662.

[74] I.G. Druzhinin, A.I. Shepelev, No Title, Tr. Instituta Khimii AN KirgCCP. 7 (1956).

[75] J. Milikan, Die oxyhaloide der alkalischen erden. Gleichgewichte in ternaren systemen II, Z. Phys. Chem. 92 (1918) 496–520.

[76] V. Grushvitskii, N. Schmidt, No Title, Bols. Emba. Izd. An. USSR I (1937) 671–676.

[77] C. Christov, S. Velikova, K. Ivanova, Study of (m1LiX + m2CaX2)(aq) where mi denotes molality and X denotes Cl, or Br at the temperature 298.15 K, J. Chem. Thermodyn. 32 (2000) 1505–1512. http://www.sciencedirect.com/science/article/B6WHM-45FC60C-K/2/8afb2673671401218e29e5f4ae1c8a66.

[78] V.P. Blidin, No Title, Izv. Akad. Nauk SSSR, Otd. Khim. Nauk. 3 (1954) 400.

[79] D. Zeng, W. Xu, W. Voigt, X. Yin, Thermodynamic study of the system (LiCl + $CaCl_2$ + H_2O), J. Chem. Thermodyn. 40 (2008) 1157–1165. http://www.sciencedirect.com/science/article/B6WHM-4RXJYTY-1/2/7f24e696f5c7d82c34731e76195ac477.

[80] X. Xu, Y. Wang, X. Sun, Y. Zhou, Vapor−Liquid Equilibria Study of the LiCl + $CaCl_2$ + H_2O System, (2019). doi:10.1021/acsomega.8b03570.

[81] X. Wang, K. Zhao, Y. Guo, T. Deng, L. Meng, Experimental Determination and Thermodynamic Model of Solid-Liquid Equilibria in the Ternary System (LiCl+ $CaCl_2$+ H_2O) at 273.15 K, J. Chem. Eng. Data 64 (2018) 249–254.

[82] A.B. Zdanovskii, E.F. Solov'eva, E.I. Lyakhovskaya, N.E. Shestakov, R.E. Shleimovich, L.M. Abutkova, Experimental solubility data on salt - water systems. Vol. 1, Three component systems, second ed., "Chemistry" Publishing, Leningrad, 1973.

[83] W. Linke, Solubilities of inorganic and metal-organic compounds, fourth ed., American Chemical Society, Washington, 1965.

[84] H.L. Silcock, Solubilities of Inorganic and Organic Compounds. Ternary and multicomponent systems of inorganic substances, Pergamon Press, 1979. https://books.google.fr/books?id=FwW8kgEACAAJ.

[85] J. Yang, X. Liu, P.-P. Liang, Solubilities of salts in the ternary systems NaCl + $CaCl_2$ + H_2O and KCl + $CaCl_2$ + H_2O at 75°C, Russ. J. Phys. Chem. A 85 (2011) 1149–1154, https://doi.org/10.1134/S0036024411070090.

[86] P.P.S. Saluja, D.J. Jobe, J.C. LeBlanc, R.J. Lemire, Apparent molar heat capacities and volumes of mixed electrolytes:[$NaCl_{(aq)}$ + $CaCl_{2(aq)}$],[$NaCl_{(aq)}$ + $MgCl_{2(aq)}$], and [$CaCl_{2(aq)}$ + $MgCl_{2(aq)}$], J. Chem. Eng. Data 40 (1995) 398–406.

[87] W.J. Lightfoot, C.F. Prutton, Equilibria in Saturated Salt Solutions. II. The Ternary Systems $CaCl_2$-$MgCl_2$-H_2O, $CaCl_2$-KCl-H_2O and $MgCl_2$-KCl-H_2O at 75°, J. Am. Chem. Soc. 69 (1947) 2098–2100.

[88] W.J. Lightfoot, C.F. Prutton, Equilibria in Saturated Solutions. I. The Ternary Systems CaCl2-$MgCl_2$-H_2O, $CaCl_2$-KCl-H_2O, and $MgCl_2$-KCl-H_2O at 35°, J. Am. Chem. Soc. 68 (1946) 1001–1002.

[89] G.O. Assarsson, Equilibria in Aqueous Systems Containing K^+, Na^+, Ca^{+2}, Mg^{+2} and Cl^-. I. The Ternary System $CaCl_2$-KCl-H_2O, J. Am. Chem. Soc. 72 (1950) 1433–1436.

[90] V.N. Sveshnikova, No Title, Dokl. Akad. Nauk. S.S.S.R. 79 (1951) 447–50.

[91] V.N. Sveshnikova, No Title, Izvest. Akad. Nauk. S.S.S.R. Otd. Khim. (1952) 44–51.

[92] A.G. Bergman, A.I. Kuznetsova, Diagramma rastvorimosti troinoi sistemy H_2O-KCl-$CaCl_2$ ot temperatury polnogo zamerzaniya do 300-gradusakh, Zhurnal Neorg. Khimii. 4 (1959) 194–204.

[93] E.I. Lukyanova, D.N. Shoikhet, No Title, Tr. Gos. Inst. Prikl. Khim. 34 (1940).

[94] N.A. Vlasov, S.V. Ogienko, Solubility polytherms of the system $CaCl_2$–KCl–H_2O from the temperature of complete freezing to+ 40, Izv. Fiz.-Khim. Nauchn.-Issled. Inst. Pri Irkutsk. Univ. 4 (1959) 62–80.

[95] C. Christov, Isopiestic Determination of the Osmotic Coefficients of an Aqueous $MgCl_2$ + $CaCl_2$ Mixed Solution at (25 and 50)°C. Chemical Equilibrium Model of Solution Behavior and Solubility in the $MgCl_2$ + H_2O and $MgCl_2$ + $CaCl_2$ + H_2O Systems to High Concentration at (25 and 50)°C, J. Chem. Eng. Data 54 (2009) 627–635. http://pubs.acs.org/doi/abs/10.1021/je8005634.

8.4 Appendix 4

Lassin A., Felipe dos Santos P., Ducousso M., Cézac P., André L. (2022). *Experimental measurements and modelling of thermodynamic properties of NaCl-$CaCl_2$ aqueous solutions up to high temperatures and CO_2 pressures.* **European Geothermal Congress 2022, Berlin, Germany, extended abstract.**

Experimental measurements and modelling of thermodynamic properties of NaCl-$CaCl_2$ aqueous solutions up to high temperatures and CO_2 pressures

Arnault Lassin[1], Pedro Felipe dos Santos[2], Marion Ducousso[2], Pierre Cézac[2], Laurent André[1,3]

[1] BRGM, 3 avenue C. Guillemin, 45060 Orléans, France

[2] Universite de Pau et des Pays de l'Adour, E2S UPPA, LaTEP, Pau, France

[3] Université d'Orléans, CNRS, BRGM, ISTO UMR 7327, 45071 Orléans, France

a.lassin@brgm.fr

Keywords: Brines chemistry, thermodynamics, geochemical modelling, CO_2 solubility.

ABSTRACT

Geothermal energy currently uses hot deep brines. However, their exploitation can raise issues specifically due to their high salinity and the variations of temperature and pressure during their pumping. Main disorders are the potential degassing of fluids, including CO_2, but also the precipitation of minerals in the facilities (production/injection wells, heat exchangers…) involving expensive maintenance works.

The chemical and physical properties of the geothermal fluids are key control factors, determining the heat-carrying potential for energy transfer over the lifetime of the well. An improved understanding of the properties of these fluids is therefore necessary to avoid exploitation issues as mentioned above, and even optimize site developments and operations. Additionally, the future for exploration, prediction and utilization of novel geothermal technologies – namely enhanced geothermal systems and supercritical resources – is intimately tied to the understanding of the physical and chemical properties of the reservoir fluids.

The REFLECT project aims to improve the accuracy and consistency of key thermodynamic and kinetic input data in order to optimize sustainable geothermal reservoir management, power and heat production and reinjection strategies. Geochemical modelling, which relies on the measurement of high quality data, is one of the numerical approaches needed to reach this goal.

In a first step, published laboratory measurements were collected to estimate the properties of saline chloride fluids (NaCl and $CaCl_2$) containing dissolved CO_2. A focus was made on properties such as CO_2 solubility for medium temperature brines up to 473.15 K.

In parallel to data collection, a modelling work was set-up to calculate these fluid properties using the specific tool named PhreeSCALE. Relying on the Pitzer equations, it is able to compute thermal and volumetric properties of aqueous solutions such as heat capacity or density of the geothermal fluids.

The methodology relies on successive steps that include the estimation of Pitzer's interaction parameters for the $CaCl_2$-H_2O, $CaCl_2$-NaCl-H_2O, and $CaCl_2$-NaCl-CO_2-H_2O systems to reproduce literature data. The model applies from 298.15 up to 473.15 K, and to elevated pressures.

1. INTRODUCTION

Geothermal energy currently uses hot deep brines. However, their exploitation can raise issues specifically due to their high salinity and the variations of temperature and pressure during their pumping. Main disorders are the potential degassing of fluids including CO_2, but also the development of scaling in the facilities (production/injection wells, heat exchangers…) involving expensive maintenance works (Eroini, 2011; Boch et al., 2017; Todd and Bluemle, 2022).

Moreover, these processes are interrelated since the degassing of CO_2 is generally concomitant with water evaporation, pressure and temperature decrease during heat extraction operations (Alt-Epping et al., 2013). The chemical disturbances induced by the outgassing (increase of concentrations and of pH) strongly favour mineral precipitation, and thus scaling (Thomas and Gudmundsson, 1989; Benoit, 1989; Simmons and Christenson, 1994). It is therefore of major interest to develop a sound knowledge of CO_2 solubility in hot and pressurized brines. The REFLECT project (https://www.reflect-h2020.eu/) aims to improve the accuracy and consistency of key thermodynamic and kinetic input data in order to optimize sustainable geothermal reservoir management, power and heat production and reinjection strategies. More specifically and in line with the scaling issues, one objective of the project is to improve the modelling capacity to predict CO_2 degassing in the facility.

Because of the environmental issues related to the climate change resulting (at least partly) from human activity, the exploitation of the underground as a source of decarboned energy, or as a large volume to store permanently waste gases (e.g., CO_2) or temporarily energy vectors (natural gas, hydrogen, heat), has regained much interest (Kelemen et al., 2019; Zivar et al., 2021; Mahon et al., 2022). The knowledge developed in these domains can be beneficial to geothermal energy. This is particularly true for experimental CO_2 solubility data in brines, acquired in the context of the carbon capture and underground storage technology (CCUS) (Carvalho et al., 2015; Mohammadian et al., 2015; Chabab et al., 2019).

In this context, various chemical systems have been studied until recently and are now well known (dos Santos et al., 2021a, 2021b, 2020; Messabeb et al., 2017, 2016; Poulain et al., 2019; and references there in). However, many chemical systems still need to be investigated or their description improved. As an additional contribution to these developments, the present work focuses on the $CaCl_2$-NaCl-CO_2-H_2O system. It relies on the collection of bibliographic CO_2 solubility data and on their numerical exploitation to develop a robust geochemical model with predictive capabilities.

2. BACKGROUND AND METHOD

2.1 Collection of experimental CO_2 solubility data

In order to study the $CaCl_2$-NaCl-CO_2-H_2O system, focus must be made on the simpler $CaCl_2$-CO_2-H_2O and NaCl-CO_2-H_2O systems first. The latter is already well known (see the extensive experimental data collection by dos Santos et al., 2021b) and described with dedicated models (dos Santos et al., 2021b; Duan et al., 2006; Shi and Mao, 2017; Zhaoa et al., 2015). The former is a little less known, despite some thermodynamic models have been developed (Appelo, 2015; Bastami et al., 2014; Shi and Mao, 2017; Springer et al., 2012; Zhao et al., 2015). New experimental CO_2 solubility data in $CaCl_2$ synthetic brines have been acquired since (Lara Cruz et al., 2021; Messabeb et al., 2017; Poulain et al., 2019). They cover ranges of pressures and temperatures that are complementary to previously published data. Indeed, they either extend the pressure and salinity ranges or refine the pressure intervals between measurements (see below). In summary, the temperature, pressure and $CaCl_2$ concentration values covered by all published CO_2 solubility data range between 293 and 424 K, 0.1 and 40 MPa, and 0 and 6.3 mol·kg^{-1}, respectively. Some inconsistencies can be noticed among all these sets of data and, in some occasions, within datasets from same authors. More specifically, Prutton and Savage (1945) indicate experimental uncertainties of 3%, but when compared with other datasets, discrepancies of up to 20% can be found. Bastami et al. (2014) do not provide any indication on their uncertainties, which complicates the comparison with other datasets and models. Tong et al. (2013) and Liborio (2017) also reported experimental errors of up to 10 and 15% in their respective datasets. Consequently, a lower weight was given to these datasets while developing the geochemical model for the $CaCl_2$-CO_2-H_2O system.

Experimental CO_2 solubility data for the $CaCl_2$-NaCl-CO_2-H_2O system were essentially acquired by Lara Cruz et al. (2021), Liu et al. (2011), Poulain et al. (2019), Zhao et al. (2015a), representing almost 70 data points. The temperature, pressure, NaCl and $CaCl_2$ concentration values covered by these data range between 318 and 453 K, 1.2 and 40 MPa, 0.95 and 2.99 mol·kg^{-1}, and 0.2 and 0.67 mol·kg^{-1}, respectively.

2.2 Numerical modelling

Thermodynamic equilibrium between the CO_2-rich phase and the aqueous solution in the autoclave can be described according to the equality of the chemical potential of CO_2 in the two phases. This results in the following equation that corresponds to Henry's law (Appelo et al., 2014):

$$m_{CO_2} = \frac{\varphi_{CO_2}^{vap} \times P \times y_{CO_2}}{\gamma_{CO_2}^{m}} \times K_H \times exp\left(-\frac{V_{m,CO_2}(P-P_0)}{RT}\right) \times \frac{m_0}{P_0} \quad [1]$$

m_{CO_2} is the molality of aqueous CO_2 (mol·kg^{-1}), $\varphi_{CO_2}^{vap}$ is the fugacity coefficient of CO_2 in the gas (or supercritical) phase (unitless), P is the total gas pressure (Pa), y_{CO_2} is the mole fraction of CO_2 in the gas phase (unitless), $\gamma_{CO_2}^{m}$ is the activity coefficient of aqueous CO_2 (unitless), K_H (unitless) is the Henry's law constant for the dissolution reaction of CO_2(g) into CO_2^0, V_{m,CO_2} is the partial molar volume of aqueous CO_2 (m^3·mol^{-1}), P_0 is the reference pressure (= 10^5 Pa), R is the ideal gas constant (= 8.31446 J·mol^{-1}·K^{-1}), T is the absolute temperature (K) and m_0 is the reference molality (=1 mol·kg^{-1}).

m_{CO_2} and y_{CO_2} are the unknowns of equation [1], P and T are constraints, V_{m,CO_2} is described by the HKF equation of state for aqueous species (Helgeson et al., 1981; Tanger and Helgeson, 1988), $\varphi_{CO_2}^{vap}$ is determined by the Peng-Robinson equation of state, $\gamma_{CO_2}^{m}$ is computed according to the Pitzer equations. More details about the latter equations can be found in Pitzer (1991). More specifically, the activity coefficient of aqueous CO_2 can be expressed as follows (dos Santos et al., 2021b):

$$\ln\left(\gamma_{CO_2}^{m}\right) = 2m_{CO_2}\lambda_{CO_2,CO_2} + \sum_{c=1}^{n_c} 2m_c\lambda_{CO_2,c} + \sum_{a=1}^{n_a} 2m_a\lambda_{CO_2,a} + \sum_{c=1}^{n_c}\sum_{a=1}^{n_a} m_c m_a \zeta_{CO_2,c,a} \quad [2]$$

λ_{CO_2,CO_2}, $\lambda_{CO_2,c}$, $\lambda_{CO_2,a}$ are binary Pitzer interaction parameters between two molecules of CO_2^0, one molecule of CO_2^0 and a cation c, and one molecule of CO_2^0 and an anion a, respectively. $\zeta_{CO_2,c,a}$ is a ternary Pitzer interaction parameter between one molecule of CO_2^0, a cation c and an anion a. n_c and n_a are the number of different cations and anions in the solution, respectively. As the Pitzer equation are semi-empirical, these specific interaction parameters cannot be determined *a priori* and must be fitted using

experimental data, like gas solubility in brines amongst others.

In the present work, geochemical calculations are done at thermodynamic equilibrium using the PhreeSCALE software (Lach et al., 2016). It results from an evolution of PhreeqC (Parkhurst and Appelo, 2013), a software that is widely used in the geochemical modelling community. The Pitzer equations that are implemented in these two calculation codes can handle partial dissociation of electrolytes but are limited to ionic strength-dependent viral contributions of second order. Compared to PhreeqC, PhreeSCALE includes a more rigorous treatment of the partial derivatives of the Pitzer equations of the excess Gibbs free energy of the solutes. Consistent thermal and volumetric properties of aqueous solutions such as heat capacity or density of geothermal fluid can be calculated too.

To fit the specific interaction parameters involving CO_2^0, an additional numerical tool named PEST (Doherty, 2004) is used in combination with PhreeSCALE. Starting from an initial set of interaction parameter values, PEST launches PhreeSCALE, which computes the concentration of dissolved CO_2. PEST then compares the results to the experimental values. As long as convergence criterion is not met, PEST suggests a new set of parameter values and launches PhreeSCALE again. When the convergence criterion is met, the fitting procedure stops and the last set of parameters proposed by PEST is saved.

The development of a consistent thermodynamic database is a long term process, and thus necessarily incremental. Therefore, the procedure above must be applied based on pre-existing models for the investigated brines. In the present work, we use the chemical model recently developed by Lassin et al. (submitted) for the NaCl-$CaCl_2$-H_2O system, and the one developed by (dos Santos et al., 2021b) for the CO_2-NaCl-H_2O system. Indeed, the models mentioned previously (section 2.1) mostly apply to the solubility of CO_2 in simple binary brines, while the objective here is to consider a mixture of brines whose description is not a straightforward addition of two models for binary brines.

The model of Lassin et al. (submitted) for the NaCl-$CaCl_2$-H_2O system is based on the Pitzer equations and includes the partial dissociation of the $CaCl_2$ electrolyte. The standard partial molar properties of the aqueous species involved (namely, Ca^{2+}, Cl^-, $CaCl^+$, and $CaCl_2^0$) are described according to the HKF equation of state (Sverjensky et al., 1997). The model is able to describe the osmotic coefficient of the $CaCl_2$ aqueous brines and salt solubility up to 523 K. It is also able to describe salt solubility in the NaCl-$CaCl_2$-H_2O system over the whole range of mixture ratios, at least up to 403 K (experimental solubility data not available at higher temperatures). Moreover, the models of Lassin et al. (submitted) and dos Santos et al. (2021b) are consistent with each other since they both include the interaction parameters of Lach et al. (2017) for the NaCl-H_2O system.

3. RESULTS AND DISCUSSION

3.1 CO_2 solubility in the $CaCl_2$-H_2O binary system

Only two new specific binary interaction parameters involving the CO_2^0 aqueous species were found necessary to describe CO_2 solubility in $CaCl_2$ and (NaCl + $CaCl_2$) brines, up to 6 M $CaCl_2$, 40 MPa of CO_2 and 423 K. These parameters, namely $\lambda_{CO_2,Ca^{2+}}$ and $\lambda_{CO_2,CaCl^+}$ are temperature dependent, according to the following equation:

$$\lambda_{CO_2,c}(T) = A + BT + C/T \qquad [3]$$

The corresponding coefficients are given in Table 1.

Table 1: Coefficients for the temperature function [3] of the CO_2^0-Ca^{2+} and CO_2^0-$CaCl^+$ specific interaction parameters.

Parameter	A	B×10^3	C
$\lambda_{CO_2,Ca^{2+}}$	1.45781	-1.44809	-258.144
$\lambda_{CO_2,CaCl^+}$	-4.05504	5.83521	708.627

Results are plotted in Figure 1 for the solubility of CO_2 in $CaCl_2$ binary aqueous solution as a function of CO_2 pressure, and at various $CaCl_2$ concentrations and temperatures. For each condition, errors σ were calculated according to the following equation (Christov and Møller, 2004), and reported in Table 2:

$$\sigma = \sqrt{\frac{\sum(m_{CO_2,exp} - m_{CO_2,calc})^2}{N}} \qquad [4]$$

where $m_{CO_2,exp}$ and $m_{CO_2,calc}$ are the experimental a and calculated molalities of dissolved CO_2, respectively, at a given condition of $CaCl_2$ concentration, pressure and temperature. The sum covers all conditions of pressure at a given temperature and $CaCl_2$ concentration, represented by *N* data points.

Table 2: Errors σ between experimental and calculated CO_2 solubility in $CaCl_2$ brines, for each condition of temperature and $CaCl_2$ concentration.

Temper-ature (K)	$CaCl_2$ (mol·kg^{-1})	Number of data points N	Error σ
323	1	11	0.015
	3	4	0.013
	6	4	0.013
373	1	30	0.043
	3	7	0.035
	6	5	0.009
423	1	17	0.022
	3	8	0.032
	6	4	0.011

Figure 1 and Table 2 show that the model satisfactorily describes the experimental data within their dispersion intervals, between 323 and 423 K, and up to 6 M $CaCl_2$. Beyond the pressure values investigated experimentally, the calculated CO_2 solubility smoothly increases, demonstrating the numerical stability of the

model and suggesting extrapolation capabilities with respect to pressure, temperature and salinity.

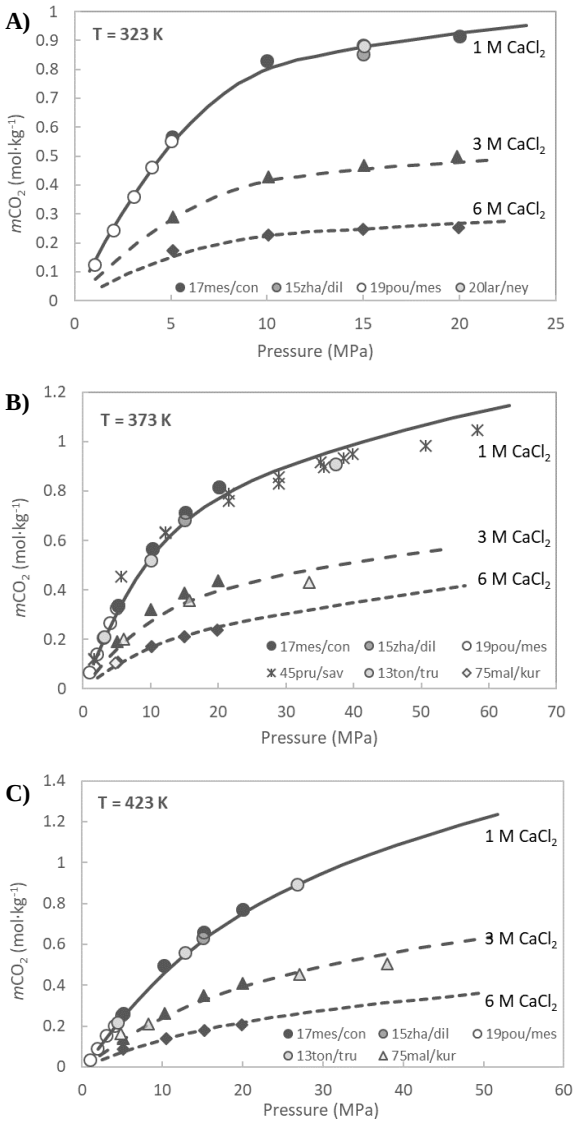

Figure 1: CO_2 solubility in $CaCl_2$ aqueous brines as a function of pressure, for various $CaCl_2$ concentrations, at A) 323 K, B) 373 K, and C) 423 K. Symbols: experimental data (45pru/sav = Prutton and Savage, 1945; 75mal/kur = Malinin and Kurovskaya, 1975; 15zha/dil = Zhao et al., 2015; 13ton/tru = Tong et al., 2013; 17mes/con = Messabeb et al., 2017; 19pou/mes = Poulain et al., 2019; 20lar/ney = Lara Cruz et al., 2021). Lines: model (this work).

3.2 CO_2 solubility in the ternary NaCl-$CaCl_2$-H_2O system

Results obtained for the solubility of CO_2 in ($CaCl_2$ + NaCl) aqueous brines are plotted in Figure 2. Errors σ are reported in Table 3. They show that the calculated solubility of CO_2 can reproduce satisfactorily the experimental data using only binary CO_2-cation interaction parameters (where cation = Na^+, Ca^{2+} or $CaCl^+$). Note that the set of Pitzer interaction parameters proposed by dos Santos et al. (2021b) and used in the present study, can describe the solubility of CO_2 in NaCl brines up to 473 K. Therefore, it is not surprising that our model is able to describe the solubility of CO_2 in the (NaCl + $CaCl_2$) aqueous mixture at 423 K.

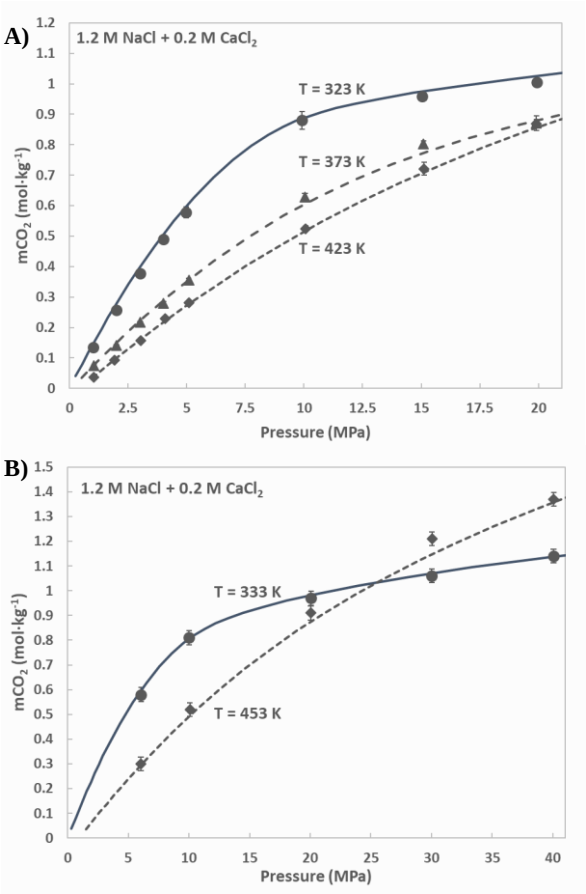

Figure 2: CO_2 solubility in (NaCl + $CaCl_2$) aqueous brines as a function of pressure, at A) 323, 373, and 423 K, and B) 333 and 453 K. Symbols: experimental data, A) Poulain et al. (2019, B) Lara Cruz et al. (2021). Lines: model (this work).

Table 3: Errors σ between experimental and calculated CO_2 solubility in (NaCl + $CaCl_2$) brines, for each condition of temperature.

Temperature (K)	Number of data points N	Error σ
323	8	0.022
333	5	0.018
373	8	0.016
423	8	0.035
453	5	0.086

These encouraging results make it possible, by means of geochemical modelling, exploring the solubility of CO_2 in extended (NaCl + $CaCl_2$) aqueous mixtures. Thus, a parametric study was done considering the whole range of compositions for the *x*NaCl + (0.5-*x*/2)$CaCl_2$ mixture, where $0 < x < 1$, for three total Cl concentration (i.e., 1.6, 3.6 and 6 mol·kg^{-1}), three temperatures (i.e., 323, 373, and 423 K), and two CO_2 fugacity values (i.e., 5 and 15 MPa).

The latter constraint is a convenient way to set the concentration of dissolved CO_2. Indeed, according to Henry's law and because the chloride content is constant when the mole fraction *x* of Na varies from 1 to 0, the molality of dissolved CO_2 is proportional to its fugacity in the CO_2-rich phase. Thus, the effect of the brine mixture composition on the calculated equilibrium pressure can be compared for different salinities. Results are plotted in Figure 3.

They suggest that whatever the temperature and the chloride concentration, the composition of the NaCl+$CaCl_2$ mixture does not affect the pressure required to equilibrate the system with a CO_2 fugacity of 5 MPa. At higher CO_2 fugacity, namely 15 MPa, the calculated equilibrium pressure varies with the chemical composition of the brine mixture. This variation is more pronounced at high salinity with large Na proportions, and lower temperatures. In these conditions, increasing Ca (at the expense of Na) increases the pressure required to equilibrate with the CO_2 fugacity (Figure 3-A). In other words, the presence of Ca in the brine has a salting-out effect on CO_2. This effect can be reversed at high temperature and high salinity: the equilibrium pressure slightly decreases when small quantities of Ca replace Na at 423 K (Figure 3-C). At higher Ca content (c.a. 5 mol.%), the salting-in effect of Ca stops and turns to a salting-out effect.

3. CONCLUSIONS

A new set of specific interaction parameters has been developed to describe the solubility of CO_2 in $CaCl_2$ + NaCl aqueous brines according to a geochemical model based on the HKF and Pitzer equations. The model is valid for $CaCl_2$ concentrations up to 6 M, temperatures up to 453 K and pressures up to 40 MPa.

Predictive calculations using this model suggest that, at high pressure, low temperature and high NaCl concentration, the presence of $CaCl_2$ in the mixture increases the salting-out effect of the brine, event at low Ca/Na ratios.

An extension of the model to larger chemical systems may help describing the behaviour of brines that are more representative of the fluids involved in geothermal exploitation plants.

Acknowledgements (optional)

The REFLECT project has received funding from the European Union's Horizon 2020 research and innovation programme under grant agreement n° 850626. The Carnot ISIFoR and BRGM are also gratefully acknowledged for their support.

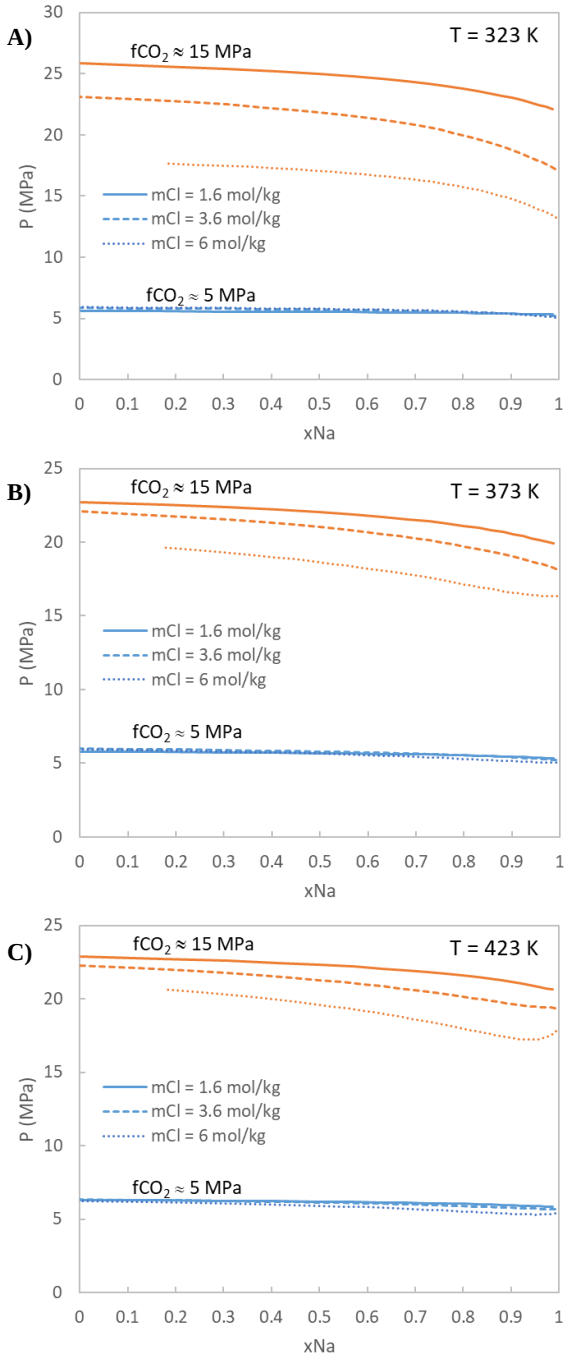

Figure 3: Predicted CO_2 solubility in (NaCl + $CaCl_2$) aqueous brines as a function of Na mole fraction, for Cl molality of 1.6, 3.6 and 6 M, CO_2 fugacity of 5 and 15 MPa, at A) 323, B) 373, and C) 423 K.

REFERENCES

Alt-Epping, P., Waber, H.N., Diamond, L.W., Eichinger, L.: Reactive transport modeling of the geothermal system at Bad Blumau, Austria:

Implications of the combined extraction of heat and CO_2. *Geothermics*, **45**, (2013), 18-30.

Appelo, C.A.J.: Principles, caveats and improvements in databases for calculating hydrogeochemical reactions in saline waters from 0 to 200°C and 1 to 1000 atm. *Appl. Geochemistry*, 55, (2015), 62–71.

Appelo, C.A.J., Parkhurst, D.L., Post, V.E.A.: Equations for calculating hydrogeochemical reactions of minerals and gases such as CO_2 at high pressures and temperatures. *Geochim. Cosmochim. Acta*, **125**, (2014), 49–67.

Bastami, A., Allahgholi, M., Pourafshary, P.: Experimental and modelling study of the solubility of CO_2 in various $CaCl_2$ solutions at different temperatures and pressures. *Pet. Sci.*, **11**, (2014), 569–577.

Benoit W.R.: Carbonate scaling characteristics in Dixie Valley, Nevada geothermal wellbores. Geothermics, **18**, (1989), 41-48

Boch, R., Leis, A., Haslinger, E. et al.: Scale-fragment formation impairing geothermal energy production: interacting H_2S corrosion and $CaCO_3$ crystal growth. *Geotherm. Energy*, **5**, (2017), 4.

Carvalho, P.J., Pereira, L.M.C., Gonçalves, N.P.F., Queimada, A.J., Coutinho, J.A.P.: Carbon dioxide solubility in aqueous solutions of NaCl: Measurements and modeling with electrolyte equations of state. *Fluid Phase Equilibria*, **388**, (2015), 100–106.

Chabab, S., Théveneau P., Corvisier, J., Coquelet, C., Paricaud, P., Houriez, C., Ahmar, E.: Thermodynamic study of the CO_2-H_2O-NaCl system: Measurements of CO_2 solubility and modeling of phase equilibria using Soreide and Whitson, electrolyte CPA and SIT models. *Int. J. Greenh. Gas Control*, **91**, (2019), 102825.

Christov, C., Møller, N.: A chemical equilibrium model of solution behavior and solubility in the H-Na-K-Ca-OH-Cl-HSO_4-SO_4-H_2O system to high concentration and temperature. *Geochim. Cosmochim. Acta*, **68**, (2004), 3717–3739.

Doherty, J.: PEST. Model-independent parameter estimation. User manual: 5th Edition, (2004).

dos Santos, P.F., André, L., Ducousso, M., Contamine, F., Cézac, P.: Experimental measurements of CO_2 solubility in aqueous $MgCl_2$ solution at temperature between 323.15 and 423.15 K and pressure up to 20 MPa. *J. Chem. Eng. Data*, **66**, (2021a), 4166-4173.

dos Santos, P.F., André, L., Ducousso, M., Contamine, F., Cézac, P.: Experimental measurement of CO_2 solubility in aqueous Na_2SO_4 solution at temperatures between 303.15 and 423.15 K and pressures up to 20 MPa. *J. Chem. Eng. Data*, **65**, (2020), 3230–3239.

dos Santos, P.F., Andre, L., Ducousso, M., Lassin, A., Contamine, F., Lach, A., Parmentier, M., Cézac, P.: An improved model for CO_2 solubility in aqueous Na+–Cl^-–SO_4^{2-} systems up to 473.15 K and 40 MPa. *Chem. Geol.*, **582**, (2021b), 120443.

Duan, Z., Sun, R., Zhu, C., Chou, I.-M.: An improved model for the calculation of CO_2 solubility in aqueous solutions containing Na^+, K^+, Ca^{2+}, Mg^{2+}, Cl^-, and SO_4^{2-}. *Mar. Chem.*, **98**, (2006), 131–139.

Eroini, V.: Kinetic Study of Calcium Carbonate Formation and Inhibition by using an in-situ Flow Cell. *PhD Thesis*, University of Leeds, (2011).

Helgeson, H.C., Kirkham, D.H., Flowers, G.C.: Theoretical prediction of the thermodynamic behavior of aqueous electrolytes at high pressures and temperatures: IV. Calculation of activity coefficients, osmotic coefficients, and apparent molal and standard and relative partial molal properties to 600°C. *Am. J. Sci.*, **281**, (1981), 1249–1516.

Kelemen, P., Benson, S.M., Pilorgé, H., Psarras, P., Wilcox, J.: An Overview of the Status and Challenges of CO_2 Storage in Minerals and Geological Formations. *Frontiers in Climate*, **1**, (2019).

Lach, A., Ballerat-Busserolles, K., André, L., Simond, M., Lassin, A., Cézac, P., Neyt, J.C., Serin, J.P.: Experimental data and modeling of solution density and heat capacity in the Na-K-Ca-Mg-Cl-H_2O system up to 353.15 K and 5 mol·kg^{-1} ionic strength. *J. Chem. Eng. Data*, **62**, (2017) 3561–3576.

Lach, A., Boulahya, F., André, L., Lassin, A., Azaroual, M., Serin, J.P., Cézac, P.: Thermal and volumetric properties of complex aqueous electrolyte solutions using the Pitzer formalism - The PhreeSCALE code. *Comput. Geosci.*, **92**, (2016), 58–69.

Lara Cruz, J., Neyrolles, E., Contamine, F., Cézac, P.: Experimental study of carbon dioxide solubility in sodium chloride and calcium chloride brines at 333.15 and 453.15 K for pressures up to 40 MPa. *J. Chem. Eng. Data*, **66**, (2021), 249–261.

Lassin, A., André, L.: A revised description of the binary $CaCl_2$-H_2O chemical system up to solution-mineral equilibria and temperatures of 250°C using Pitzer equations. Extension to the multicomponent HCl-LiCl-NaCl-KCl-$MgCl_2$-$CaCl_2$-H_2O system. *J. Chem. Thermod.*, (submitted).

Liborio, B.: Dissolution of carbon dioxide in aqueous electrolyte solutions, in the context of geological storage: A thermodynamic approach. *Ph.D. Thesis*, Université Clermont Auvergne, Clermont-Ferrand, (2017), 231 p.

Liu, Y., Hou, M., Yang, G., Han, B.: Solubility of CO_2 in aqueous solutions of NaCl, KCl, $CaCl_2$ and their

mixed salts at different temperatures and pressures. *J. Supercrit. Fluids*, **56**, (2011), 125–129.

Mahon, H., O'Connor, D., Friedrich, D., Ben, H.: A review of thermal energy storage technologies for seasonal loops. *Energy*, **239**, (2022), 122207.

Malinin, S.D., Kurovskaya, N.A.: *Geochem. Int.*, **12**, (1975), 199.

Messabeb, H., Contamine, F., Cézac, P., Serin, J.P., Gaucher, E.C.: Experimental Measurement of CO_2 Solubility in Aqueous NaCl Solution at Temperature from 323.15 to 423.15 K and Pressure of up to 20 MPa. *J. Chem. Eng. Data*, **61**, (2016), 3573–3584.

Messabeb, H., Contamine, F., Cézac, P., Serin, J.P., Pouget, C., Gaucher, E.C.: Experimental measurement of CO_2 solubility in aqueous $CaCl_2$ solution at temperature from 323.15 to 423.15 K and pressure up to 20 MPa using the conductometric titration. *J. Chem. Eng. Data*, **62**, (2017), 4228–4234.

Mohammadian, E., Hamidi, H., Asadullah, M., Azdarpour, A., Motamedi, S., Junin, R.: Measurement of CO_2 Solubility in NaCl Brine Solutions at Different Temperatures and Pressures Using the Potentiometric Titration Method. *J. Chem. Eng. Data*, **60**, (2015), 2042-2049.

Parkhurst, D.L., Appelo, C.A.J.: Description of input and examples for PHREEQC version 3: a computer program for speciation, batch-reaction, one-dimensional transport, and inverse geochemical calculations. *U.S. Geological Survey, Techniques and Methods*. Reston, VA, (2013).

Pitzer, K.S. (Ed.): Activity coefficients in electrolyte solutions. *CRC Press*, Boca Raton, CA, (1991).

Poulain, M., Messabeb, H., Lach, A., Contamine, F., Cézac, P., Serin, J.P., Dupin, J.C., Martinez, H.: Experimental measurements of carbon dioxide solubility in Na-Ca-K-Cl solutions at high temperatures and pressures up to 20 MPa. *J. Chem. Eng. Data*, **64**, (2019), 2497–2503.

Prutton, C.F., Savage, R.L.: The solubility of carbon dioxide in calcium chloride-water solutions at 75, 100, 120° and high pressures. *J. Am. Chem. Soc*., **67**, (1945), 1550.

Simmons, S.F., Christenson, B.W.: Origins of calcite in a boiling geothermal system. *Am. J. Sci.*, **294**, (1994), 361-400.

Shi, X., Mao, S.: An improved model for CO_2 solubility in aqueous electrolyte solution containing Na^+, K^+, Mg^{2+}, Ca^{2+}, Cl^- and SO_4^{2-} under conditions of CO_2 capture and sequestration. *Chem. Geol.*, **463**, (2017), 12–28.

Springer, R.D., Wang, Z., Anderko, A., Wang, P., Felmy, A.R.: A thermodynamic model for predicting mineral reactivity in supercritical carbon dioxide: I. Phase behavior of carbon dioxide–water–chloride salt systems across the H_2O-rich to the CO_2-rich regions. *Chem. Geol.*, **322–323**, (2012), 151–171.

Sverjensky, D.A., Shock, E.L., Helgeson, H.C.: Prediction of the thermodynamic properties of aqueous metal complexes to 1000°C and 5 kb. *Geochim. Cosmochim. Acta*, **61**, (1997), 1359–1412.

Tanger, J.C., Helgeson, H.C.: Calculation of the thermodynamic and transport properties of aqueous species at high pressures and temperatures: Revised equations of state for the standard partial molal properties of ions and electrolytes. *Am. J. Sci*., **288**, (1988), 19–98.

Thomas, D.M., Gudmundsson, J.S.: Advances in the study of solids deposition in geothermal systems. *Geothermics*, **18**, (1989), 5-15.

Todd, M.A., Bluemle, M.J.: Chapter 12 - Formation and mitigation of mineral scaling in geothermal power plants. In *Water-Formed Deposits* Ed.: Zahid Amjad, Konstantinos D. Demadis, (2022), 269-282,

Tong, D., Trusler, J.P.M., Vega-Maza, D.: Solubility of CO_2 in aqueous solutions of $CaCl_2$ or $MgCl_2$ and in a synthetic formation brine at temperatures up to 423 K and pressures up to 40 MPa. *J. Chem. Eng. Data*, 58, (2013), 2116–2124.

Zhao, H., Dilmore, R., Allen, D.E., Hedges, S.W., Soong, Y., Lvov, S.N.: Measurement and modeling of CO_2 solubility in natural and synthetic formation brines for CO_2 sequestration. *Environ. Sci. Technol*., **49**, (2015a) 1972–1980.

Zhao, H., Fedkin, M. V., Dilmore, R.M., Lvov, S.N.: Carbon dioxide solubility in aqueous solutions of sodium chloride at geological conditions: Experimental results at 323.15, 373.15, and 423.15K and 150bar and modeling up to 573.15K and 2000bar. *Geochim. Cosmochim. Acta*, **149**, (2015b), 165–189.

Zivar, D., Kumar, S., Foroozesh, J.: Underground hydrogen storage: A comprehensive review. *Int. J. Hydrog. Energy*, **46**, (2021), 23436-23462.